U.S.NRC
United States Nuclear Regulatory Commission
Protecting People and the Environment

RIL 2021-XX
NIST TN XXXX
SAND2021-XXXX

REPORT ON HIGH ENERGY ARCING FAULT EXPERIMENTS

Experimental Results from Open Box Enclosures

Date Published: December 2021

Prepared by:
G. Taylor
Office of Nuclear Regulatory Research

A.D. Putorti Jr.
National Institute of Standards and Technology

C. LaFleur
Sandia National Laboratories

Mark Henry Salley, NRC Project Manager

Sandia National Laboratories is a multimission laboratory managed and operated by National Technology & Engineering Solutions of Sandia, LLC, a wholly owned subsidiary of Honeywell International Inc., for the U.S. Department of Energy's National Nuclear Security Administration under contract DE-NA0003525.

This report was published as National Institute of Standards and Technology (NIST) Technical Note XXXX as part of a series of experiments funded by the U.S. Nuclear Regulatory Commission's Office of Nuclear Regulatory Research. The report has been re-published as an NRC Research Information Letter (RIL).

Sandia National Laboratories is a multimission laboratory managed and operated by National Technology & Engineering Solutions of Sandia, LLC, a wholly owned subsidiary of Honeywell International Inc., for the U.S. Department of Energy's National Nuclear Security Administration under contract DE-NA0003525.

Disclaimer

Legally binding regulatory requirements are stated only in laws, NRC regulations, licenses, including technical specifications, or orders; not in Research Information Letters (RILs). A RIL is not regulatory guidance, although NRC's regulatory offices may consider the information in a RIL to determine whether any regulatory actions are warranted.

Certain commercial equipment, instruments, or materials are identified in this paper in order to specify the experimental procedure adequately. Such identification is not intended to imply recommendation or endorsement by the US Nuclear Regulatory Commission or the National Institute of Standards and Technology, or Sandia National Laboratories, nor is it intended to imply that the materials or equipment identified are necessarily the best available for the purpose.

NIST Technical Note XXXX

Report on High Energy Arcing Fault Experiments

Experimental Results from Open Box Enclosures

Anthony Putorti
Scott Bareham
Edward Hnetkovsky
Christopher Brown
Wai Cheong Tam
Andre Thompson
Michael Selepak
Philip Deardorff
National Institute of Standards and Technology

Kenneth Hamburger
Nicholas Melly
Kenneth Miller
Gabriel Taylor
U.S. Nuclear Regulatory Commission

Kenneth Armijo
Paul Clem
Alvaro Augusto Cruz-Cabrera
Byron Demosthenous
Austin Glover
Chris LaFleur
Raymond Martinez
James Taylor
Rana Weaver
Caroline Winters
Sandia National Laboratories

This publication is available free of charge from:
https://doi.org/10.6028/NIST.TN.XXXX

December 2021

U.S. Department of Commerce
Gina M. Raimondo, Secretary

National Institute of Standards and Technology
James K. Olthoff, Performing the Non-Exclusive Functions and Duties of the Under Secretary of Commerce for Standards and Technology & Director, National Institute of Standards and Technology

National Institute of Standards and Technology Technical Note XXXX
Natl. Inst. Stand. Technol. Tech. Note XXXX, NNN pages (December 2021)
CODEN: NTNOEF

This publication is available free of charge from:
https://doi.org/10.6028/NIST.TN.XXXX

Abstract

This report documents an experimental program designed to investigate High Energy Arcing Fault (HEAF) phenomena. The experiments focus on providing data to better characterize the arc to improve the prediction of arc energy emitted during a HEAF event. An open box experiment allow for direct observation of the arc, which allows diagnostic instrumentation to record the phenomenological data needed for better characterization of the arc energy source term. The data collected supports characterization of the arc and arc jet, enclosure breach, material loss, and electrical properties. These results will be used to better characterizing the hazard for improvements in fire probabilistic risk assessment (PRA) realism.

The experiments were performed at KEMA Labs located in Chalfont, Pennsylvania. The experimental design, setup, and execution were completed by staff from the NRC, the National Institute of Standards and Technology (NIST), Sandia National Laboratories (SNL) and KEMA Labs. In addition, representatives from the Electric Power Research Institute (EPRI) observed some of the experimental setup and execution.

The HEAF experiments were performed between August 22, 2020 and September 18, 2020 on near-identical 51 cm (20 in) cube metal boxes suspended from a Unistrut support structure. The three-phase arcing fault was initiated at the ends of the conductors oriented vertically and located at the center of the box. Either aluminum or copper conductors were used for the conductors. The low-voltage experiments used 1 000 volts AC, while the medium-voltage experiments used 6 900 volts AC consistent with other recently completed experiments [1]. Durations of the experiment ranged from 1 s to 5 s with fault currents ranging from 1 kA to 30 kA. Real-time electrical operating conditions, including voltage, current and frequency, were measured during the experiments. Heat fluxes and incident energies were measured with plate thermometers, radiometers, and slug calorimeters at various locations around the electrical enclosures. The experiments were documented with normal and high-speed videography, infrared imaging and photography.

Key words

High Energy Arcing Fault, Arc Flash, Electrical Enclosure, Electric Arc, Fire Probabilistic Risk Assessment

Table of Contents

List of Tables

List of Figures

EXECUTIVE SUMMARY

PRIMARY AUDIENCE: Fire protection, electrical and probabilistic risk assessment engineers conducting or reviewing fire risk assessments related to high energy arcing faults.

SECONDARY AUDIENCE: Engineers, reviewers, utility managers, and other stakeholders who conduct, review, or manage fire protection programs and need to understand the underlying technical basis for the hazards associated with high energy arcing faults.

KEY RESEARCH QUESTION: How does the energy of electrical arcs change with variation to influencing parameters?

RESEARCH OVERVIEW

Operating experience has shown that high energy arcing faults pose a hazard to the safe operation of nuclear facilities. Current regulations and probabilistic risk assessment methods were developed using limited information and these uncertainties required the use of safety margins to bound the hazard. Experiments aimed at providing additional data to improve realism identified a concern that high energy arcing faults involving aluminum may increase the hazard potential. Due to the limited number of experiments where this phenomenon was observed, the NRC pursued additional experiments focused on assessing the specific impact of aluminum on the hazard. This report documents a set of experiments performed in 2019.

A series of open box electrical arcing experiments were performed under a variety of conditions believed to influence the arc energy characteristics. These influencing parameters included conductor material type, arc duration, fault current, system voltage, and conductor size. Each experiment consisted of an arcing fault initiated and sustained within a five-sided cubical metal enclosure. Numerous measurements were taken to characterize the environment within and surrounding the box, including external heat flux, external incident energy, electromagnetic field, air breakdown strength, and mass loss of electrical conductors and steel box enclosure. Photometric equipment and techniques were deployed to capture the event using a combination of devices to characterize the thermal environment, particulate trajectory and velocity, and event timing.

This report documents the experiments performed, including the experimental methods, experiment facility, open box, instrumentation, experiment observations, and results. Videos and photometric data files are provided by laboratories contracted to the NRC and information on accessing that information is identified. This report does not provide detailed evaluation of the results or comparisons of the results to other methods or data. Those efforts will be documented in subsequent report(s).

KEY FINDINGS

This research yields a data set of information to characterize the effects of electrical arcing faults involving aluminum or copper electrodes. The results from this research include:

- External heat flux and incident energy measurements which provide direct comparison between aluminum and copper electrodes.

- Mass loss data was collected for the electrodes and the steel enclosure. This information can be subsequently used to evaluate or develop prediction models to support hazard modeling.
    - For the electrodes, more mass was lost for copper electrodes then aluminum when normalized to an equivalent electrical experimental energy.
    - The steel box enclosure mass lost was observed to be larger for the aluminum electrode experiments versus the copper electrode experiments when normalized to an equivalent electrical experimental energy.
- Air conductivity and breakdown strength measurements were made during a number of experiments. The results indicated that a conductive cloud is unlikely to cause equipment arc over.
- Surface conductivity measurement of HEAF byproduct surface deposition showed a decrease in resistance. Impact on plant safety equipment is not likely, but highly dependent on the design, configuration, location, and sensitivity of the equipment.
- Electromagnetic interference measurements showed that the EMI signature was small and not likely to impact sensitive plant equipment.

WHY THIS MATTERS

This report provides empirical evidence to assist U.S. NRC staff and stakeholders who are evaluating the adequacy of current methods. The information provided will support advances in state-of-the-art methods and tools to assess the high energy arcing fault hazard in nuclear facilities. This information may also be applicable to fossil fuel and alternative energy facilities and other buildings with low-voltage and medium-voltage electrical distribution equipment such as switchgear and bus duct.

HOW TO APPLY RESULTS

Engineers and scientist advancing hazard and fire probabilistic risk assessment methods should focus on Section 3 and 4 of this report.

LEARNING AND ENGAGEMENT OPPORTUNITIES

Users of this report may be interested in the following learning opportunities:

Nuclear Energy Institute (NEA) HEAF Project to conduct experiments in order to explore the basic configurations, failure modes and effects of HEAF events. Primary objectives include (1) development of a peer-reviewed guidance document that could be readily used to assist regulators of participants, and (2) joint nuclear safety project report covering all testing and data captured. More information on the project and opportunities to participate in the program can be found online at https://www.oecd-nea.org/.

CITATIONS

This report was prepared by the following:

National Institute of Standards and Technology (NIST)
Engineering Laboratory; Fire Research Division
Gaithersburg, Maryland 20899

Anthony D. Putorti Jr.
Scott Bareham
Edward Hnetkovsky
Christopher Brown
Wai Cheong Tam
Eric Link
Michael Selepak
Phil Deardorff

Sandia National Laboratories (SNL)
Albuquerque, New Mexico 87185

Kenneth Armijo
Alvaro Augusto Cruz-Cabrera
Paul Clem
Byron Demosthenous
Austin Glover
Chris LaFleur
Ray Martinez
James Taylor
Rana Weaver
Caroline Winters

U.S. Nuclear Regulatory Commission
Washington, DC 20555-0001

Kenneth Hamburger
Nicholas Melly
Kenneth Miller
Gabriel Taylor

ABBREVIATIONS AND ACRONYMS

AC	alternating current
ASTM	ASTM International
AWG	American Wire Gauge
DC	direct current
DIN	Deutsches Institut für Normung
EMI	electro-magnetic interference
EPRI	Electric Power Research Institute
GI	generic issue
GIRP	Generic Issue Review Panel
HEAF	high energy arcing fault
IEEE	Institute of Electrical and Electronic Engineers
IN	information notice
IR	infra-red
ISO	International Organization for Standardization
MD	management directive
NEA	Nuclear Energy Agency
NIST	National Institute of Standards and Technology
NRC	Nuclear Regulatory Commission
OECD	Organisation for Economic Co-operation and Development
OBMV	open box medium-voltage
PIRT	Phenomena Identification and Ranking Table
PRA	probabilistic risk assessment
PT	plate thermometer
RES	Office of Nuclear Regulatory Research
RIL	research information letter
SNL	Sandia National Laboratories
T_{cap}	Tungsten slug Calorimeter
U.S.	United States of America

1. Introduction

Infrequent events such as fires at a nuclear power plant can pose a significant risk to safe plant operations. Licensees combat this risk by having robust fire protection programs designed to minimize the likelihood and consequences of fire. These programs provide reasonable assurance of adequate protection of the facility from known fire hazards. However, several hazards remain subject to a larger degree of uncertainty, requiring significant safety margins in plant analyses.

One such hazard comprises an electrical arcing fault involving electrical distribution equipment and components comprised of aluminum. While the electrical faults and subsequent fires are considered in existing fire protection programs, recent research [2] has indicated that the presence of aluminum during the electrical fault can exacerbate the damage potential of the event. The extended damage capacity could exceed the protection provided by existing fire protection features for specific fire scenarios and increase plant risk estimated in fire probabilistic risk assessments (PRAs).

The U.S. Nuclear Regulatory Commission (NRC) Office of Nuclear Regulatory Research (RES) studies fire and explosion hazards to the safe operation of nuclear facilities. This includes developing data, tools and methodologies to support risk and safety assessments. Through recent research efforts and collaboration with international partners, a non-negligible number of reportable high energy arcing fault (HEAF) events have been identified as occurring in nuclear facilities [2]. HEAF events pose a unique hazard in nuclear facilities and additional research in this area is needed to ensure that the hazard is accurately characterized and assessed for its impact on nuclear safety.

1.1. Background

In June 2013, an OECD/NEA report [3] on international operating experience documented 48 HEAF events, accounting for approximately 10 percent of the total fire events reported. These HEAF events are often accompanied by loss of essential power and complicated shutdowns. Existing PRA methodology for HEAF analysis is prescribed in NUREG/CR-6850 “EPRI/NRC-RES Fire PRA Methodology for Nuclear Power Facilities Vol. 2 [4],” and its Supplement 1 [5]. To confirm these methods, the NRC led an international experimental campaign from 2014 to 2016. This experimental campaign is referred to as “Phase 1 experiments.” The results of these experiments [6] uncovered a potential increase in hazard posed by aluminum components in or near electrical equipment, as well as unanalyzed equipment failure mechanisms.

In response to this new information, the NRC performed a thorough review of U.S. operating experience with a focus on instances where HEAF-like events have occurred in the presence of aluminum. This review uncovered six events where aluminum effects like those observed in the experiments were present. An Information Notice 2017-004, “High Energy Arcing Faults in Electrical Equipment Containing Aluminum Components (IN 2017-04)” detailing the relevant aspects of the licensee event reports and Phase 1 experiments was published in August of 2017 [2].

Additionally, the staff in the Office of Nuclear Regulatory Research (RES) proposed a potential safety concern as a generic issue (GI) in a letter dated May 6, 2016 [7]. The Generic Issue Review Panel (GIRP) completed its screening evaluation [8] for proposed Generic Issue (GI) PRE-GI-018, "High-Energy Arc Faults (HEAFs) Involving Aluminum," and concluded that the proposed issue met all seven screening criteria outlined in Management Directive (MD) 6.4, "Generic Issues Program." Therefore, the GIRP recommended that this issue continue into the Assessment Stage of the GI program. The GIRP has completed an assessment plan, issued July 10, 2019 [9]. Though the HEAF research project will result in updated fire PRA guidance for all arcing faults, much of the HEAF research program exists to resolve PRE-GI-018 in accordance with the assessment plan.

These actions resulted in the identification of a need for more data to better understand the hazard. The NRC developed an experimental plan in collaboration with its international collaborative partners under the OECD/NEA program and based on information from a Phenomena Identification and Ranking Table (PIRT) exercise performed in 2017 [10].

On August 31, 2021, the NRC closed the proposed generic issue PRE-GI-018, "High Energy Arc Faults involving Aluminum," [11] based on fact that the proposed GI did not meet one of the seven screening criteria. The GIRP concluded that the risk and safety significance of HEAFs involving aluminum cannot be adequately determined without performing additional, long-term research to develop the methodology for such a determination. As such, Criterion 5 of the screening criteria in NRC Management Directive 6.4 is no longer being met and the proposed GI exited the program.

1.2. Objectives

The research objectives for this experimental series include: 1) observe and record electrical arc behavior to support model development and refinement, 2) measure arc optical emissions, 3) measure electric field, 4) evaluate arc effluent impact on air breakdown strength, 5) measure the air conductivities of the arc effluent, and 6) document the experiments and results.

1.3. Scope

The scope of this research includes performing experiments on low and medium electric arc characteristics using a variety of instrumentation. This effort involves measurement and documentation of electrical and thermal parameters, along with physical evidence. Detailed data analysis for specific applications is beyond the scope of this report.

1.4. Approach

The approach taken for this work follows practices from past efforts but makes several deviations to achieve the objectives. Specifically, the electrical arc is initiated using a three-phase power system. The arc persists for a specified duration, current, and system voltage. Measurements taken prior to, during, and after the experiments are performed to assess specific characteristics of the arc and the influence of parameter variation. KEMA Labs provided electrical energy for the experiment at the specified experimental parameters (system voltage, current, duration). Measurements internal and external to the arc were made using robust measurement devices fielded by the National Institute of Standards and

Technology (NIST), KEMA Labs and Sandia National Laboratories (SNL). Measurements were recorded, scaled, and reported. Feedback received during the developmental stage of this project was incorporated into the experimental approach.

2. Experimental Method

This section provides information on methods used to perform the experiments[1], including experiment planning, an overview of the experiment facility, the experimental apparatus, and the various instrumentation that were used.

2.1. Experiment Planning

The experiments are designed to complement small scale arc experiments that were performed at SNL in 2018 and 2019 [12]. The small-scale experiments were limited in the amount of energy that could be delivered to the arc. The experiments performed at KEMA Labs provide more representative energy (voltage, current and duration) to ensure that the small-scale experimental results are applicable, and to understand the impacts of changes in the configuration. In addition, three phase faults were performed instead of single phase to ground faults. The small-scale experimental results are documented in SAND2019-11145, "Electrical Arc Fault Particle Size Characterization [12]."

The experiment plan was developed in 2019. Lessons learned from the Phase 1 experiments [6], results from the Phenomena Identification and Ranking Table (PIRT) exercise [10], the literature, and input from the SNL modeling team were used to develop the initial experimental plan. Feedback was received and discussed with the Electric Power Research Institute (EPRI). These discussions resulted in changes to the plan that provided improvements to the overall approach and confidence in the execution of the effort.
In addition to the experiments that support model development, additional needs were identified through stakeholder feedback. These include a better understanding of the electrical conductivity characteristics of the arc effluent and the strength of the electromagnetic field of the arc. Two additional experimental plans were developed to address those aspects.

The key parameters that the experimental plan evaluates include:

- Material – copper vs. aluminum electrical conductors
- Voltage – low-voltage vs. medium-voltage
- Current – selection of credible arcing current(s)
- Duration – low-to-mid range HEAF duration(s)

[1] The term 'test' implies the use of a standardized test method promulgated by a standards development organization such as the International Organization for Standardization (ISO), ASTM International, Institute of Electrical and Electronics Engineers (IEEE), etc. The experiments described in this report are not standardized tests and were specifically developed to examine HEAF phenomena. The term 'test' is used in some contexts to preserve continuity with previous programs or to describe facilities where standard tests are frequently performed. Standard test methods, where they exist, are used for some measurements.

2.2. Experiment Facility

The full-scale experiments were performed at KEMA Labs (referred to in the remainder of this report as "KEMA"), located in Chalfont, Pennsylvania. Two rounds of experiments were performed, one in August and the other in September of 2019. The second round of experiments was not planned in advance but became viable as a result of cancelation of planned medium-voltage bus duct experiments. The experiment facility was chosen for its ability to meet the requirements of the program, specifically the electrical voltages, currents, and energies needed for sustained arcing within the subject enclosures, and ability to permit fire conditions for a period after completion of the arcing phase of the HEAF experiment. KEMA provided the electrical measurements required to quantify the characteristics of the power supplied to the enclosures during the arcing experiments. KEMA also provided incident thermal energy measurements.

The experiment cell was composed of a cubical space with one open side. The open side was equipped with a roll-up door for security and weather protection when not in use. The open side of the experiment cell faces the operator control room, with a courtyard area in-between. The control room is equipped with impact resistant glazing so that the operators, clients, and guests can observe the experiments. A door in the rear of the experiment cell leads to a protected space where SNL data acquisition equipment was located and operated. NIST data acquisition equipment was located adjacent to the test cells in an air-conditioned van.

Two different experiment cells were used during this experiment series. Experiment Cell #7 was used in August to perform the low-voltage experiments. Experiment Cell #9 was used in September for the medium-voltage experiments. The experiment cells are shown in Fig. 1 and Fig. 2. Detailed drawings of the facility are provided in Appendix B. Drawings of the experiment cell are courtesy of KEMA Labs.

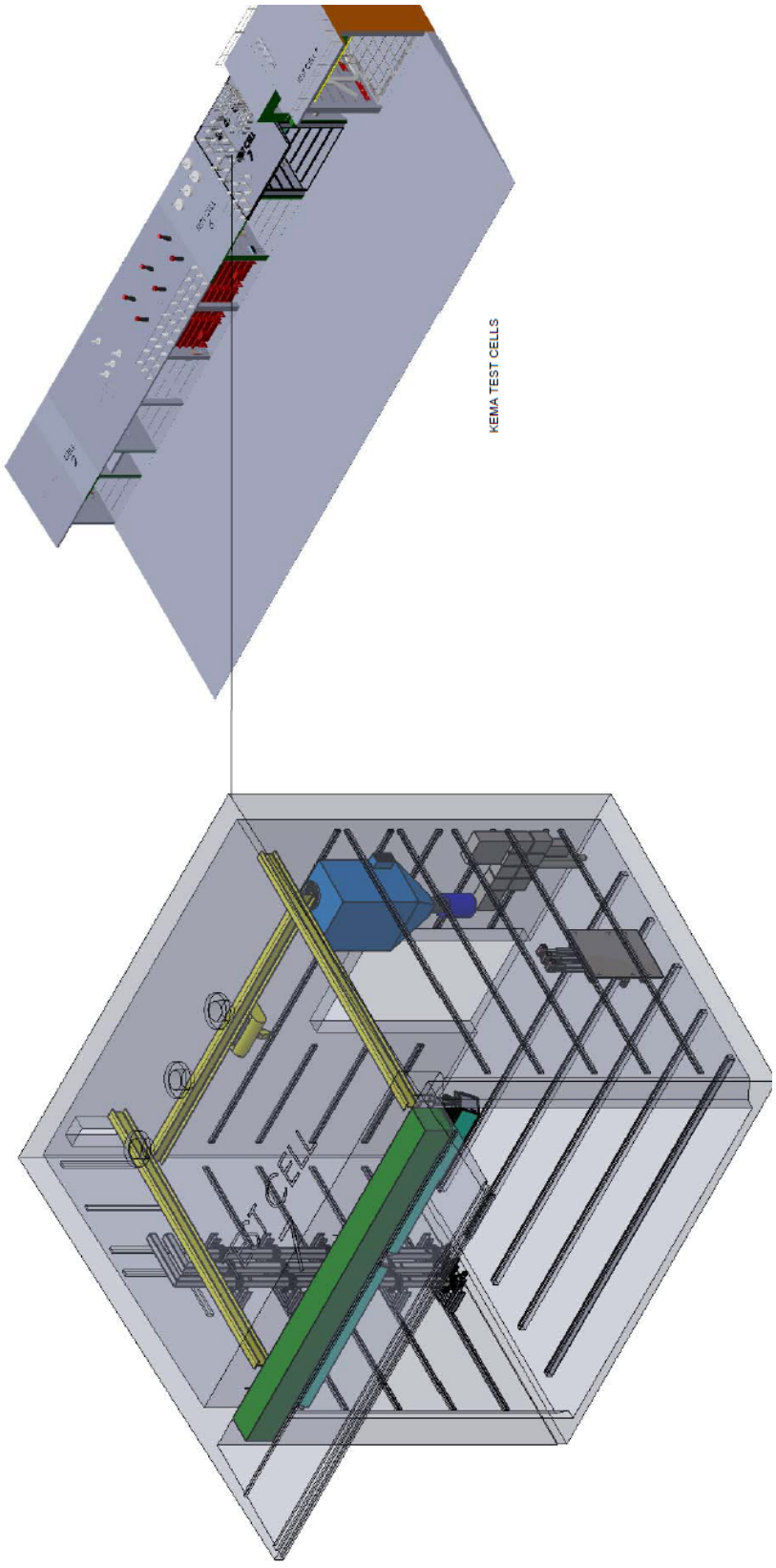

Fig. 1. Isometric drawing of Experiment Cell #7 (Left) and Location of Experiment Cell #7 (Right with respect to KEMA facility)

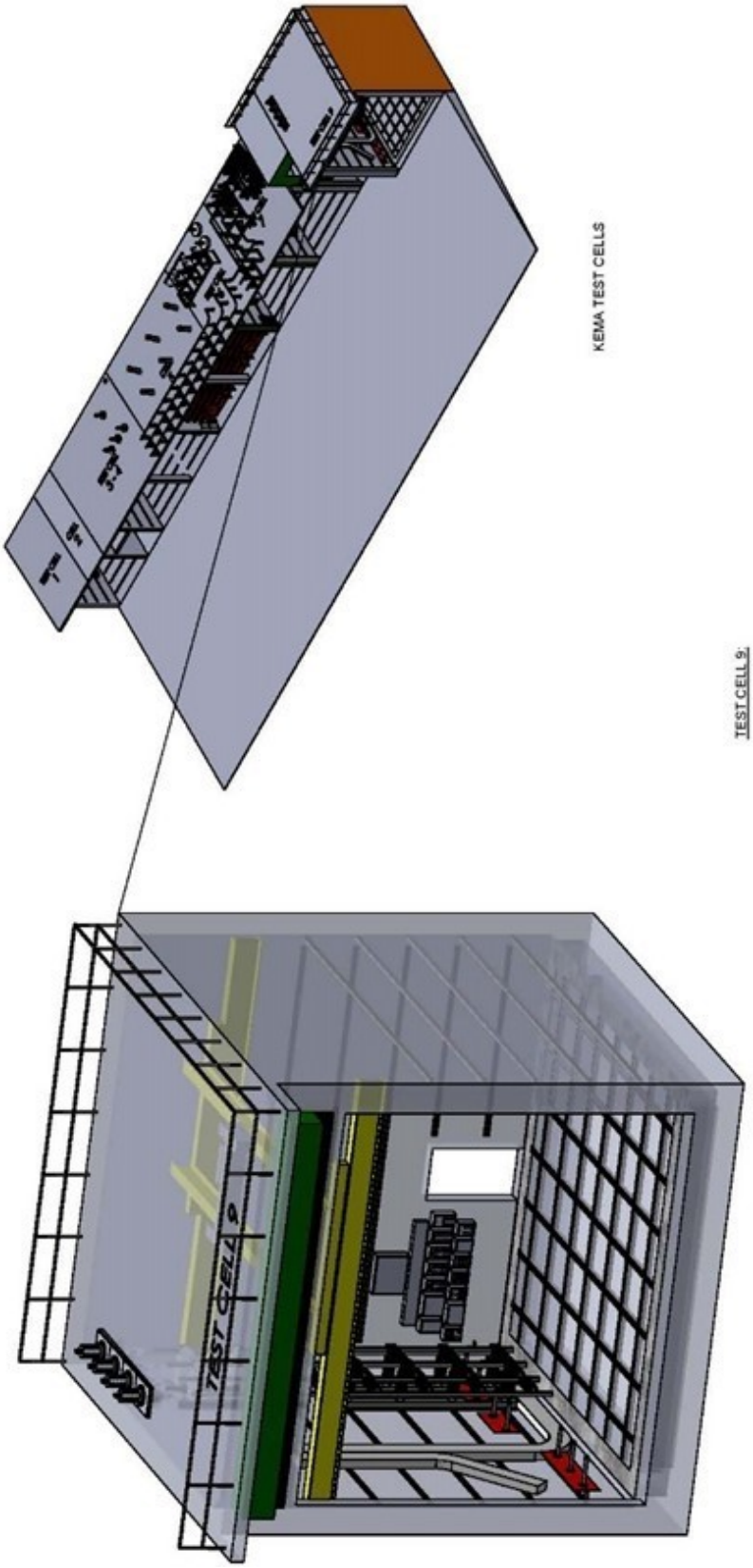

Fig. 2. Isometric drawing of Experiment Cell # 9 (Left) and Location of Experiment Cell #9 (Right with respect to KEMA facility)

2.3. Open Box

The open box is shown in Fig. 3 for low-voltage and Fig. 4 for medium-voltage experiments. The box dimensions were approximately 51 cm by 51 cm by 51 cm (20 in by 20-in by 20-in). The box was made of sheet steel with a nominal thickness of 0.18 cm (0.07 in). Three electrodes were spaced approximately 8.9 cm (3.5 in) on center for low-voltage and approximately 13 cm (5.0 in) on center for the medium-voltage experiments. Ends of the electrodes were near the centerline of the box (approximately 25 cm [10 in] from top and bottom). The electrodes were held in place by a prefabricated two-piece insulator block that affixed to the top of the box through a rectangular opening. The box was elevated approximately 127 cm (50 in) from the floor to the bottom of the open box. This configuration supported easier implementation of the instrumentation deployed by SNL (see Section 2.4) and allowed for evaluation of arc burn-through of the steel box.

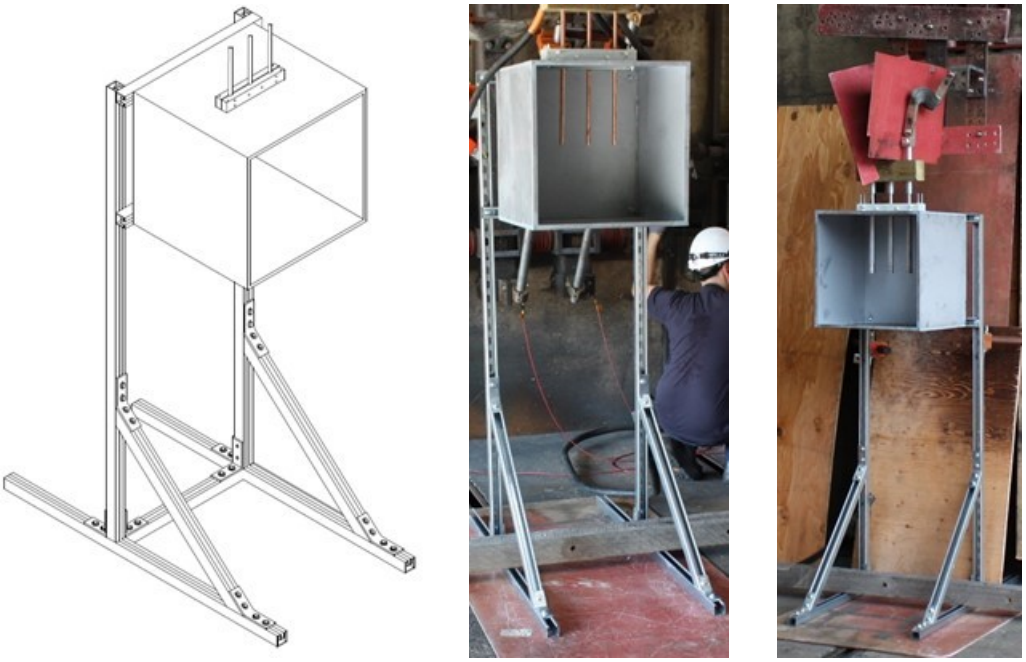

Fig. 3. Open Box Configuration Low-voltage experiments [Left – isometric, Center – 1.3 cm [0.5 in] copper electrode, Right – 2.5 cm [1 in] aluminum electrode]

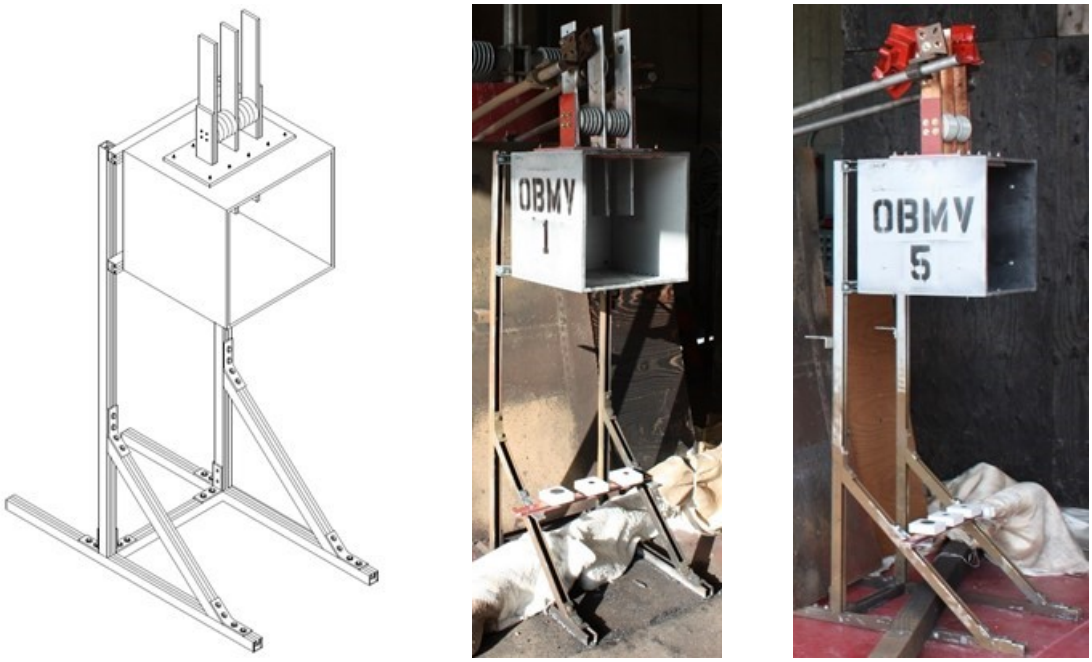

Fig. 4. Open box configuration medium-voltage experiments [Left - isometric, Center – aluminum 10.2 cm [4 in] bars, Right – copper 7.62 cm [3 in] bars]

One series of low-voltage experiments was performed in August 2019. The planned experiments are shown in Table 1. The experiments used 1 000 Vac instead of a more typical 480 Vac or 600 Vac system voltage to ensure that the arc could be maintained for the desired experiment duration. The actual arc voltage is dependent on arc impedance which is a function of the conductor gap and arc current, thus the selection of a higher low-voltage was made to support arc restrike for the planned experimental duration, rather than influence arc energy. The nominal currents of 1 kA, 5 kA, 15 kA, or 30 kA varied between experiments. The planned experimental duration of 1 s, 2 s, or 4 s experiments was also varied. Either aluminum or copper electrodes were installed in the open boxes. The electrodes for the low-voltage experiments were cylindrical rods. Two rod diameters were used, namely, a nominal 1.3 cm (0.5 in) diameter rod or 2.5 cm (1.0 in) diameter rod. The larger rod was milled down to a nominal 1.3 cm (0.5 in) in the center of the rod to allow for a single rod support bracket to be used for all low-voltage box experiments.

The second series of experiments was performed at medium-voltage levels in September 2019. The planned experiments are shown in Table 2. The medium-voltage experiments used 6 900 Vac, with various arc currents and experimental durations to allow for comparisons to the low-voltage experiments and for evaluation of material effects (aluminum versus copper). Nominal currents of either 15 kA or 30 kA and nominal durations of 1 s, 2 s, or 5 s were used. The electrodes for the medium-voltage experiments were rectangular bars approximately 1.3 cm (0.5 in) thick and 7.6 cm (3.0 in) wide for copper electrodes and 10.2 cm (4.0 in) for aluminum electrodes. One exception was OBMV6, a repeat of OBMV1, which used 7.6 cm (3.0 in) wide aluminum electrode bars.

Table 1. Low-voltage box experimental matrix (planned)

EXPERIMENT	Rod Material		Rod Diameter (cm)		Voltage	Current	Duration
#	Al	Cu	0.5	2.5	kV	kA	Seconds
OB01		X	X		1.0	1.0	2.0
OB02		X		X	1.0	15.0	2.0
OB03		X		X	1.0	15.0	4.0
OB04		X		X	1.0	30.0	1.0
OB05	X		X		1.0	1.0	2.0
OB06	X			X	1.0	15.0	2.0
OB07	X			X	1.0	15.0	4.0
OB08	X			X	1.0	30.0	1.0
OB09		X	X		1.0	5.0	2.0
OB10	X		X		1.0	5.0	2.0

Table 2. Medium-voltage box experimental matrix (planned)

EXPERIMENT	Rod Material		Rod Width (in)		Voltage	Current	Duration
#	Al	Cu	3.0	4.0	kV	kA	Seconds
OBMV1	X			X	6.9	15	2
OBMV2	X			X	6.9	30	1
OBMV3	X			X	6.9	15	5
OBMV4		X	X		6.9	15	2
OBMV5		X	X		6.9	30	5

2.4. Instrumentation

Thermal, optical emission, electromagnetic, conductivity and electrical measurements were made using a variety of instruments and techniques. This section provides an overview of each, along with the methods and location of measurement.

2.4.1. Overview of Instruments

Table 3 lists the measurement equipment arranged throughout the test cell and the corresponding measurements. A general configuration is shown in Fig. 5 followed by a photograph in Fig. 6. A brief description of each device follows.

Table 3. List of measurement equipment

Measurements	Instrument / Technique
Temperature	Infrared (IR) Imaging, Plate Thermometer (PT)
Electromagnetic Interference	Free-Field d-Dot Sensors
Air Conductivity	Planar Conductivity Sensors
Air Breakdown Strength	Breakdown Sensors
Heat Flux (time-varying)	Plate Thermometer (PT)
Heat Flux (average)	Plate Thermometer (PT), Thermal Capacitance Slug (T_{cap} slug), Radiometer
Incident Energy	ASTM Slug Calorimeter (slug) ,Thermal Capacitance Slug (T_{cap} slug)
Arc Plasma / Fire Dimensions	Videography, IR Imaging
Surface Deposit Analysis	Sample Collection (carbon tape), Post-Experiment Laboratory Analysis (Energy Dispersive Spectroscopy)
Qualitative Information	High Speed / High Dynamic Range Imaging

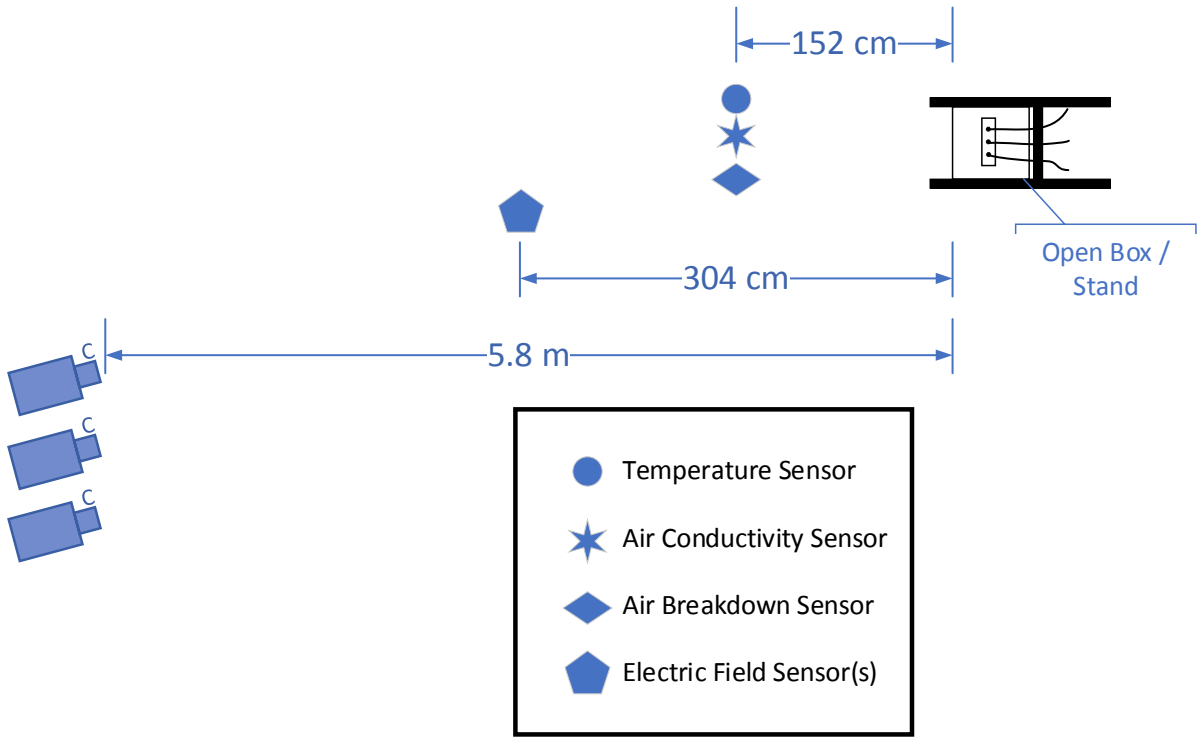

Fig. 5. Plan view of instrumentation locations (note that locations and instruments used varied by experiment and illustration is not to scale). Three cameras (labeled 'C' are shown in the far left of the figure and were approximately 5.8 m from the open box.

Fig. 6. Instrumentation cluster covered with heat resisting fabric for protection during experiments (from Left-to-right, air breakdown, radiometer, d-dot, air conductivity, high speed IR and visible videography

2.4.2. Optical Emission Spectroscopy

An Ocean Optics HR4000 Spectrometer was used to monitor the spectral radiation profile emitted from the arcing fault at a data acquisition rate of 100 Hz for the entire experimental duration. A UV-VIS optical fiber collects light from the arc and disperse it by wavelength/energy using a grating and imaged onto a detector. This provides information on how many photons of a given energy are present during the collection time. This energy is specific to the emitting species and the temperature and density of the emitter. By analyzing the emission spectra produced, quantitative time-resolved measurements are produced of both the arc temperature and surrounding graybody temperature. Emission spectra also provide species identification in the arc and the surrounding gas environment. The resulting temperatures measurements will be used for model validation and will be made available for comparison to all physical and analytical models. The spectrometer is shown in Fig. 7.

Fig. 7. The spectrometer is mounted to the top of the base plate

2.4.3. Digital Imaging

NIST and SNL fielded numerous imaging technologies to provide high-speed quantitative and qualitative imaging during this HEAF experimental series evolution. The measurement methods included visible high-speed and high definition imaging, high-speed high dynamic range visible imaging, and high-speed thermal imaging. The equipment fielded by NIST included high definition video cameras and a high definition thermal imager like that used in the Phase 1 experiments [6] and 2018 medium-voltage HEAF experiments [1] to capture high definition visible and high-speed thermal images. NIST also fielded a high speed, high dynamic range, thermal imager equipped with a rotating filter wheel. Equipment fielded by SNL was a subset of equipment fielded in the 2018 experiment [1]. The equipment selection was scaled down based on results and lessons learned. SNL reports document the approach, and uncertainties [13].

The processed images can be accessed from the NRC RIL website[2]:
https://www.nrc.gov/reading-rm/doc-collections/research-info-letters/index.html

[2] The RIL website can be accessed by visiting http://www.NRC.gov, selecting the "NRC Library" >> "Document Collections" >> "Research Information Letters".

2.4.3.1. High Speed Videography

One video camera provided high-speed high-resolution quantitative and qualitative imaging of the arcing fault in the open box. The camera was located on the opposite side of the cell from the open box, and adjacent to the thermal imaging camera(s). The camera view included the open-end side of the box under experiment. Images from this camera were used with data fusion products to visualize instrumentation data (current and voltage) and imaging measurements. All imaging was time-synchronized to the start of the arcing event via a trigger signal from the DNV GL KEMA facility. Fusion of the short-wave high-speed infrared imager with the high-resolution high-speed visible imager provided quantitative temperature data in the overlaid images. A color legend shows the calibrated temperature range with uncertainties. A screenshot of the video compilation is shown in Fig. 8.

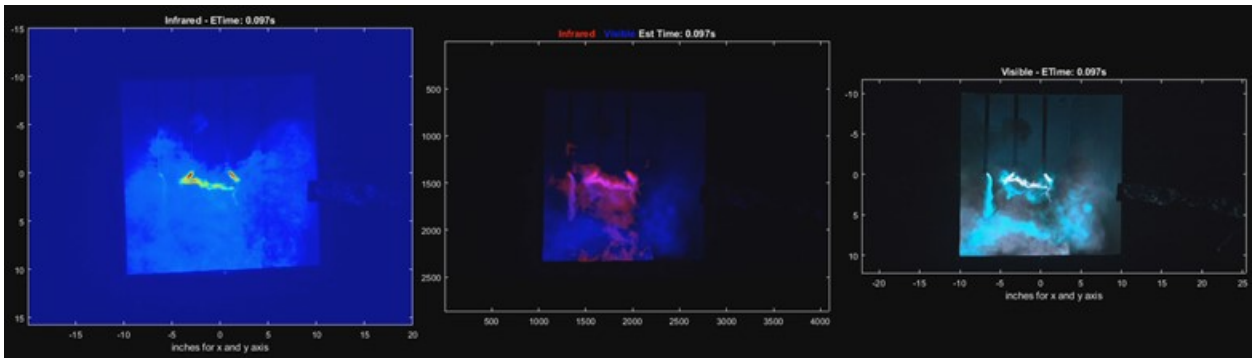

Fig. 8. High-speed high-resolution imaging (left – IR image, center - IR image fused with visible image, right – visible image)

2.4.3.2. High Definition Videography

High definition (HD) video imaging was used to provide additional angles for each experiment. In the experimental cell, cameras were placed in protective housings and located on the floor or attached to the experiment cell wall. Their wide view angle and proximity provided a high resolution and detail of the early portion of the experiments. However, as the experiment progressed the effluent quickly obscured the camera view. A second set of HD cameras were located approximately 27 m (90 ft) from the front of the cell adjacent to the thermal imaging cameras. The camera placement and zoom allowed for a macroscopic view of the entire experimental cell or an area surrounding the open box. These cameras were 90-degrees orthogonal to the action camera attached to the experiment cell wall. Half of these cameras were equipped with IR pass filters to better image the plasma / fire from the HEAF to improve the image captured during an arcing event.

2.4.3.3. Thermography

Up to four thermal imaging cameras were used per experiment. Two of the cameras were supplied by NIST, while the other two were provided by SNL. The camera settings such as frame-rate, thermal calibration range, and resolution were varied. The cameras were also placed in different locations. The NIST cameras were located outside the test cell approximately 27 meters (90 ft) from, and orthogonal to, the front face of the KEMA

experimental cell. The SNL cameras were located in the experimental cell and were housed within a mechanically ventilated metal enclosure. The thermal imagers used in this series are shown in Fig. 9.

Fig. 9. Thermal imagers used inside and outside the test cell (Left – Thermal imaging cameras located approximately 30 yards from open box, Right – Imaging cameras located within the experiment cell, from left to right [thermal, high speed visible, thermal])

2.4.3.4. SNL Imaging

The SNL thermal imagers were each housed in an enclosure that provided protection for the camera and networking components. An opening in the box allowed for the camera lenses to protrude out of the enclosure. The camera locations, non-orthogonal axis, and distance from the HEAF effluent provided protection for the camera and lens. During the medium-voltage open box experiments, however, a thermal imaging camera lens was impacted by molten metal. Subsequent medium-voltage open box experiments were therefore configured such that the camera lens was not in direct alignment to the HEAF effluent using a mirror and concrete barrier.

2.4.3.5. NIST Imaging

The NIST thermal imagers were only used during the medium-voltage experiments. The thermal imaging was performed with two main goals. The first goal was to obtain qualitative information about the development and movement of the arc, the development of plumes of hot gases and HEAF products issuing from the open box, the impingement of the arc jets on the targets and thermal transducers, and the penetrations formed in the enclosure. The second goal was to provide quantitative measurements of box temperatures during and after the HEAF event. The thermal imaging measurements were performed by a FLIR model SC8243 imaging system and a Telops MS M350 imaging system.

The FLIR thermal imager is equipped with a 50 mm f/4.0 lens, with an InSb detector that has a nominal response range from 3 µm to 5 µm and a nominal pixel pitch of 18 µm by 18 µm. The imager can operate in full resolution mode of 1024 pixels by 1024 pixels at approximately 125 frames per second and can cover the temperature range of -20 °C to 1500 °C (- 4 °F to 2732 °F) using dynamic range extension techniques. For these experiments, to compliment the imaging performed by SNL imagers, the resolution was

lowered to 319 x 255 pixels, and the temperature range limited to 250 °C to 600 °C, so that the frame rate could be increased to approximately 400 Hz.

The Telops thermal imager was equipped with a 50 mm f/2.3 lens, with a detector that has a nominal response range from 3.0 µm to 4.9 µm and a nominal pixel pitch of 16 µm by 16 µm. The imager was operated in full resolution mode of 640 pixels by 512 pixels at approximately 350 frames per second. The video capture was performed using a spinning filter wheel with eight positions, filled with two consecutive series of four different transmittance neutral density filters. A dynamic range extension technique is applied, where the images from each series of four filters are captured, and post-processing software combines the images into one image with an expanded temperature range. After dynamic range extension is applied, the video images are 640 x 512 pixels in size, covering from – 0 °C to 2500 °C (- 4 °F to 4532 °F), with an effective video frame rate of approximately 88 Hz.

The uncertainty of the temperature results from the FLIR and Telops imagers are both specified by the manufacturer as ± 2 °C or ± 2 percent, with a 99 percent confidence interval. Using the NIST Uncertainty Machine [14], the expanded uncertainty in the temperature measurements of the metal surfaces is given in Table 4. Details of the uncertainty analysis can be found in a previous HEAF report [1].

Table 4. Expanded uncertainty for IR imager temperatures

Surface	Mean Emissivity	Temperature (°C)	Uncertainty (°C)	Confidence	Coverage Factor	Approximate Uncertainty Contribution
Paint	0.94	100	± 2.6	95%	1.7	Imager: 30% Emissivity: 70%
Paint	0.94	650	± 10.5	95%	1.9	Imager: 70% Emissivity: 30%
Oxidized Steel	0.80	100	± 3.0	95%	1.8	Imager: 20% Emissivity: 80%
Oxidized Steel	0.80	650	± 11.1	95%	1.9	Imager: 65% Emissivity: 35%

2.4.4. Calorimetry

Several types of calorimeters were used in these experiments. For all experiments, an SNL provided radiometer was used. This device was used in the previous small-scale experiments allowing direct comparisons. During the medium-voltage box experiments, several thermal

capacitance slug calorimeters (T_{cap}), ASTM calorimeters, and plate thermocouples were used. These devices were available because the planned medium-voltage bus duct experiments were cancelled. The types and configurations were selected based on the expected thermal exposure and ability of the device to survive.

2.4.4.1. Radiometer

A mobile radiometer was placed near the open end of the box to measure heat flux. The location (approximately 0.5 m (18 in), 1.8 m (72 in), or 3.0 m (120 in)) and thickness (nominally 1 mm (0.04 in) or 3 mm (0.12 in) thick, black copper plates) varied based on the energy of the experiment, projected temperature rise based on copper plate heat capacity, and the expected ability of the sensor to survive experiments up to 400 °C (750 °F). The surface area of the square copper plate was 25.8 cm^2 (4 in^2). Type K thermocouples were used due to their high upper maximum temperature of 1 250 °C (2 192 °F), and display a manufacturer specified uncertainty of ± 1.1 °C (± 2.0 °F). The limit of temperature resolution during data acquisition was ± 0.1 °C (± 0.2 °F). Identical radiometers were used in EPRI DC HEAF experiments [12, 15] conducted at Detroit Edison in July 2019, under DOE EERE PVRD2 funding, for comparison to and validation of DC HEAF models for open box and component (combiner box, string inverter, and central inverter components). These types of devices were also used in fragility experiments [16]. The radiometer was covered for thermal protection as shown in Fig. 10.

Fig. 10. Radiometer apparatus in its thermal protected configuration

The evolved calorimeter energy can be determined using the measured radiometer temperature change as follows:

$$4\pi d^2 \rho_{cu} C_{v-cu} t_{Cu} \Delta T$$

where ρ_{cu} is the density of copper (g/m^3), C_{v-cu} is the heat capacity of copper (J/g·K), t_{Cu} is the copper plate thickness (m), ΔT is the peak heat rise of the copper plate from ambient (K),

and $4\pi d^2$ is the surface area (m^2) to which arc energy is radiated at a calorimeter distance d (m). This calculation assumes 100% absorption of incident radiation on the black copper calorimeter plates and either uniform arc radiation during the 1-3 second arc duration or similar spatial radiation for the Al and Cu arcs.

2.4.4.2. Plate Thermometer

Modified plate thermometers (PTs) are robust thermal sensors that can survive in hostile HEAF environments [1, 6, 17]. They were chosen for heat flux measurements in the HEAF experiments due to their rugged construction, low cost, lack of cooling water, and known emissivity and convective heat flux coefficients.

The modified plate thermometer used in the HEAF experiments is shown in Fig. 11. It consists of two 0.51 mm (0.02 in) nominal diameter (24 AWG) Type-K thermocouple wires welded directly to the rear of an 0.787 mm ± 0.051 mm (0.031 in ± 0.002 in, 99 percent confidence interval per manufacture specifications) thick Inconel 600 plate, approximately 100 mm (3.94 in) by 100 mm (3.94 in) in size. The plate is backed by a mineral fiber blanket approximately 25.4 mm (1.0 in) thick to decrease heat loss. Machine screws with ceramic washers allow for legs to be attached at the rear of the plate thermometer to simplify installation onto instrumentation racks.

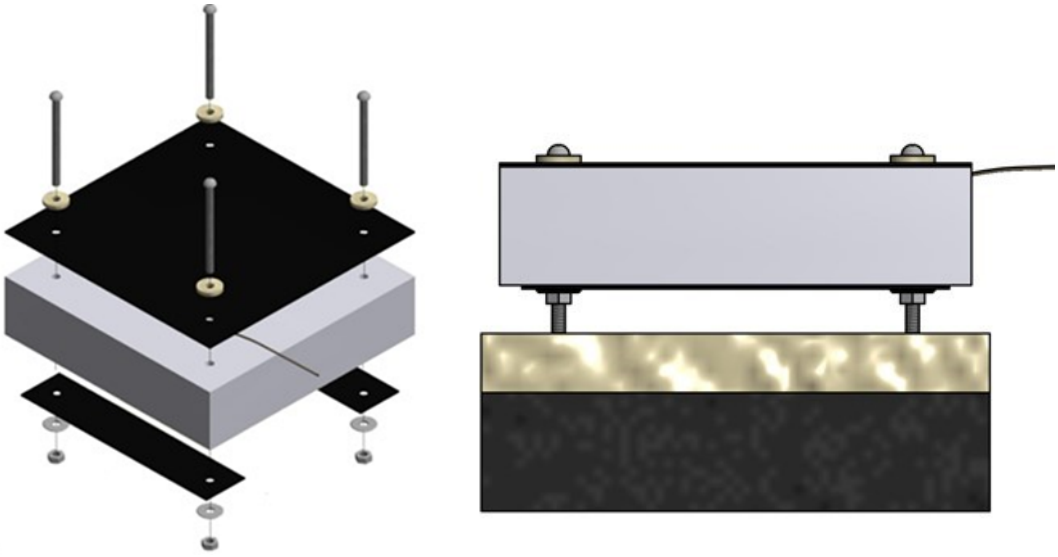

Fig. 11. Exploded view of modified plate thermometer (left); Cross-sectional view of modified plate thermometer placed on cone calorimeter sample holder (right)

The incident heat flux on a plate thermometer can be calculated from a heat balance using the following relation, a rearrangement of Equation 18 from Ingason and Wickstrom [21]:

$$\dot{q}''_{inc} = \sigma \cdot T_{PT}^4 + \frac{(h_{PT} + K_{cond})(T_{PT} - T_\infty)}{\varepsilon_{PT}} + \frac{\rho_{ST} \cdot C_{ST} \cdot \delta \cdot \left(\frac{\Delta T_{PT}}{\Delta t}\right)}{\varepsilon_{PT}} \quad (1)$$

Here $\dot{q}''_{inc}$ is the incident heat flux, σ is the Stefan-Boltzmann Constant, 5.670×10^{-8} W/(m^2·K^4), T_{PT} is the temperature of the plate (K), h_{PT} is the convection heat transfer coefficient, 10 W/(m^2·K), K_{cond} is the conduction correction factor determined from NIST cone calorimeter data, 4 W/(m^2·K), T_∞ is the ambient temperature (K), ε_{PT} is the plate emissivity, 0.85 at 480 °C as rolled and oxidized and specified by the alloy manufacturer, ρ_{PT} is the alloy plate density, 8470 kg/m^3 from the alloy manufacturer, C_{ST} is the alloy plate heat capacity, 502 J/(kg·K) at 300 °C from the alloy manufacturer, δ is the alloy plate thickness, 0.79 mm (0.03 in), and Δt is the data acquisition time step of 0.1 s.

The gauge heat flux can also be calculated and is the heat flux listed in the tables of this report. The gauge heat flux is the heat flux that would be reported by an ideal water-cooled transducer such as a Schmidt-Boelter or Gardon gauge operating at a constant temperature of T_{gauge}. The gauge heat flux, $\dot{q}''_{gauge}$, is calculated from [18]:

$$\dot{q}''_{gauge} = \sigma \cdot T_{PT}^4 + \frac{(h_{PT} + K_{cond})(T_{PT} - T_\infty)}{\varepsilon_{PT}} + \frac{\rho_{ST} \cdot C_{ST} \cdot \delta \cdot \left(\frac{\Delta T_{PT}}{\Delta t}\right)}{\varepsilon_{PT}} - \sigma \cdot T_{gauge}^4 \qquad (2)$$

Type A evaluation of uncertainty is performed by the statistical analysis of a series of measurements. Type B evaluation of uncertainty is based on scientific judgement using relevant available information such as manufacturer specifications, calibration data, handbook data, previous experiments, and knowledge of the behaviors of materials and measurement equipment [19, 20, 21].

The plate thermometer temperature increase, ΔT_{PT}, is reported along with the gauge heat flux. The uncertainty in the temperature of the Type-K thermocouple wire is given by the manufacturer as ±1.1 °C or 0.4 percent with a 99 percent confidence interval [22]. The expanded uncertainty in a PT temperature change of 0 °C to 1250 °C is 0.3 percent, with a coverage factor of 2, which corresponds to a confidence interval of 95 percent [19].

2.4.4.3. ASTM Slug Calorimeters (Slug)

Incident energy was measured using slug calorimeters described in ASTM F1959 [23] and shown in Fig. 12. These instruments are customarily used to measure radiant energy and determine the arc flash hazard to personnel in the area of electrical enclosures. Due to the characteristics of the HEAF phenomena, which can result in convective arc jets, the calorimeters are reacting to convective heat transfer in addition to radiant heat transfer. ASTM slug calorimeters consist of a copper disc with an approximate thickness of 1.6 mm (0.063 in) and diameter of 40 mm (1.6 in). An iron-constantan thermocouple (Type J), composed of two 0.255 mm (0.01 in) nominal diameter (30 AWG) wires, is soldered to in the back of the copper disc using silver solder. The ASTM standard specifies that the copper disc be installed in an insulation board. The KEMA slug calorimeters were installed in a G-11 fiberglass epoxy phenolic cup, which was then placed in a calcium silicate board holder nominally 100 mm by 100 mm by 32 mm thick (4 in by 4 in by 1.25 in nominal thickness) for mounting on instrument rack. The instruments were provided by KEMA. The slug temperatures were reported by the KEMA data acquisition system at a rate of 20 Hz.

The incident energy absorbed by the slug calorimeter during the HEAF experiments is calculated according to the methodology in ASTM F1959 [19]. The method reports the net heat absorbed over the arc duration and assumes that there are no losses from the disc due to re-radiation, convection, or conduction to the disc holder. The absorptivity of the disc is assumed to be one.

The total energy per unit area, Q'', is calculated by:

$$Q'' = \frac{m \cdot \overline{C_p} \cdot (T_f - T_i)}{A} \quad (3)$$

where m is the mass of the copper disc, C_p is the average heat capacity of the copper disc, T_f is the temperature of the disc at the end of the arc, T_i is the temperature of the disc before the arc, and A is the front surface area of the disc. The total energy per unit area resulting from the arc is reported in a summary table for each sensor location in each experiment. The ASTM F1959 standard also refers to the total energy per unit area as incident energy (cal/cm^2 or kJ/m^2).

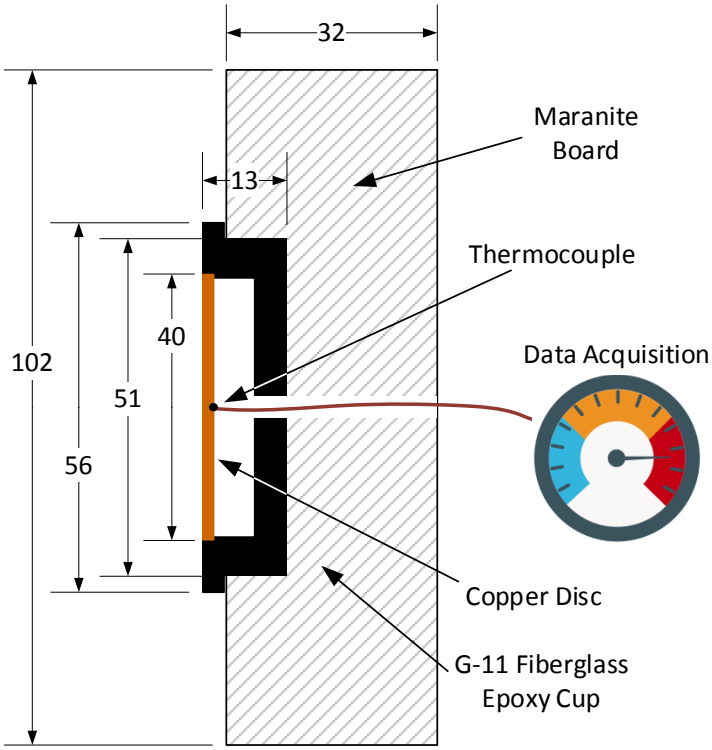

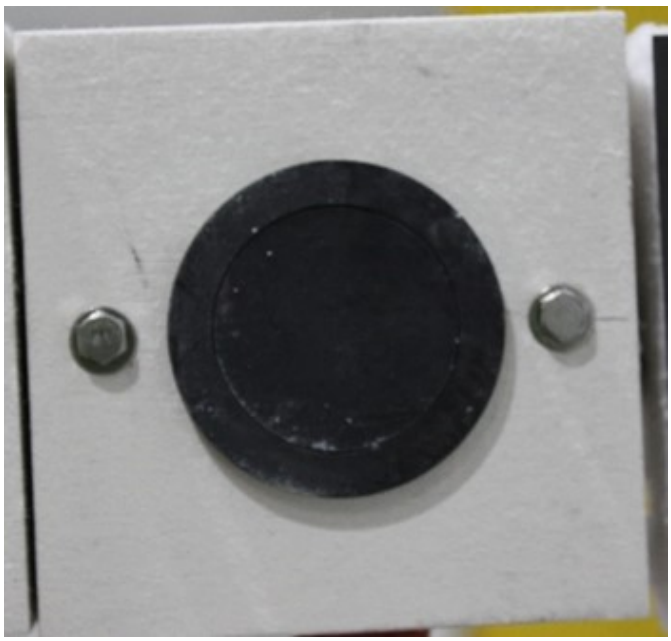

Fig. 12. Cross-section of ASTM Slug (top) nominal dimensions in millimeters, photo of device being prepared in the field (bottom). Note that the two bolts on each side of the device are used for mounting to the DIN rail of the instrumentation rack.

The Type B standard uncertainty in the thermocouple measurement, derived from typical thermocouple manufacturer data, with a coverage factor of 2, is 2.2 °C or 0.75 percent. The ASTM calculation method assumes that the absorptivity of the disc is 1.0, however inspection of the discs over the course of the experiments suggests that the emissivity may

vary from approximately 0.9 to 1.0, in a rectangular probability distribution. It was found that the uncertainty in the thermocouple wire drives the uncertainty at low energies, while the uncertainty in the absorptivity drives the uncertainty at high energies [14]. The combined standard uncertainty in the absorbed energy, composed of Type A and Type B uncertainties, is 17 percent at 50 kJ/m^2 and 4 percent at 500 kJ/m^2. The expanded uncertainty in the steady-state absorbed energy measurement is 35 percent at 50 kJ/m^2 and 8 percent at 500 kJ/m^2, with a coverage factor of 2, which corresponds to a confidence interval of 95 percent [19]. Additional detail on the ASTM calorimeter uncertainty determination, using Type A and Type B uncertainties, can be found in a previous report [1].

2.4.4.4. Thermal Capacitance Slugs (T_{cap} slug)

Tungsten thermal capacitance slugs (T_{cap} slug) were used to measure the heat flux and incident energy during the HEAF experiment. These sensors were developed as a result of experience gained in Phase 1, where the thermal conditions during some experiments exceeded the measurement capabilities and caused destruction of the ASTM slug calorimeters and modified plate thermometers. A cross section of a T_{cap} slug is shown in Fig. 13, which is a modified example of the thermal capacitance slug described in ASTM E457-08 [24]. The slug is composed of a tungsten cylinder approximately 15 mm (0.59 in) long mounted in calcium silicate board. A type-K thermocouple is attached to the rear of the tungsten to measure the temperature during heating. The development of the T_{cap} is descried in a previous report [1].

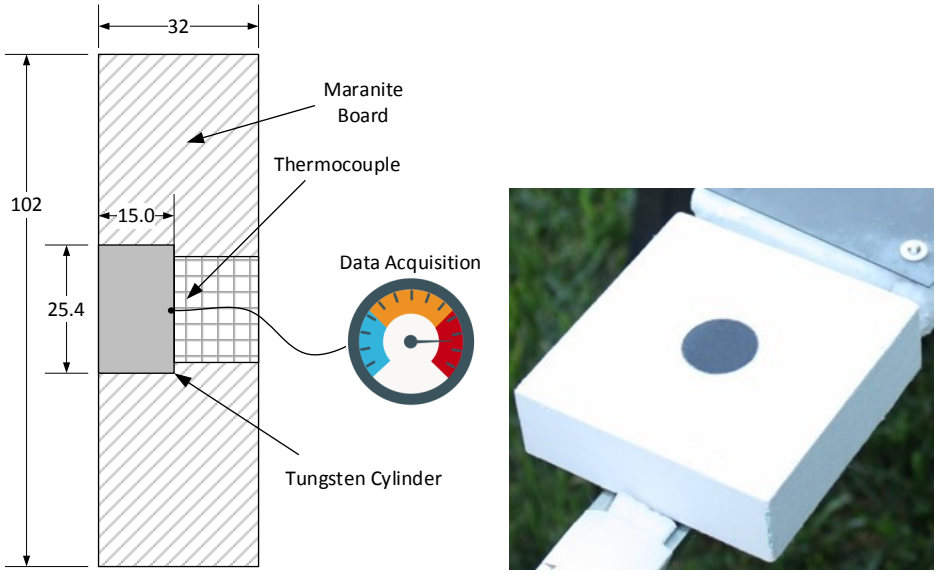

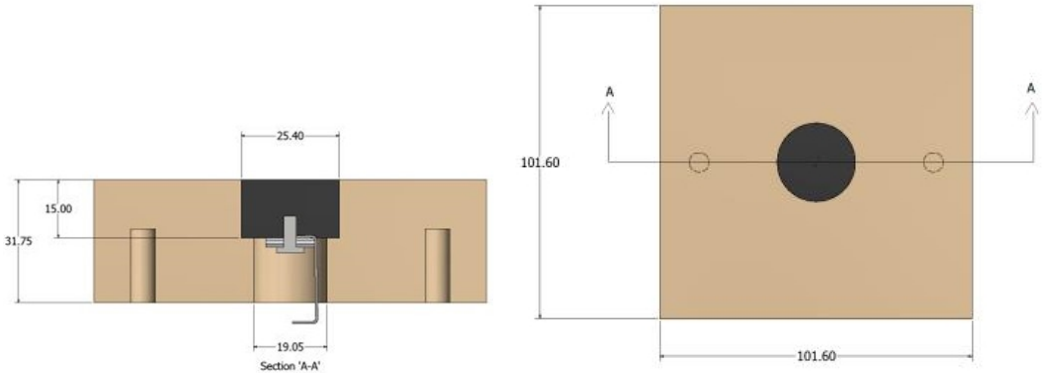

Fig. 13. Thermal capacitance style slug, illustration (top left), photo of device being prepared in the field (top right), dimensional drawings showing internal construction (bottom left and right). All dimensions in mm.

The maximum heat flux was determined from Equation (4), where $(\dot{q}")$ is the heat flux into the surface of the tungsten slug (kW/m^2), ρ is the density of the tungsten slug (kg/m^3), (C_p) is the average heat capacity of the tungsten slug (kJ/[kg · K]), ΔT is the change in temperature of the tungsten slug (°C), and Δt is the corresponding change in time (s).

$$\dot{q}" = \rho \cdot \overline{C_P} \cdot l \cdot \left(\frac{\Delta T}{\Delta t}\right) \quad (4)$$

An uncertainty analysis using Type A and Type B components was performed on the T_{cap} slug at 50 kW/m^2 and 5 MW/m^2 using the NIST Uncertainty Machine [14] with cone calorimeter data and FDS simulations. At a simulated heat flux of 50 kW/m^2 the expanded uncertainty was found to be 2.9 percent, with a coverage factor of 2, corresponding to a 95 percent confidence interval. At a simulated heat flux of 5 MW/m^2 the expanded uncertainty was found to be 2.0 percent, with a coverage factor 1.9, corresponding to a 95 percent confidence interval.

The experimental uncertainty of incident energy measurements was calculated using simulated data and the NIST Uncertainty Machine [14], including Type A and Type B components, with a 95 percent confidence interval. The expanded uncertainty of the incident energy over the measurement range is estimated at ± 5 percent, with a 95 percent confidence interval, which includes the estimated error due to conduction effects. additional details on development of the T_{cap}, heat transfer analysis, and uncertainty determination using cone calorimeter data and FDS simulations can be found in a previous report [1].

2.4.4.5. Placement of NIST and KEMA instrumentation for medium-voltage open box experiments

During the medium-voltage open box experiments, two small arrays of sensors were deployed by NIST. A vertical array was placed approximately 165cm (65-in) from the front of the box surface. The array was attached to a Unistrut stand and the sensor cables were routed and protected in the Unistrut U-channel using thermal ceramic fiber and GPO3 (red board). The vertical array consisted of one laboratory supplied ASTM thermal capacitance slug, one NIST tungsten thermal capacitance slug, and one NIST plate thermometer. A horizontal array was placed directly below the box approximately 84 cm (33 in) from the bottom surface of the box. This array was attached to the Uni-strut stand that supported the open box. The horizontal array consisted of two NIST thermal capacitance slug calorimeters and one laboratory supplied ASTM thermal capacitance slug calorimeter. Plate thermometers were not used on the horizontal configuration due to the expected damage. The sensor arrays are shown in Fig. 14 and Fig. 15. The expanded uncertainty in the measurement of the distance from the vertical instrumentation stand to the open box is ± 13 mm (0.5 in) with a coverage factor of 2 and an estimated confidence interval of 95 percent. The expanded uncertainty in the measurement of the other distances is ± 5 mm (0.2 in) with a coverage factor of 2 and an estimated confidence interval of 95 percent.

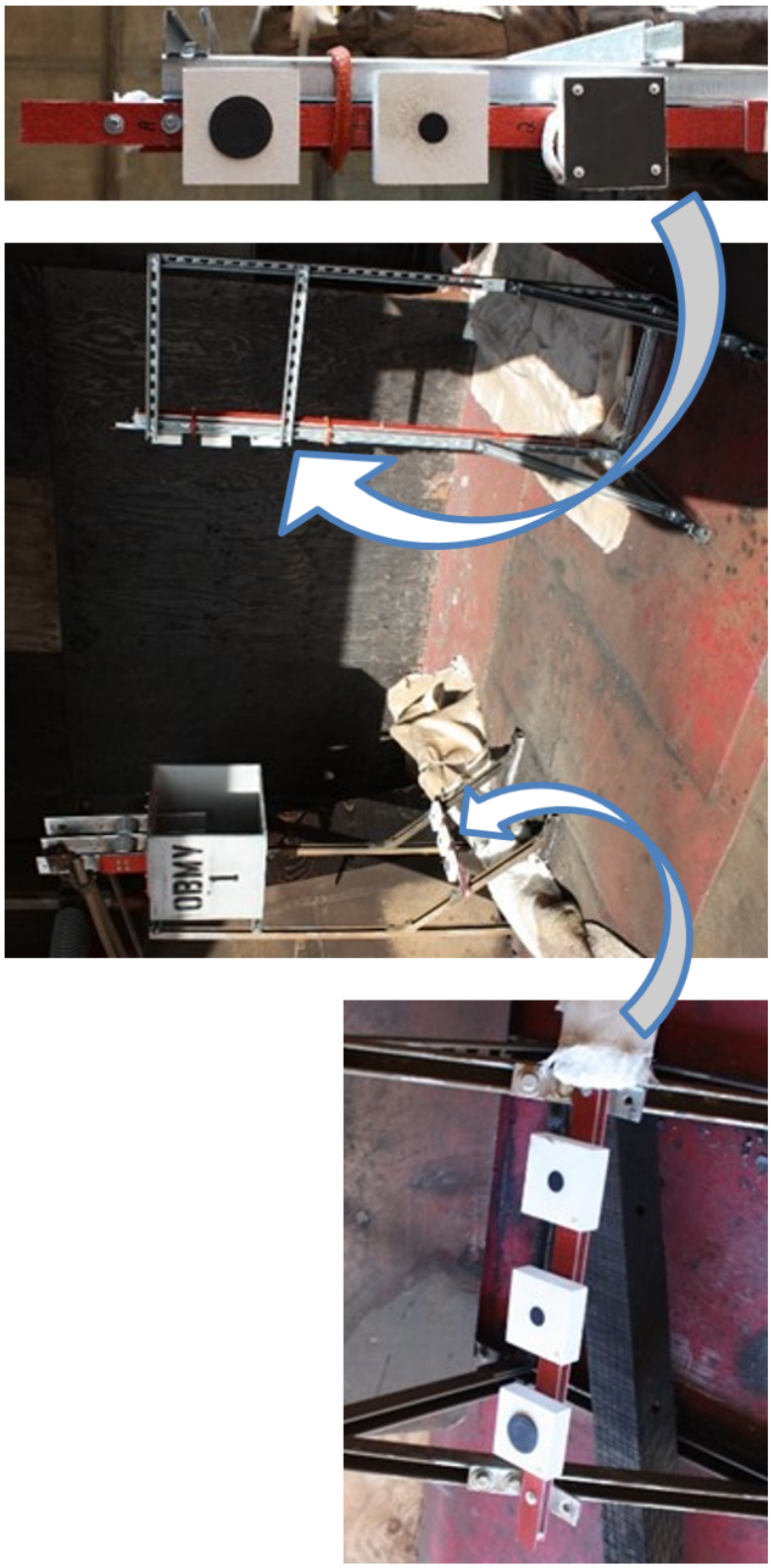

Fig. 14. Calorimeters array used during medium-voltage experiments (Left - Horizontal, Center - array location within cell, Right - vertical)

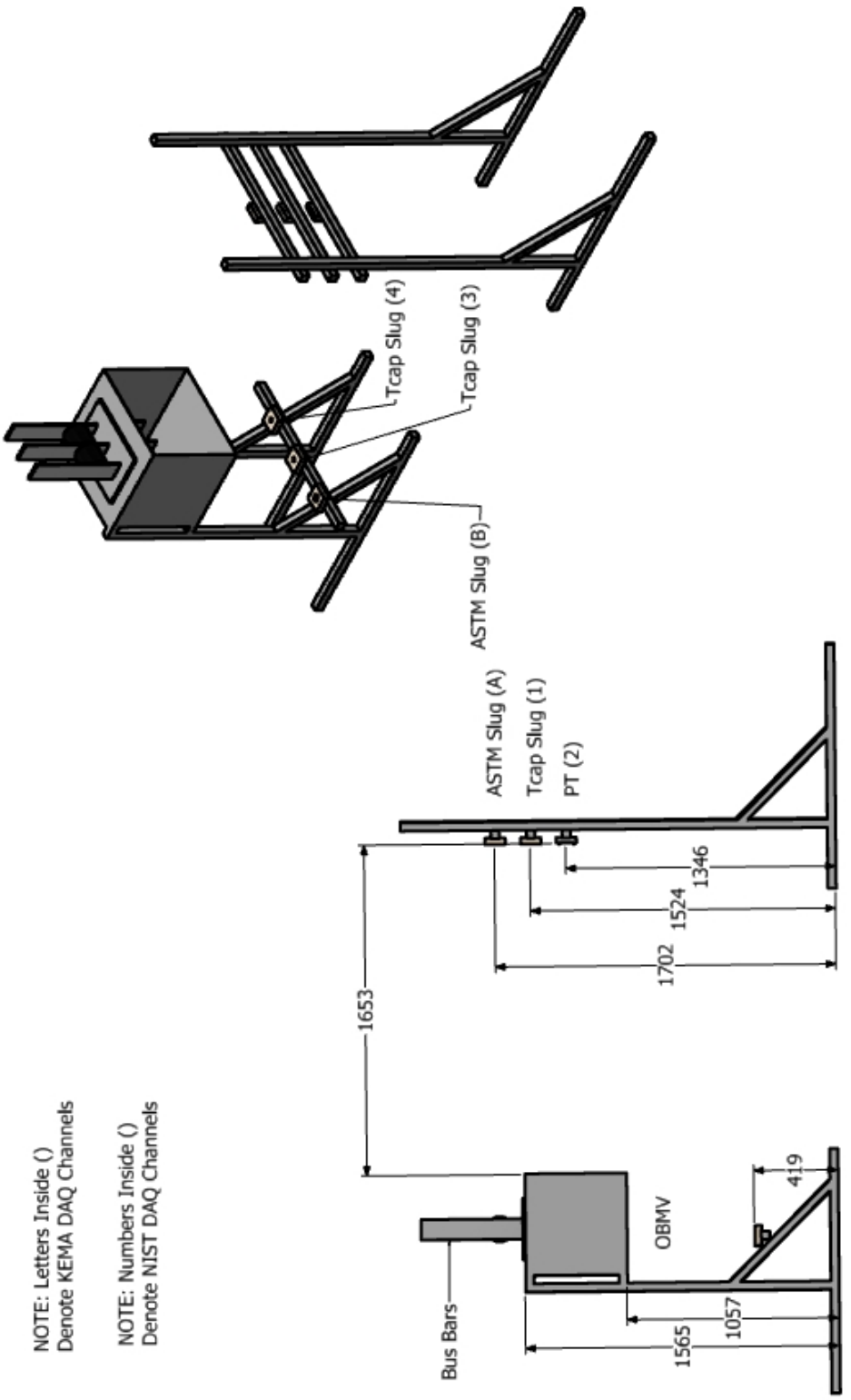

Fig. 15. Calorimeter configuration during the medium-voltage experiments. Dimensions in mm.

2.4.4.6. Data Acquisition System

The NIST data acquisition system used a combination of shielding, grounding, isolation, and system configuration that reduced the impact of electromagnetic interference (EMI), as shown in Fig. 16. This data acquisition system was used for the NIST plate thermometer and T_{cap} instruments and is described in the literature [1, 6, 17].

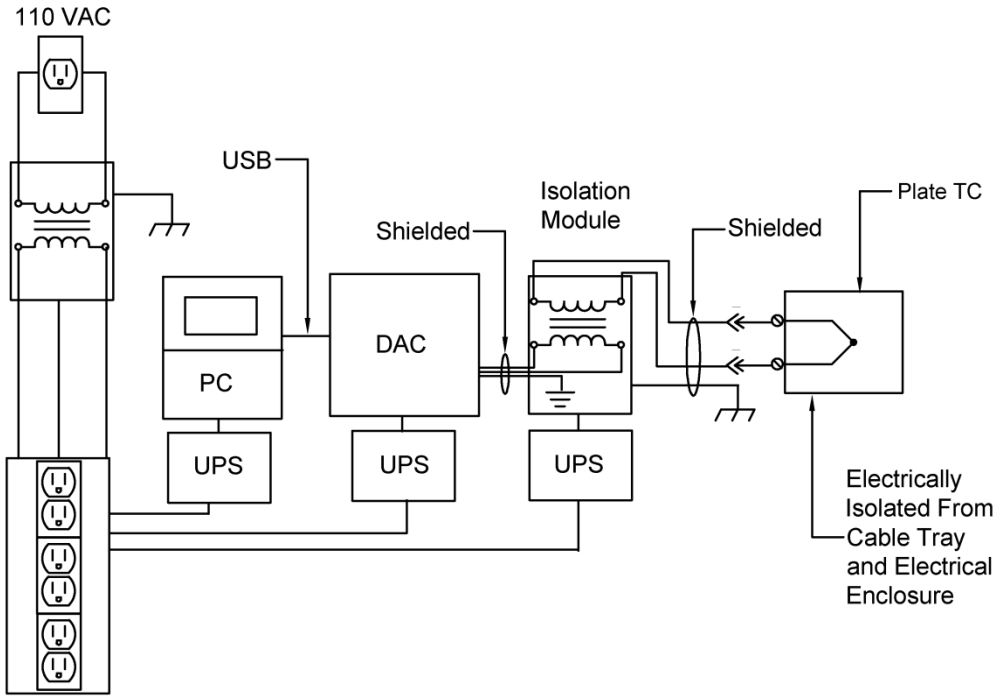

Fig. 16. Data Acquisition System Configuration with EMI rejection

The data acquisition process involved starting the data recording prior to the experiment and stopping after the experiment. Due to the system being located outside of the main control room in an air-conditioned van next to the test cell, the acquisition was manually started, and the operator traveled to the control room for safety. After the experiment was complete and deemed safe for travel back to the data acquisition location, the operator would travel back to the system and stop the recording. Due to the safety procedures, there is significant pre-experiment and post-experiment data recorded. Since the KEMA trigger signal was acquired via the DAQ system, the actual start of the experiment was post processed and the time was adjusted to set the experiment time zero to the actual start of the experiment.

2.4.5. d-Dot Sensors

During an arc, significant electromagnetic interference may potentially be generated, which could couple to nearby electronics. The electrical field content of the arc event as a function of frequency was measured using free-field d-Dot sensors, which quantify the electrical field (kV/m) as a function of frequency from 10 kHz to 1.5 GHz. These frequencies correspond to wavelengths of 4 cm (2.5 GHz) to 30 km (10 kHz) which may efficiently couple to nearby

cables or metallic traces. Because of space limitation, an RF filter/wave guide was not used. As such, a baseline measurement was required to be made prior to each experiment such that background signals were removed from HEAF measured signals. The sensor cable, optical link, and DAQ were configured to eliminate EMI corruption. This included the use of triple coaxial cable, fiber optic cable and a DAQ modules that was shielded and grounded. Generated field intensity data was transmitted to spectrum analyzers outside the experiment chamber using fiber optic links to minimize EMI coupling from transmission lines.

Probes were initially placed in "far field" outside predicted thermal plume region to limit thermal damage to probe and associated cabling. Based on the data from the initial experiments the probes were positioned in different geometrical and radial locations from the open box for subsequent experiments. This will allow for an evaluation of spatial influences on the measured field strength. A photo of the d-Dot sensors prepared for an experiment is presented in Fig. 17.

Fig. 17. d-Dot sensors arrangement prior to experiment. Note all sensors oriented in same x-direction based on results from earlier experiment indicating largest measured signal.

For the electrical field measurements, the measurement uncertainty due to the collection oscilloscope was ± 8 mV, for a trigger level set above ambient RF noise of 52 mV. No trigger was observed for any of the open box testing at an acquisition rate of 5 GS/s. The electric field level for the Prodyn AD-70 free field D-Dot sensors [25] is given by

$$E(t) = \frac{1}{RA_{eq}\epsilon_0}\int_{t_i}^{t_f} v(t)dt$$

Where ε_o is the permittivity of free space, R is the sensor characteristic load impedance in ohms and A is the equivalent sensor area (m^2), given as:

$$R = 100$$
$$A_{eq} = 10^{-3}$$

The integrated field is dependent on measurement frequency, but at 5 GHz, failure to trigger at 52 mV is consistent with an EM field level less than 11.8 V/m with an uncertainty of ± 1.8 V/m. For comparison, MIL-STD-461G EMI testing under RS103 radiated susceptibility [26], electric field specifies testing safety critical equipment under 200 V/m fields. MIL-STD-461G RS105 Transient Electromagnetic Field testing specifies a test level of 50 kV/m with a tolerance of +6 dB/-0 dB, presenting a potential test field level of up to 100 kV/m. EPRI Report TR-102323 specifies a transient equipment susceptibility field limit of 152 dB□V/m, equivalent to 40 V/m [27]. The maximum field level at which no trigger occurred (e.g. E= 11.8 V/m ± 1.8 V/m uncertainty) appears below levels of concern for military electronics, but could be repeated with specific regard to transient equipment susceptibility field level testing.

2.4.6. Conductivity Sensors

Previous experiments have identified that HEAF effluent resulted in unacceptable insulation resistance between uninsulated and non-enclosed power conductors. This observation questions the impact of HEAF effluent on the functionality of nuclear power plant electrical equipment. Understanding the impact of HEAF effluent on the performance of safety equipment is desired to better understand the hazard.

A conductivity sensor designed specifically for pulsed power research was used in the open box experiments. The sensor measures free charge and is fully enclosed with a perforated screen design to eliminate Electromagnetic Interference (EMI). The sensor geometry is shown in Fig. 18.

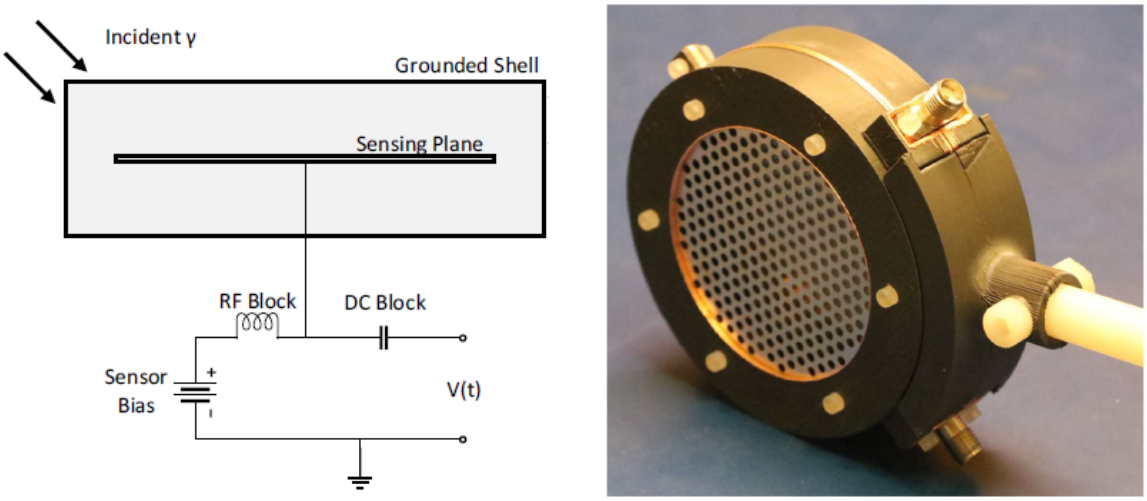

Fig. 18. Parallel plate sensors with a perforated screen design to eliminate EMI.

The sensor is formed from a hollow grounded cylinder with a suspended metal disk. A sensor bias (10 volts) is applied to the disk through a radio frequency (RF) block. As conductive particulate enters the chamber, the time change of resistance is measured as a voltage change through a DC block; the higher the conductivity or conductance, the higher the voltage is measured between the perforated sensor plates. Up to two of these devices were placed at accompanying locations of other conductivity instruments. The grounded shell and use of

coaxial cable to fiber link or metal-clad, EMI-shielded cables were used to ensure EMI reduction. The use of these sensors in pulse power applications (similar environment to HEAF experiments from an electrical interference perspective) have previously shown successful results. For the MV air conductivity measurement, the uncertainty is 9 x 10^{-6} Ω^{-1}, limited by the resolution of the data acquisition digital oscilloscope used [28].

2.4.7. Voltage Holdoff Strength

A criterion for required voltage holdoff strength was based on discussions with EPRI regarding NEC table 490.24, which specifies minimum clearance of live parts as a function of nominal voltage rating. Values in NEC table 490.24 [29] relevant to medium-voltage equipment include minimum phase-to-ground clearances of 10 cm (4 in) at 7.2 kV and 12.5 cm (5 in) at 13.8 kV. These equate to NEC-allowed maximum design electrical fields of 0.72 kV/cm to 1.10 kV/cm.

The voltage holdoff strength of air is normally 25 kV/cm to 30 kV/cm dependent on gas density, temperature, and composition. During a HEAF, high temperatures causing decreased air density and the presence of metal particulates would be expected to reduce the holdoff strength of air. An air breakdown field holdoff of less than 0.7 kV/cm to 1.1 kV/cm during HEAF events would be a significant concern. HEAFs could produce environmental conditions where the holdoff strength is not enough to maintain dielectric isolation between electrical power conductors, depending on component design.

To evaluate HEAF generated effluent air-vapor voltage holdoff properties, an approach based on ASTM D2477 [30]was followed. Two conical electrodes as shown in Fig. 19 were used. The effective gap between the electrode tips was 0.5 cm (0.2 in). A fast ramp of 10 kV/s was used instead of a steady or stepped ramp as in ASTM D2477 to enable multiple measurements of breakdown strength during a 2 s to 8 s experiment. The limited duration of a HEAF event limits the applicability of the steady or stepped approach; a fast ramp with multiple breakdown events enables statistical breakdown voltage measurements during a single HEAF experiment. The uncertainty of the breakdown voltage measurement is ± 200 V (0.2 kV) limited by the resolution of the data acquisition digital oscilloscope used [28]. A set of six ramp sequences was used during experiments as shown in Fig. 20. Current viewing transformers and a voltage monitor were connected to oscilloscopes to acquire air breakdown voltage data prior to (baseline) and during HEAF events to quantify any changes in breakdown or holdoff strength. Pre-HEAF air breakdown measurements are shown in Fig. **21**, which measured a breakdown field of 28.5 kV/cm ± 2.2 kV/cm. This is consistent with typical air breakdown strengths of 25 kV/cm to 30 kV/cm, and a holdoff well above the 0.7 kV/cm to 1.1 kV/cm NEC-allowed electrical field operation levels of concern.

Fig. 19. Breakdown Sensor (left – electrode configuration, middle – safety jumper, right – operational experiment)

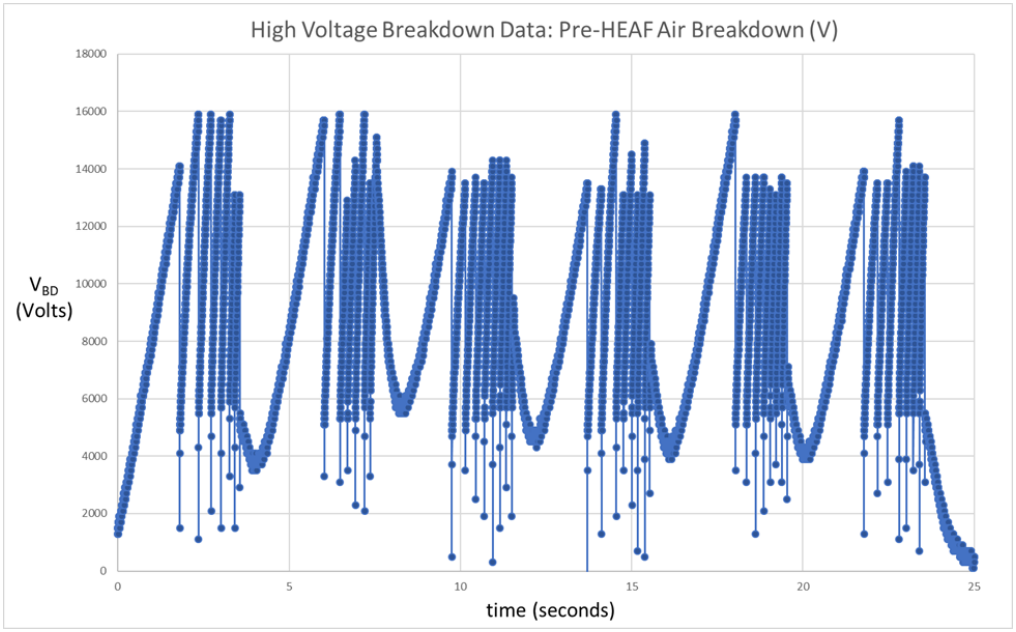

Fig. 20. Measured waveform spark gap from experiment

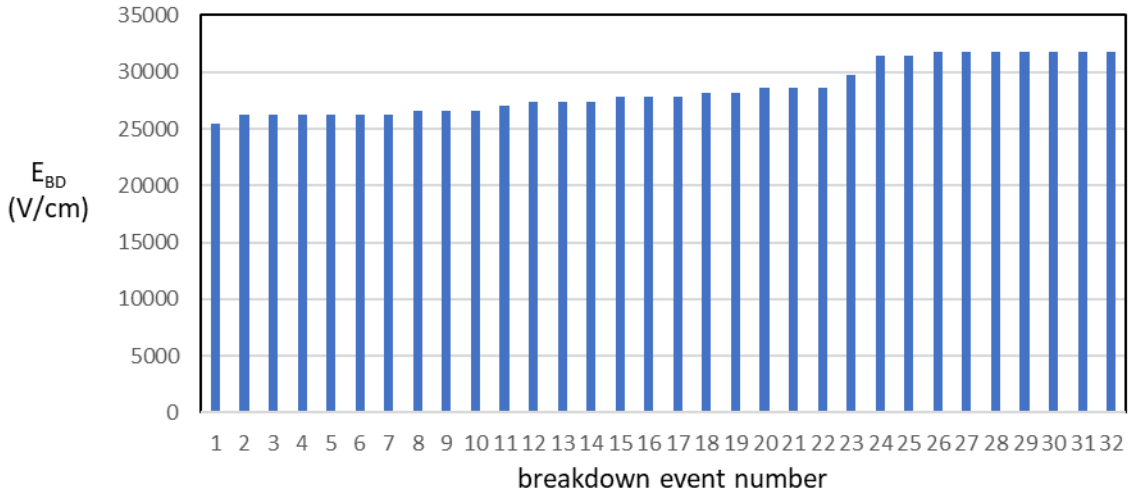

Fig. 21. High Voltage Breakdown Strength: Pre-HEAF
(E_{BD}=28.5kV/cm ± 2.2 kV/cm)

2.4.8. Mass Loss Measurements

Mass loss measurements of electrode material were made using an electronic mass balance with a measurement range of approximately 0 kg to 41 kg. The mass balance (NIST Scale 2) has an expanded uncertainty, derived from manufacturer specifications of ± 1 g, with a 95 percent confidence interval. Calibrated masses of approximately 50 g to 40.970 kg were used to verify the performance of the mass balance. Results are plotted in Fig. 22 and show good agreement. Initial (pre-experiment) and final (post-experiment) measurements were made of masses of the electrode. The electrode mass loss is reported in the experiment result Sections 3 and 4.

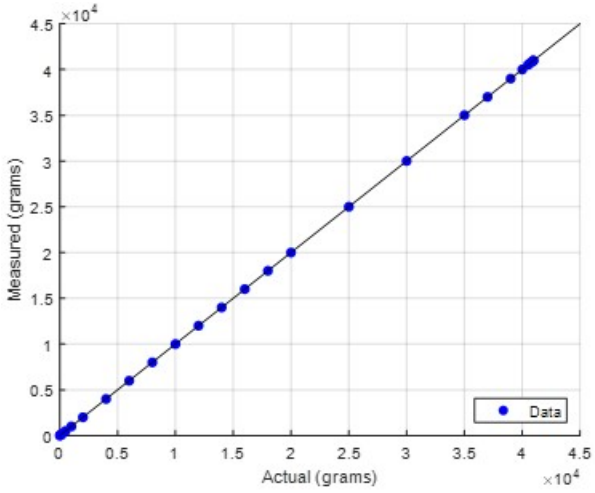

Fig. 22. Scale-calibration results

Mass loss measurements of the steel enclosure were also planned, however, during the measurements it was noted that the masses of several enclosures were greater after the experiment than prior to the experiment. It was determined that the electrode material was

plated onto the enclosure resulting in an inaccurate measurement of the actual enclosure material loss. The plated and melted electrode material was not easily removed and as such, an alternative way to estimate material loss was used. The alternative required the use of photo images with reference measurements and a computer software program. The photos were imported into the software program, size to the scale based on the measurement references and then the user outlined the area of the missing material. The program would then provide the area of the outline. With the known surface area, material thickness and nominal density of steel (7.9 g/cm^3), the mass of the breached area could be estimated. This approach required judgement by the user to outline the area of the breach and account for material that was off plane due to yielding of the metal at elevated temperatures. This method provides a reasonable measure of mass loss, but does have a higher level of uncertainty. In previous experiments [1], mass loss measured with a balance was compared with this alternative technique. The expanded uncertainty in mass measurements using the alternative technique based on area is estimated at ± 10 percent with a 95 percent confidence interval. An example of the approach is shown in Fig. 23.

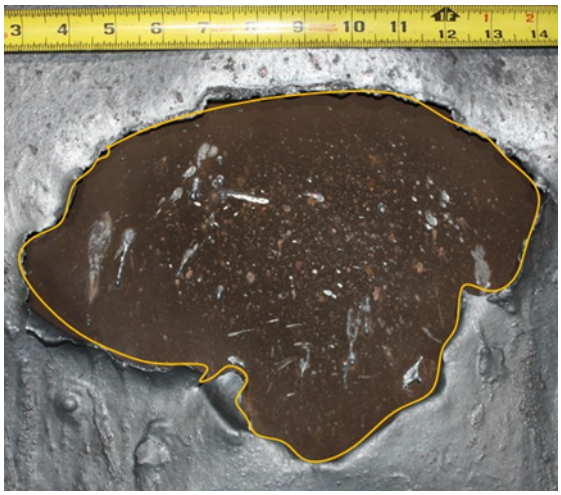

Fig. 23. Example of Mass Loss Measurement using Surface Area Estimated by Computer Software (363 cm^2 estimated area in example photo shown)

2.4.9. Electrical Data Acquisition and Processing

Electrical measurements were made by the experiments laboratory. The measurements included line-to-ground voltages at the generator and just prior to the open box in the experiment cell and current measurements downstream of the open box (not in the experiment cell) but downstream of any transformer. The voltages in this report are at the open box and are line to ground voltages (unless stated otherwise). The uncertainty in the measurements made by the test laboratory are ± 3 percent.

All experiments were run in a wye connection. However, early experiments were run with the wye neutral not connected to ground via impedance. Since the voltages are reference to

ground, the wye neutral and ground do not have a common reference, thus the neutral is floating. This becomes a problem in reporting the actual line-to-neutral voltage at the device. After this was identified subsequent experiment were performed with the wye-neutral connected to ground via impedance to ensure a common reference. To address the issue for the initial experiments, a post-processing technique was identified by the experiments laboratory and is presented below with an example case.

The zero-sequence voltage was calculated by adding all device phase voltages together. An example is shown in Fig. 24 along with the measured device voltage for each phase Next one-third of this zero-sequence voltage is removed from each of the device voltage waveforms. Fig. 24 and Fig. 26 shows how the voltage waveforms are modified for a case where the wye-neutral is not and is connected to ground via impedance. For the cases where the generator neutral is connected to ground via impedance, similarity of the pre- and post-waveforms demonstrate correctness of the MATLAB algorithm and technique. For completeness, a final figure showing the generator, device and post-processed device voltage waveforms are shown in Fig. 27 from Experiment OB08. MATLAB code used for processing is also shown.

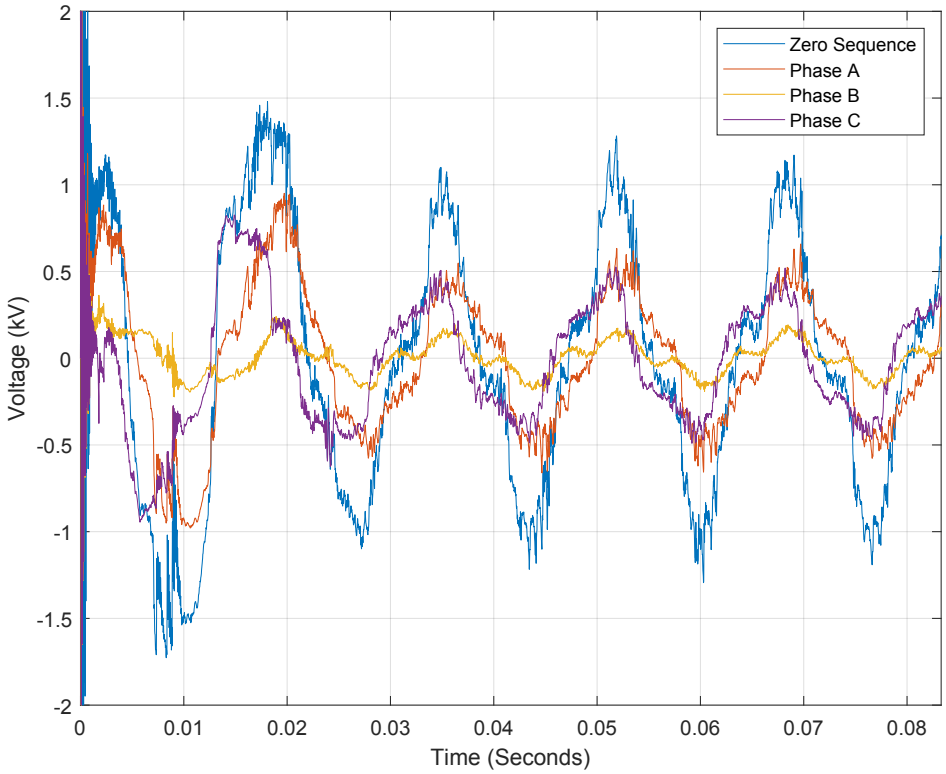

Fig. 24. Zero-sequence voltage (Experiment OB08)

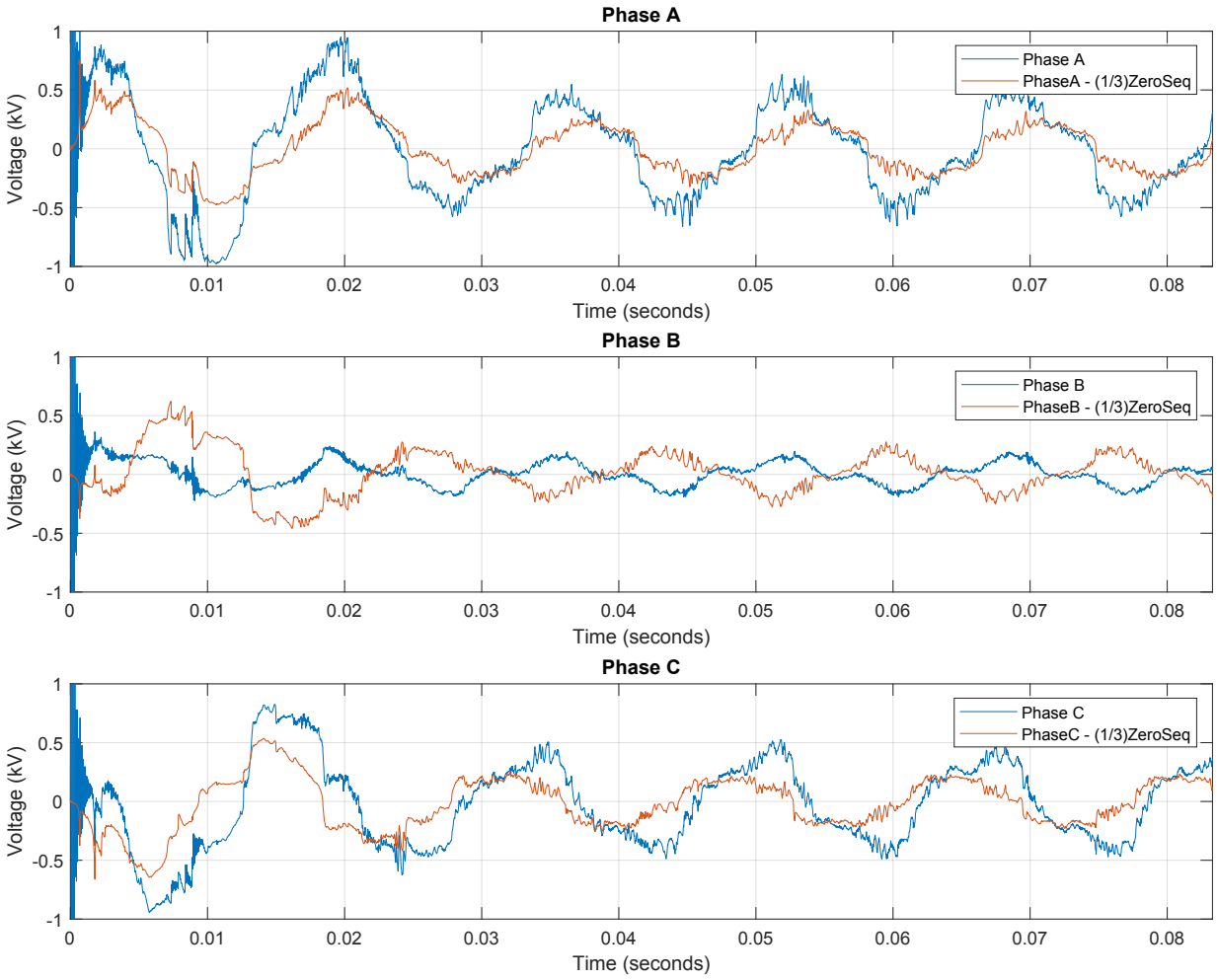

Fig. 25. Original and modified device voltage when wye-neutral is not connected to ground (Experiment OB04).

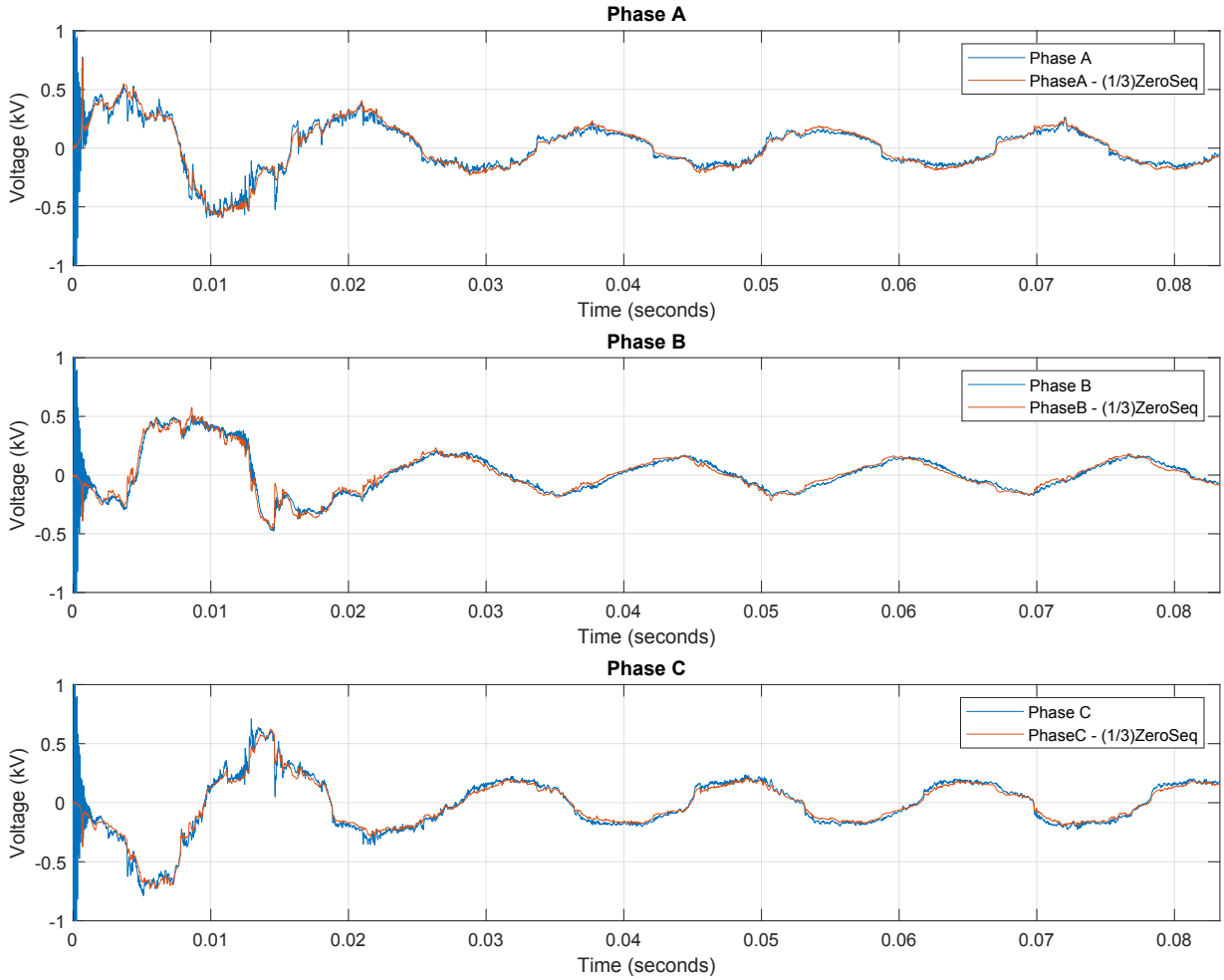

Fig. 26. Original and modified device voltage when wye-neutral is connected to ground via impedance (Experiment OB04)

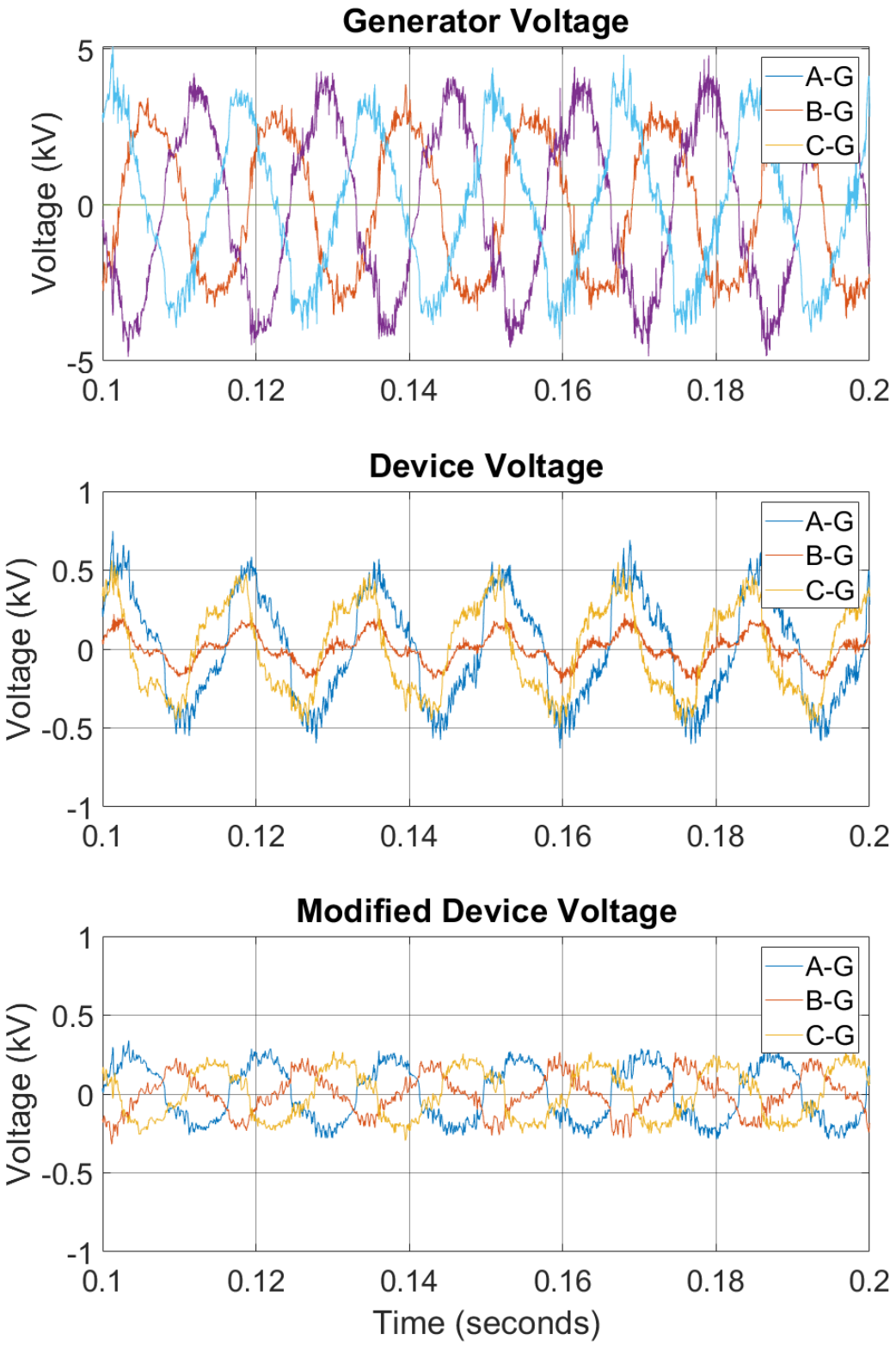

Fig. 27. Line-to-Ground Voltage at Generator (Top), at Open box (Middle), and modified Open box Voltage (Bottom) [Experiment OB08]

MATLAB Code

```
% define initial device voltage variables

A=U1TO(:,2);        % Phase A Voltage at open box
B=U2TO(:,2);        % Phase B Voltage at open box
C=U3TO(:,2);        % Phase C Voltage at open box

ABC=A+B+C;          % calculate zero sequence voltage

AM=A-(ABC./3);      % remove one-third zero sequence from each phase voltage
BM=B-(ABC./3);      % by dividing zero sequence by 3 (./3) and subtracting from phase
CM=C-(ABC./3);      % voltages
```

3. Low-voltage Experiment Results

The experiments laboratory performed calibration runs to ensure that the power circuits selected met the desired experimental parameters. The calibrations were measured at a shorting bus within the laboratory's facility and the actual experimental conditions were slightly different because of the additional circuit length to the open box and that of the open box equipment. The resulting circuit calibrations are presented in Table 5, with detail provided in the KEMA report (Appendix B).

Table 5. Low-voltage circuit calibration

Voltage (Volts)	Current Sym (kA)	Current Peak (kA)	Circuit
1,000	1.04	2.9	190822-7001
1,000	5.05	14.9	190822-7002
1,064	30.0	79.1	190823-7001
1,009	15.0	40.4	190823-7002
6,900	15.3	42.9	190916-9002
6,900	30.6	86.5	190916-9004

The circuit calibrations were performed for about 10 cycles to ensure stabilization of the waveform. The duration of the arc during actual experiments was determined by the ability to maintain the arc within the enclosure and the breaking of the circuit by the experiment laboratory's protective device(s). Provided that the arc did not prematurely extinguish prior to the desired arc time, the experiments laboratory ensured that the arc duration parameter was met by automatically triggering their protectives devices to open at the specified duration. Because there was a delay in the opening of the circuit (breaker opening time), the actual durations were longer than the desired durations. Table 6 and Table 7 present the experimental parameter variations planned for these series of experiments.

Table 6. Low-voltage experiments - planned nominal experiment parameters

Experiment No.	Rod Material		Rod Diameter (cm)		System Voltage (kV)	Current (kA)	Duration (s)	Notes
#	Al	Cu	1.3	2.5				
OB01(a)		X	X		1.0	1.0	2.0	Shorting wire issue
OB01(b)		X	X		1.0	1.0	2.0	Repeat of OB01(a)
OB02		X		X	1.0	15.0	2.0	
OB03		X		X	1.0	15.0	3.0	
OB04		X		X	1.0	30.0	1.0	
OB05	X		X		1.0	1.0	2.0	
OB06	X			X	1.0	15.0	2.0	
OB07	X			X	1.0	15.0	1.5	

Table 6. Low-voltage experiments - planned nominal experiment parameters

Experiment No.	Rod Material		Rod Diameter (cm)		System Voltage (kV)	Current (kA)	Duration (s)	Notes
#	Al	Cu	1.3	2.5				
OB08	X			X	1.0	30.0	1.0	
OB09		X	X		1.0	5.0	2.0	
OB10	X		X		1.0	5.0	2.0	

Table 7. Medium-voltage experiments - planned nominal experiment parameters

Experiment No.	Rod Material		Bus size (cm)		System Voltage (kV)	Current (kA)	Duration (s)
#	Al	Cu	7.6	10.2			
OBMV1	X			X	6.9	15.0	2
OBMV2	X			X	6.9	30.0	1
OBMV3	X			X	6.9	15.0	5
OBMV4		X	X		6.9	15.0	5
OBMV5		X	X		6.9	30.0	2

3.1. Low-Voltage Experiment Results with Copper Electrodes

Experiments OB01(a) through OB04 and OB09 are presented in this subsection. All of these experiments used copper electrodes.

For each experiment, the following information is provided:

- Experiment specifications
- Electrode length and mass
- Photo of pre- and post-experiment configuration
- Photo of enclosure breach (if applicable)
- Voltage and current profile
- SNL Measurements (if applicable)
- Notes
- Observations

A summary of the low-voltage box experiments is presented at the end of this section.

3.1.1. Experiment ID: OB01(a)

This was the first open box experiment performed. During the performance of this experiment it was determined that the low currents resulted in excessively long time for the shorting wire to vaporize. This resulted in a direct phase-to-phase bolted short for over one-half of the experimental time. The shorting wire used was based on the IEEE guidance [31].

Because the experiment didn't achieve the objectives, this experiment was designated "OB01(a)" and an identical experiment with a different shorting wire was conducted designated "OB01(b)."

This experiment was performed on August 22, 2019. The electrical characteristics are presented in Table 8. Photos of Experiment OB01(a) are presented in Fig. 28. Thermal and visual video stills are provided in Fig. 29. The electrical measurements are presented in Fig. 30 and Fig. 31. Test OB01(a) used KEMA test circuit S01. The KEMA report identifies this experiment 190822-7003.

Table 8. Experiment OB01(a) parameters

Electrical Parameter	**Target**	**Actual**	**Other**
Voltage (V_{L-L})	1 000	1 029	347 (Arc)
Current (A)	1 000	1 052	
Duration (ms)	2 000	2 010	660 (Arc)
Energy (MJ)		0.201	
Other Parameters			
Electrode Length Loss (cm)	0.5 (Phase A)	1.1 (Phase B)	0.3 (Phase C)
Electrode Mass Loss (g)	Not recorded due to limited arcing duration		
Electrode Material	Copper		
Electrode Diameter	1.27 cm (0.5in)		
Electrode Spacing	8.9 cm (3.5 in) on center		
Shorting Wire	1 – 10 AWG (2.588 mm diameter), k-strand tinned copper		
Box Electrical Configuration	Connected to Neutral		
Generator Configuration	Generator Neutral Floating		
Enclosure Breach	None		

Fig. 28. Experiment OB01(a) Pre-experiment (left) and Post-experiment (right) electrodes. Phase sequence left-to-right (C-B-A)

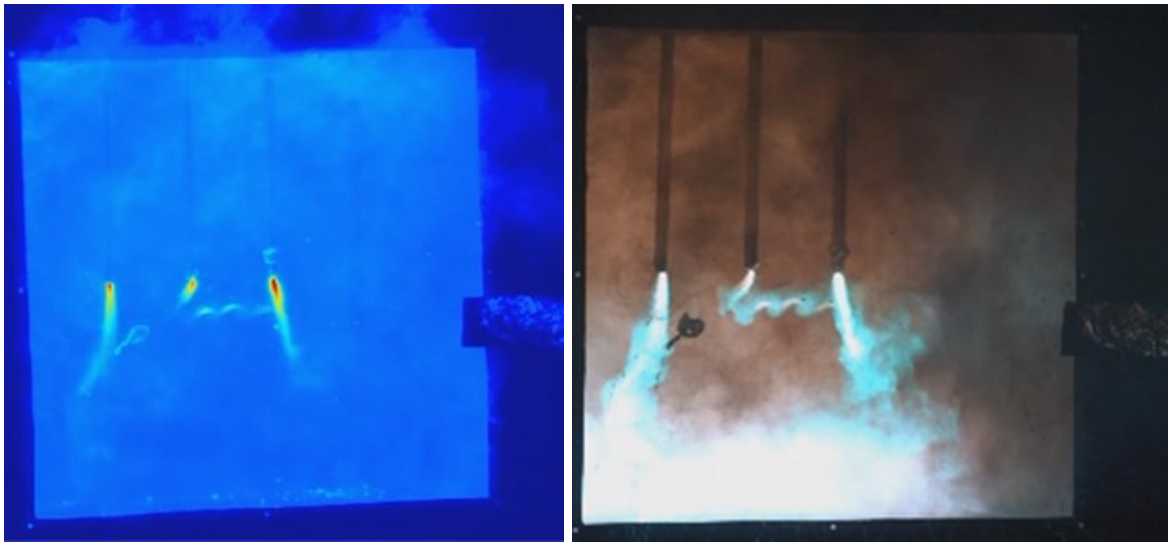

Fig. 29. Thermal (left) and Visible (right) video still shot during arc (t = 1.97s)

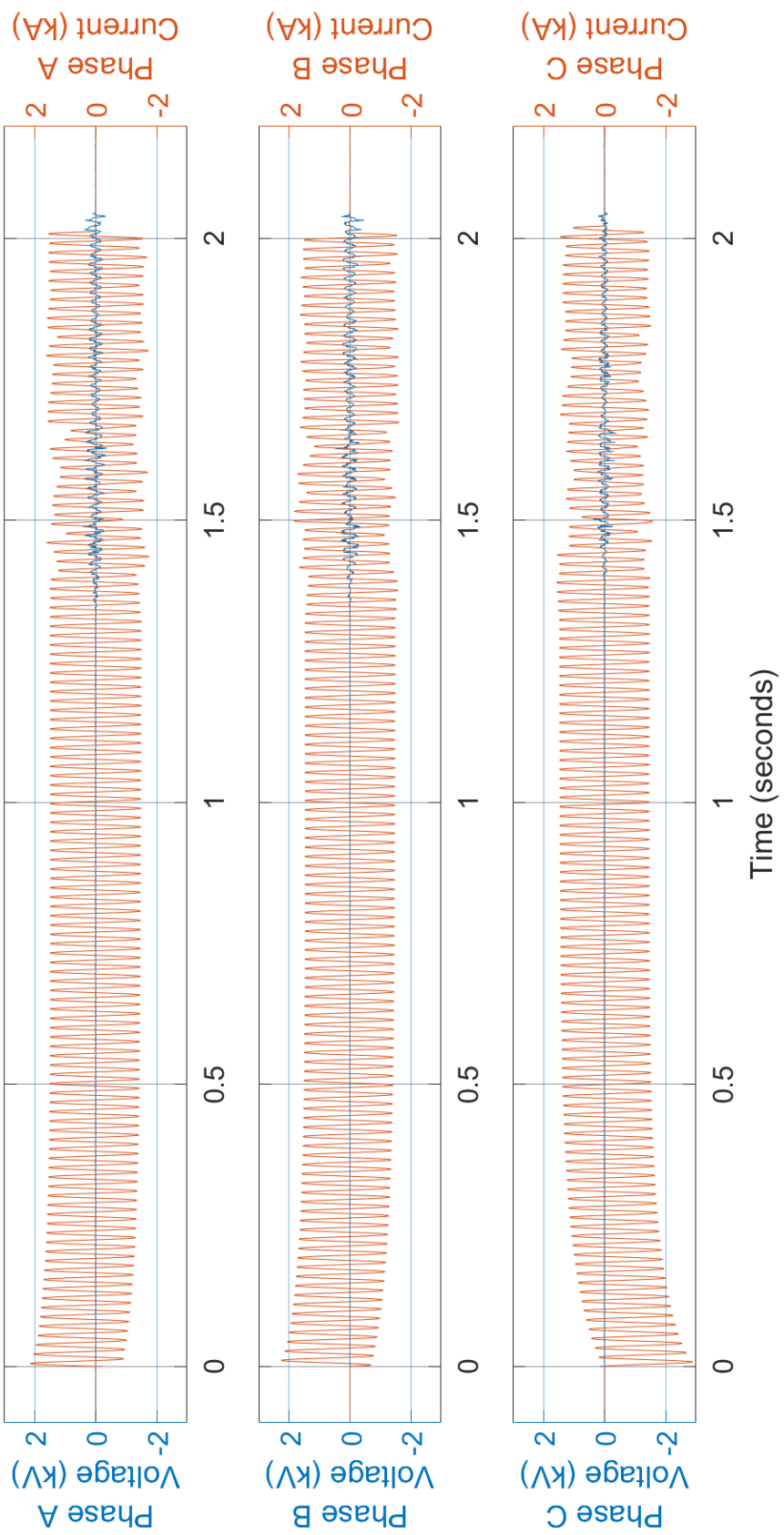

Fig. 30. Voltage and current measurements for Experiment OB01(a)

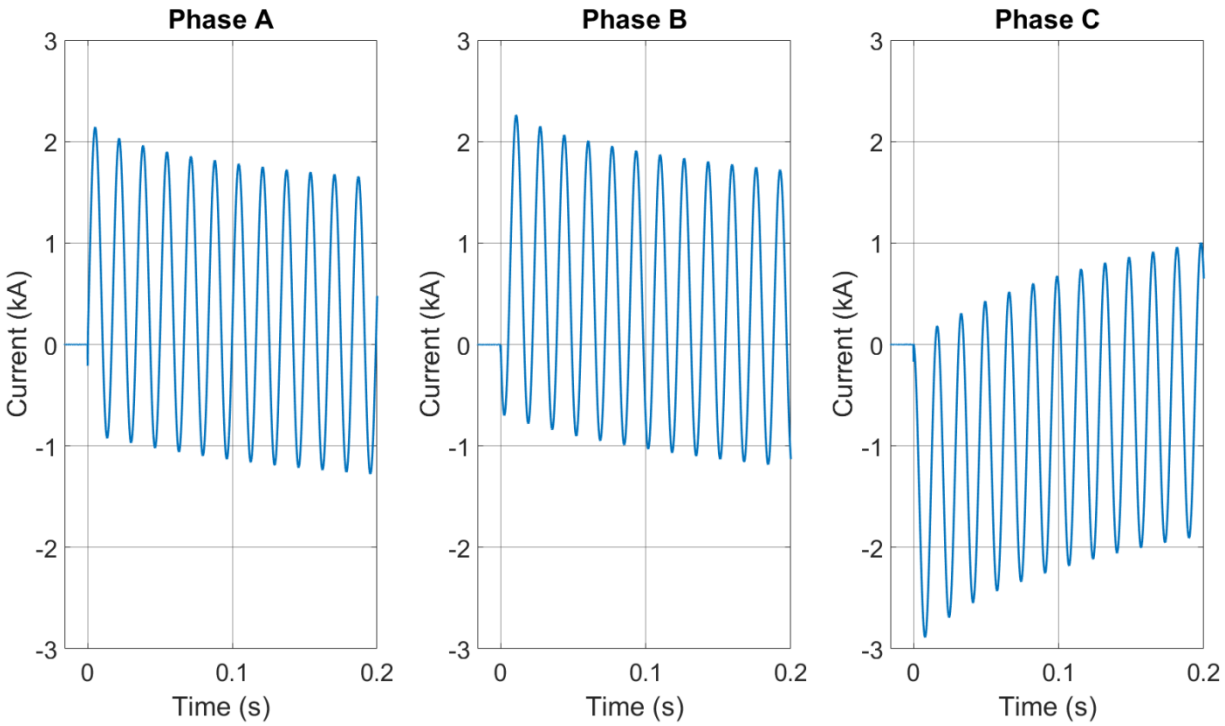

Fig. 31. Transient current profiles for Experiment OB01(a)

SNL used a radiometer to measure the incident energy during the experiment. The measurement specifics and results are presented in Table 9.

Table 9. Experiment OB01(a) radiometer measurements

Distance from Electrode (cm)	Thickness (mm)	ΔT (°C)	Calculated Incident Energy (MJ/m^2)	Calculated Energy (MJ)
45.7	1	21.6	0.07	0.20

SNL used the spectrometer during this experiment. The Iris was opened to 3 mm without the use of any optical density filter in place. During the experiment, the spectral features saturated the detectors. The detector was positioned to focus immediately below the center copper electrode tip (Phase B). The spectrum from this experiment is presented in Fig. 32. The spectrum is quite busy, with many emitting materials contributing to the signal. There was no direct characterization of the material within the box, so species and concentration are unknown. It is also important to note this data has not been processed to consider the effects of detector efficiency or non-linearity. Neither has a background been subtracted to try and remove the broad band, gray-body emission. Due to the saturation, no temperature inference was attempted.

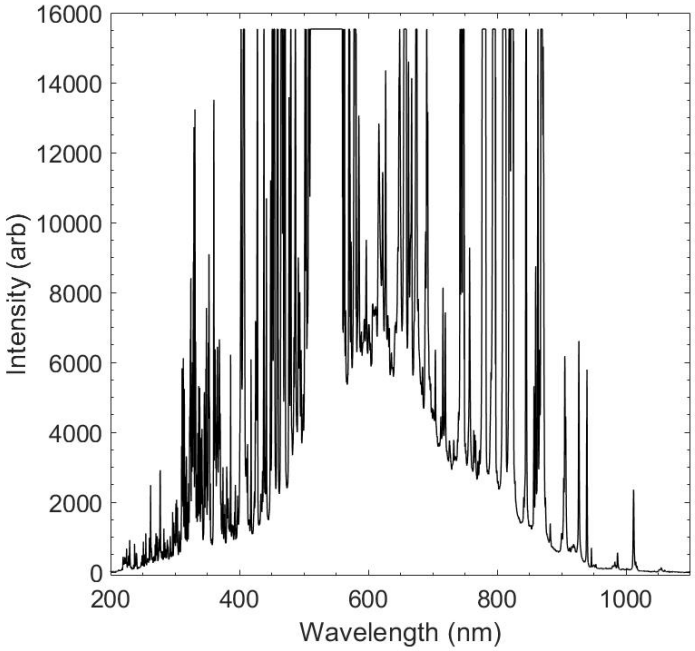

Fig. 32. Spectrum from Experiment OB01(a)

Observations and Notes

As can be observed from the photo, there was minimal material loss from the electrodes and the enclosure was not breached. Due to the minimal material loss mass measurements were not made. For this experiment a single uninsulated conductor of nominal 2.6 mm diameter (10 AWG) size with Type K-strand tinned copper was used as the shorting wire. From video evidence and the electrical measurements, the low current resulted in a significant amount of time (approximately 1.35 s) for the shorting wire to become vaporized. Therefore, the arc was only present for approximately 0.7 s versus the desired 2 s experiment duration. As such, the experiment was re-run as Experiment ID#OB01(b) using a smaller gauge wire.

3.1.2. Experiment ID: OB01(b)

This experiment was a repeat of Experiment OB01(a) except that the IEEE guidance [31] for LV experiments was not followed. The guidance uses a larger cross-sectional conductor in low-voltage experiments to ensure that sufficient conductive material is available to maintain the arc. Maintaining arcs at low-voltage is more difficult than at medium-voltage, hence the guidance to use more material. However, at the low current for this experiments, the recommended shorting wire acted as a slow blow fuse rather than an arc initiator. To provide the desired arc duration and a better arc initiation mechanism while attempting to ensure sufficient conductive medium, the following approach was followed. The shorting wire recommended for medium-voltage experiments were used. However, instead of using a single strand, a double strand configuration was used. Given the low current levels, it was believed at the time, and confirmed through later experiments, that the smaller diameter

conductor would provide a better arc initiation mechanism. This approach was found to initiate the arc in less than one cycle.

This experiment was performed on August 22, 2019. The electrical characteristics are presented in Table 10. Photos of Experiment OB01(b) are presented in Fig. 33, while the electrical measurements are presented in Fig. 34 and Fig. 35. It should be noted that the raw data file for Phase C is had a voltage divider in place and that signal needs to be multiplied by 2. This only affects the Phase C voltage and the waveforms presented below have been corrected. Experiment OB01(b) used KEMA experiment circuit S01. The KEMA Experiment report identifies this experiment as 190822-7004.

Table 10. Experiment OB01(b) parameters

Electrical Parameter	Target	Actual	Other
Voltage (V_{L-L})	1 000	1 028	308 (arc)
Current (A)	1 000	1 030	
Duration (ms)	2 000	2 020	
Energy (MJ)		0.736	
Other Parameters			
Electrode Length Loss (cm)	0.5 (Phase A)	0.4 (Phase B)	0.6 (Phase C)
Electrode Mass Loss (g)[3]	5.5	12.0	7.0
Electrode Material		Copper	
Electrode Diameter		1.27 cm (0.5in)	
Electrode Spacing		8.9 cm (3.5 in) on center	
Shorting Wire		2 – 24 AWG (0.511 mm diameter), single strand tinned copper	
Box Electrical Configuration		Neutral	
Generator Configuration		Neutral not Grounded	
Enclosure Breach		None	

[3] Mass loss for both Test OB01(a) and OB01(b)

Fig. 33. Experiment OB01(b) pre-experiment (left) and post-experiment (right) electrodes. Phase sequence from left-to-right (C-B-A)

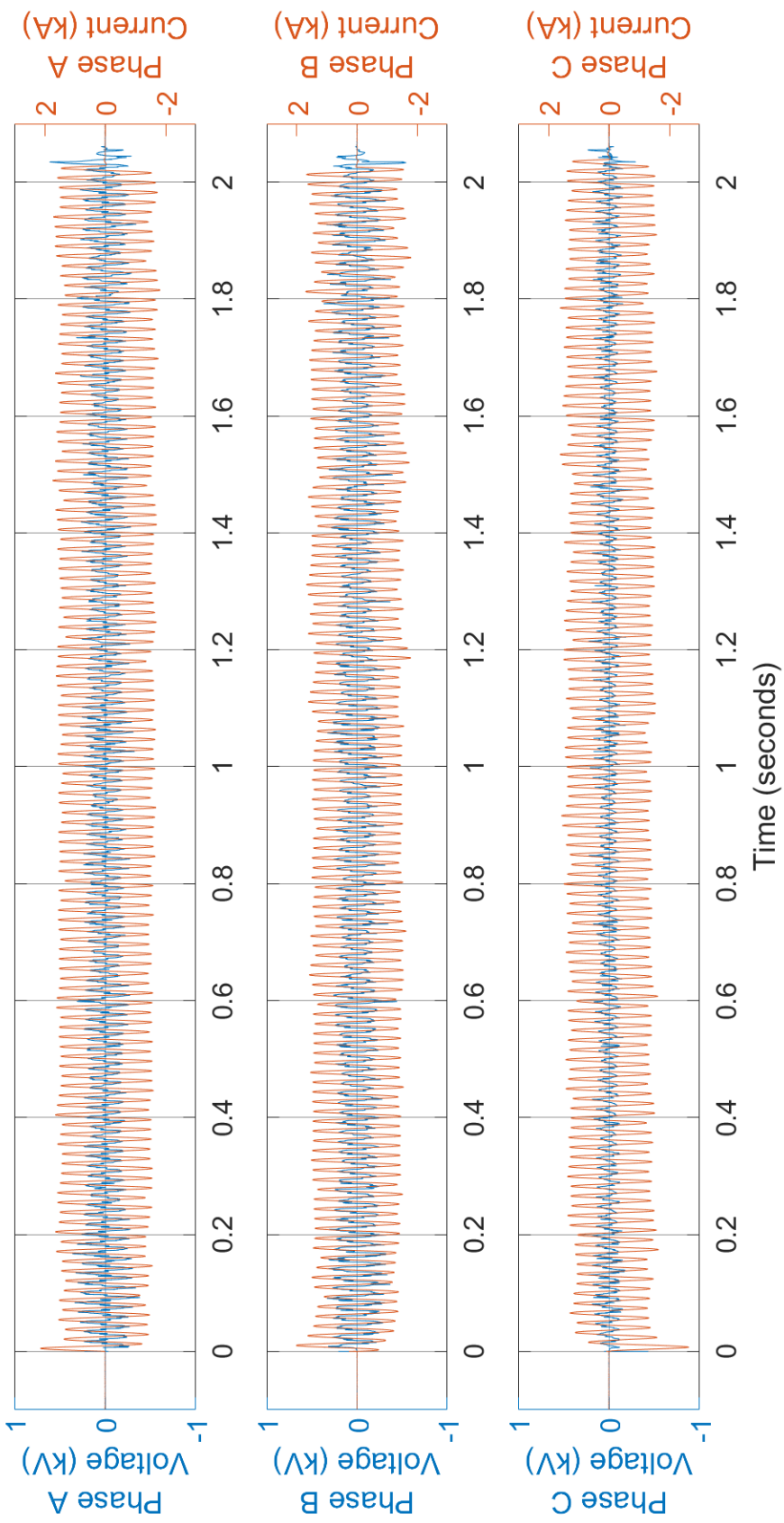

Fig. 34. Voltage and current measurements for Experiment OB01(b)

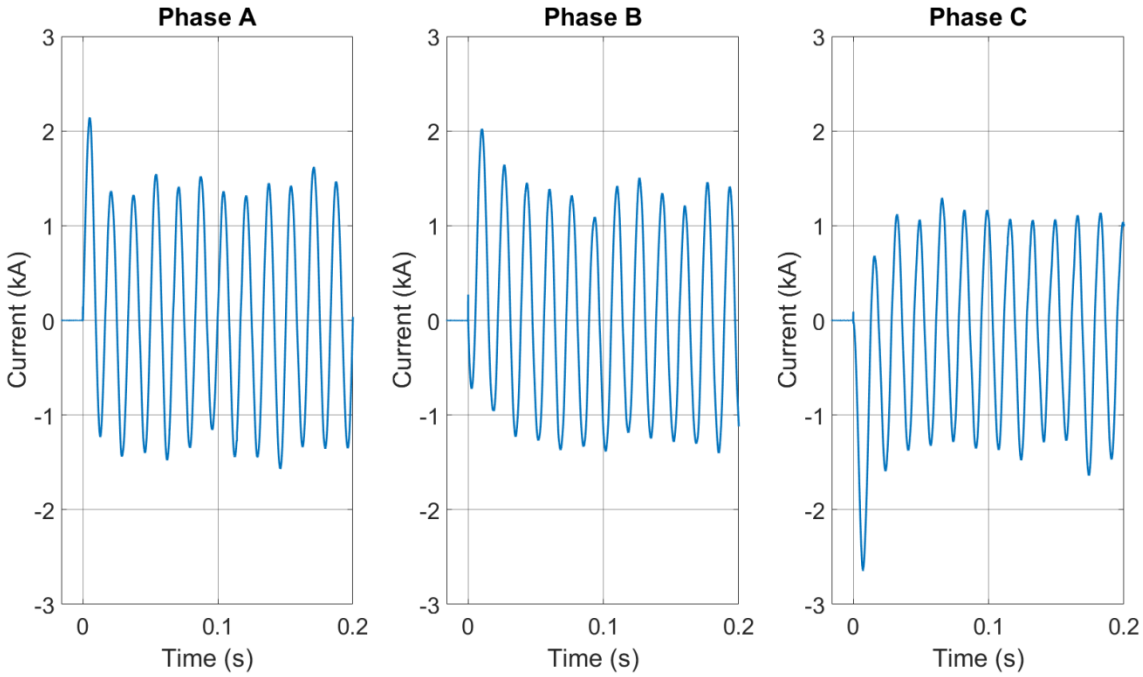

Fig. 35. Transient current profiles for Experiment OB01(b)

SNL used a radiometer to measure the incident energy during the experiment. The measurement specifics and results are presented in Table 11.

Table 11. Experiment OB01(b) Radiometer Measurements

Distance from Electrode (cm)	Thickness (mm)	ΔT (°C)	Calculated Incident Energy (MJ/m^2)	Calculated Energy (MJ)
45.7	1	45.1	0.16	0.41

SNL used the spectrometer during this experiment. The Iris was opened to 1 mm without the use of any optical density filter in place. Detector was positioned to look immediately below the center copper electrode tip. Spectral features saturated the detector at early times. By the middle of the experiment, the spectrometer was recording features that could be analyzed, and weak features were present at the end of the experiment. The spectrum from this experiment is presented in Fig. 36 and Fig. 37.

In both the left and right spectra of Fig. 37, two copper transitions at 793.3 nm, and 809.3 nm are visible and isolated. These transitions were identified as temperature sensitive in previous work. However, in order to accurately infer temperature, two additional lines at 570 nm, 578.2 nm must be resolved as well. Unfortunately, as seen in all spectra that region experiences significant interference from additional species emission. Therefore, no temperature inference was attempted, and the spectra presented have no data processing for detector non-linearity, efficiency, or background subtraction.

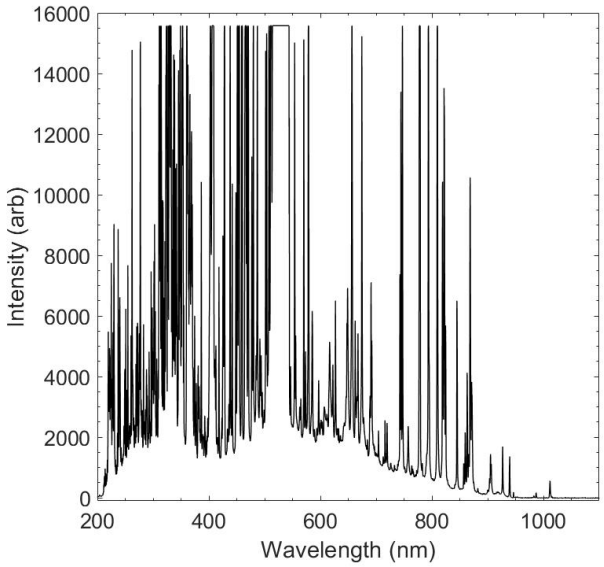

Fig. 36. Spectrum from Experiment OB01(b), early

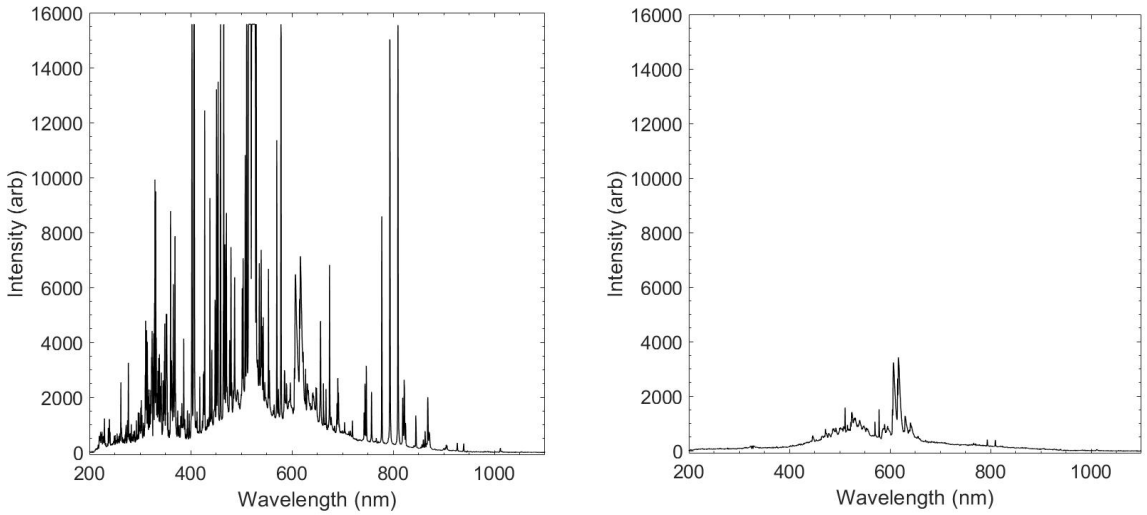

Fig. 37. Spectrum from Experiment OB01(b), mid-experiment

Observations and Notes

The use of the smaller arcing wire reduced the amount of time to vaporize the wire under these low current conditions. Review of the current and voltage profiles indicated that the nominal 0.511 mm diameter (24AWG) arc wire was vaporized in approximately 4.44 ms versus the 1 350 ms from experiment OB01(a). The steel enclosure did not breach. The electrodes from Experiment OB01(a) were re-used for this experiment. The electrodes were not repositioned due to the minimal amount of material lost during the previous experiment. Care must be used when evaluating the material lost from experiment OB01(a) and experiment OB01(b).

3.1.3. Experiment ID: OB02

This experiment was performed on August 30, 2019. The electrical characteristics are presented in Table 12. Photos of Experiment OB02 are presented in Fig. 38 through Fig. 39, while the electrical measurements are presented in Fig. 41 and Fig. 42. Experiment OB02 used KEMA experiment circuit S03. The KEMA experiment report identifies this experiment at 190830-7001.

Table 12. Experiment Parameters Experiment OB02

Electrical Parameter	Target	Actual	Other
Voltage (V_{L-L})	1 000	1 008	271 (arc)
Current (A)	15 000	14 016	
Duration (ms)	2 000	2 020	
Energy (MJ)		11.989	
Other Parameters			
Electrode Length Loss (cm)	5.1 (Phase A)	6.4 (Phase B)	4.9 (Phase C)
Electrode Mass Loss (g)	189.5	369.0	204.0
Electrode Material		Copper	
Electrode Diameter		2.54 cm (1.0 in)	
Electrode Spacing		8.9 cm (3.5 in) on center	
Shorting Wire		2 – 24 AWG (0.511 mm diameter), single strand tinned copper	
Box Electrical Configuration		Neutral	
Generator Configuration		Neutral tied to ground via impedance	
Enclosure Breach		Yes, Bottom and Top	
Enclosure Mass Loss (g)		386	

Fig. 38. Experiment OB02 pre-experiment (left) and post-experiment (right) electrodes. Phase sequence from left-to-right is C-B-A

Fig. 39. Experiment OB02 enclosure breach. Bottom side breach (left), top side breach with electrode holder removed (right).

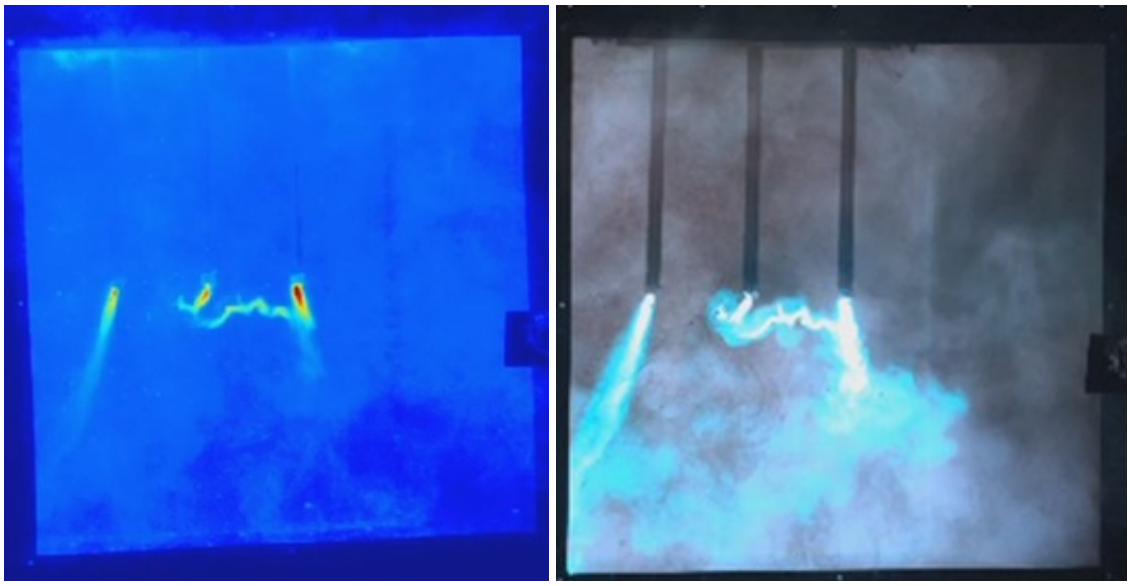

Fig. 40. Experiment OB02 thermal (left) and visible (right) video still shots during the arc (t = 1.47 s)

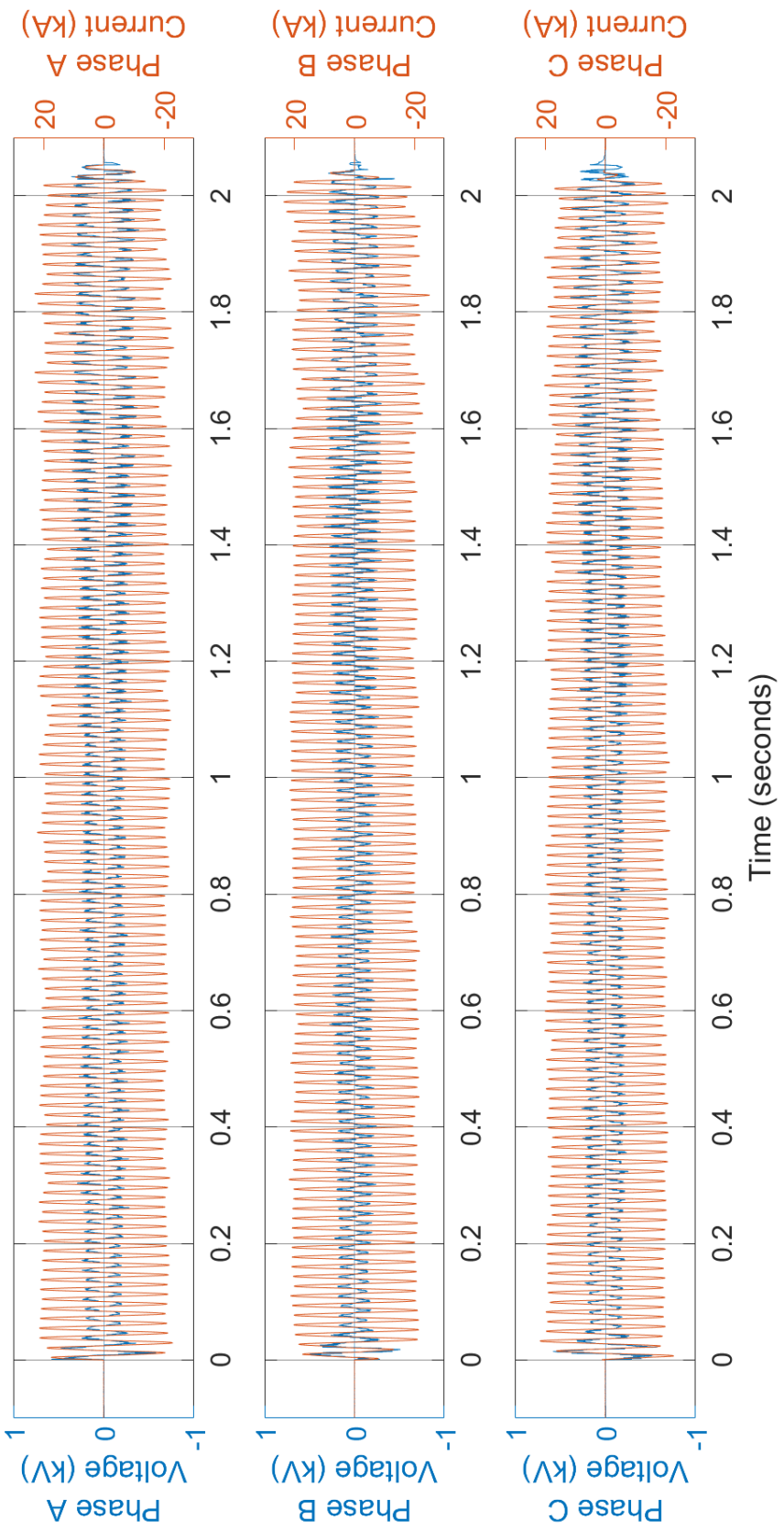

Fig. 41. Experiment OB02 voltage and current measurements

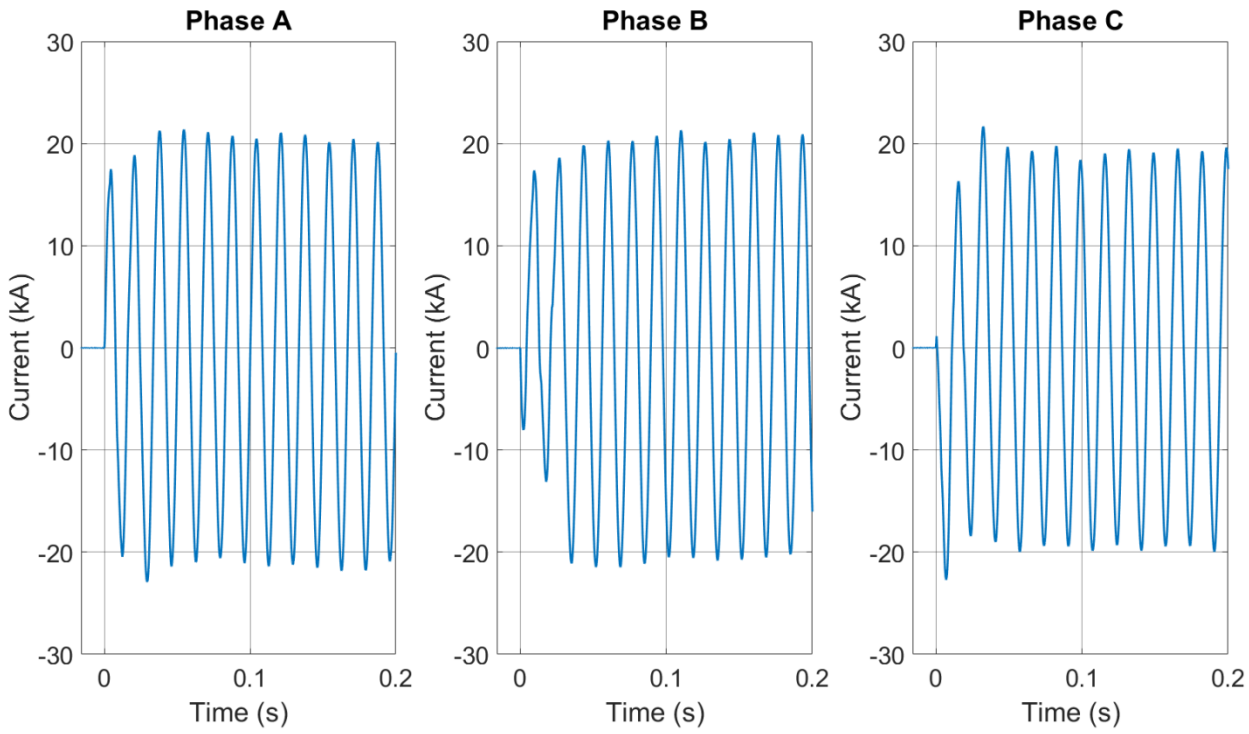

Fig. 42. Experiment OB02 transient current profiles

SNL used a radiometer to measure the incident energy during the experiment. The measurement specifics and results are presented in Table 13.

Table 13. Experiment OB02 radiometer measurement

Distance from Electrode (cm)	Thickness (mm)	ΔT (°C)	Calculated Incident Energy (MJ/m²)	Calculated Energy (MJ)
182.8	3	10.2	0.11	4.46

Observations and Notes

The steel enclosure breached at the bottom and top. The estimated mass loss from the enclosure is approximately 386 grams and a total breach opening on all sides of approximately 275 cm^2 (bottom opening of approximately 248 cm^2 and a top opening of approximately 26 cm^2).

3.1.4. Experiment ID: OB03

This experiment was performed on August 30, 2019. The electrical characteristics are presented in Table 14. Photos of Experiment OB03 are presented in Fig. 43 through Fig. 44, while the electrical measurements are presented in Fig. 46 and Fig. 47.
Experiment OB03 used KEMA experiment circuit S03. The KEMA Experiment report identifies this experiment at 190830-7002.

Table 14. Experiment OB03 experimental parameters

Electrical Parameter	Target	Actual	Other
Voltage (V_{L-L})	1 000	1 008	314 (arc)
Current (A)	15 000	13 804	
Duration (ms)	3 000	3 030	
Energy (MJ)		19.886	
Other Parameters			
Electrode Length Loss (cm)	9.8 (Phase A)	12.1 (Phase B)	8.6 (Phase C)
Electrode Mass Loss (g)	444	515	368
Electrode Material		Copper	
Electrode Diameter		2.54 cm (1.0in)	
Electrode Spacing		8.9 cm (3.5 in) on center	
Shorting Wire		2 – 24 AWG (0.511 mm diameter), single strand tinned copper	
Box Electrical Configuration		Neutral	
Generator Configuration		Neutral tied to ground via impedance	
Enclosure Breach		Bottom, side, back, top	
Enclosure Mass Loss (g)		1 799	

Fig. 43. Experiment OB03 pre-experiment (left) and post-experiment (right) electrodes. Phase sequence from left-to-right is C-B-A.

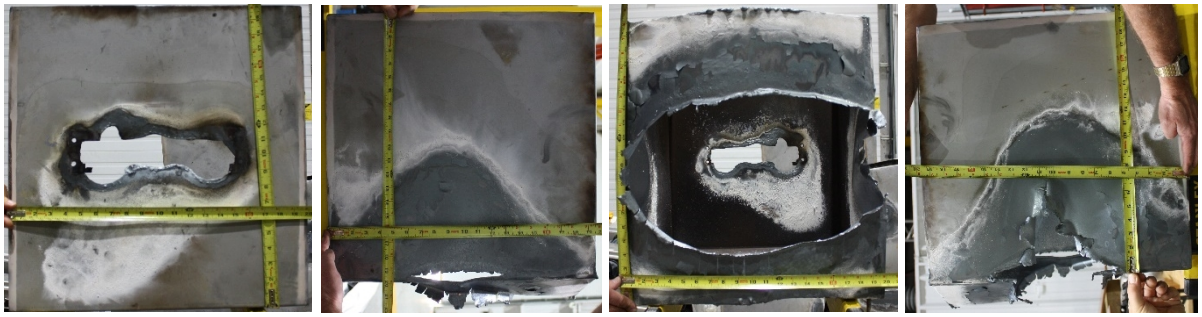

Fig. 44. Experiment OB03 enclosure breach (from left-to-right: top, left side, bottom, right side).

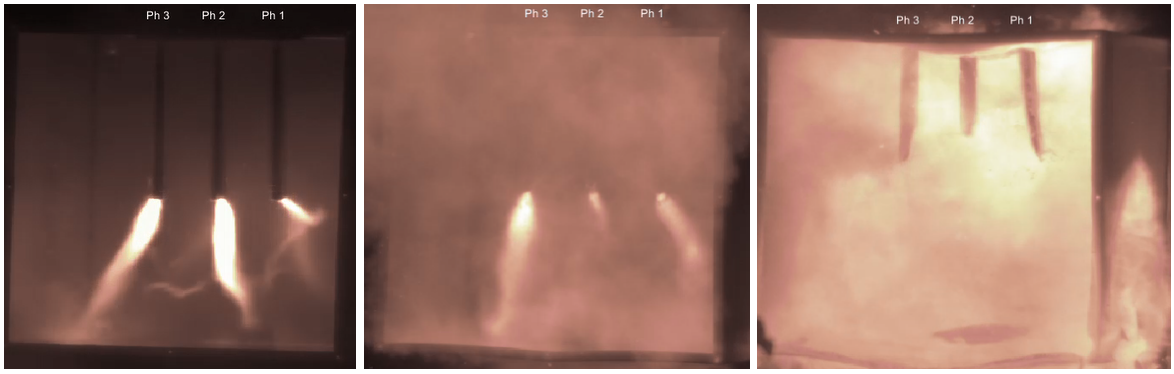

Fig. 45. Experiment OB03 still shots from the high speed visible video during the arc (Left 0.02 s, Center 1.50 s, Right 3.06 s)

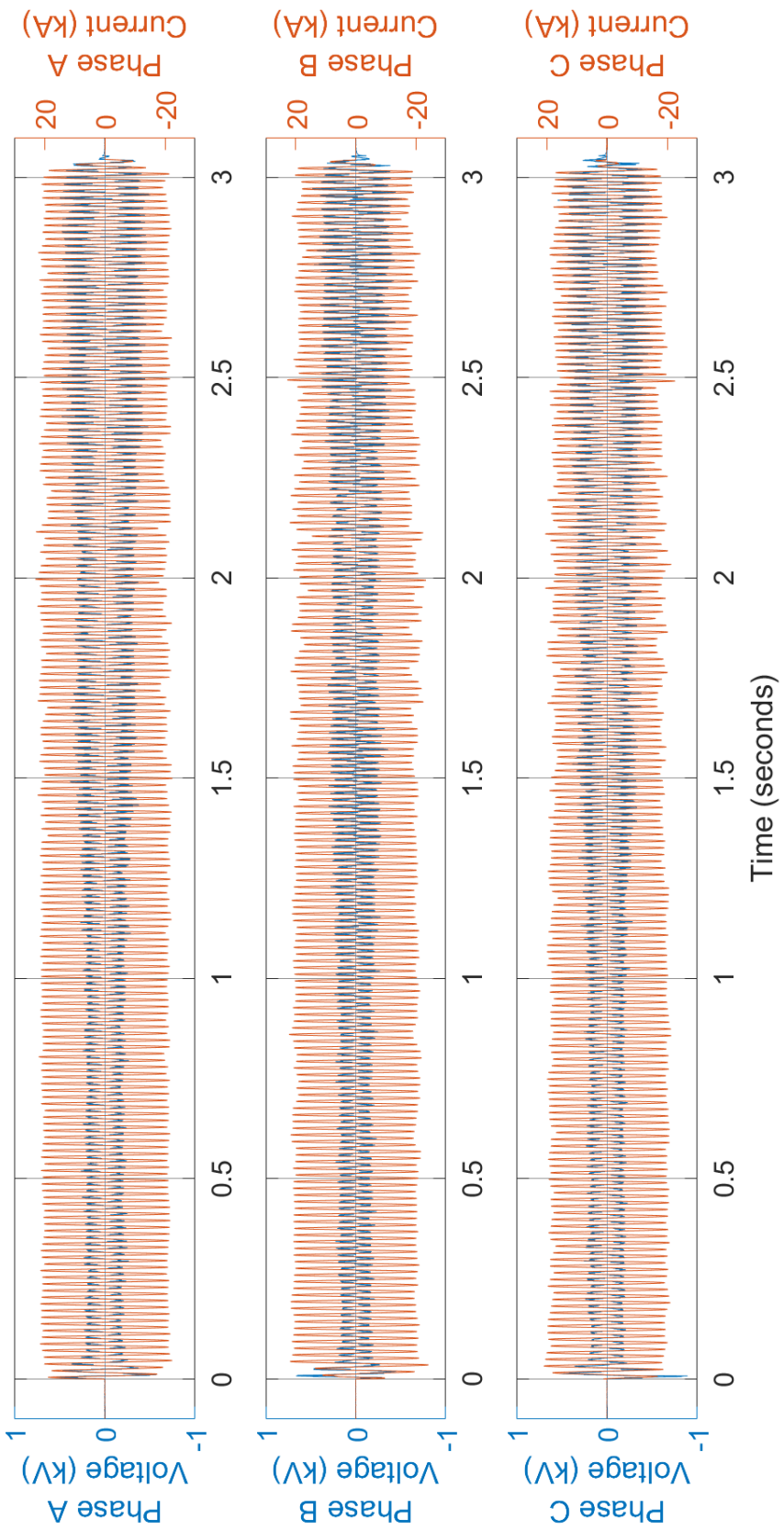

Fig. 46. Experiment OB03 voltage and current measurements

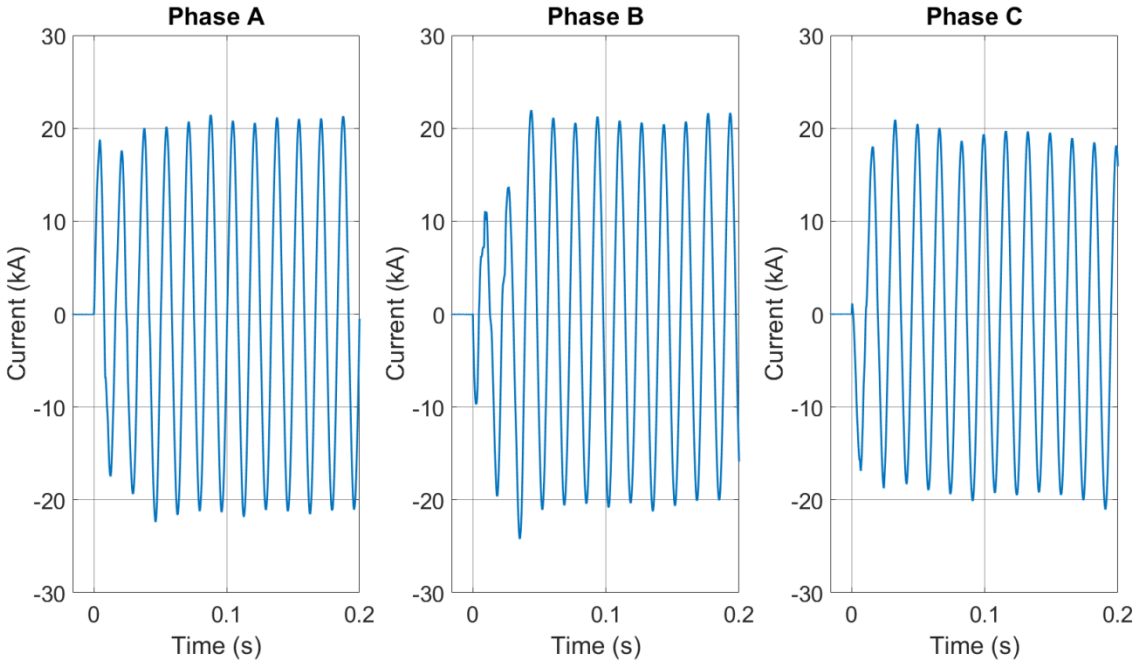

Fig. 47. Experiment OB03 transient current profiles

SNL used a radiometer to measure the incident energy during the experiment. The measurement specifics and results are presented in Table 15.

Table 15. Experiment OB03 radiometer measurement

Distance from Electrode (cm)	Thickness (mm)	ΔT (°C)	Calculated Incident Energy (MJ/m^2)	Calculated Energy (MJ)
182.9	3	17.7	0.18	7.73

Observations and Notes

The estimated mass loss from the enclosure is approximately 1 799 grams and a total breach opening on all sides of approximately 1 280 cm^2 (bottom opening of approximately 1 110 cm^2, left side approximately 20 cm^2, right side approximately 101 cm^2 and a top opening of approximately 50 cm^2).

3.1.5. Experiment ID: OB04

This experiment was performed on August 30, 2019. The electrical characteristics are presented in Table 16. Photos of Experiment OB04 are presented in Fig. 48, Fig. 49 and Fig. 50, while the electrical measurements are presented in Fig. 52 and Fig. 53. Experiment OB04 used KEMA experiment circuit S04. The KEMA Experiment report identifies this experiment as 190830-7003.

Table 16. Experiment OB04 experiment parameters

Electrical Parameter	Target	Actual	Other
Voltage (V_{L-L})	1 000	1 063	276 (arc)
Current (A)	30 000	27 786	
Duration (ms)	1 000	1 030	
Energy (MJ)		12.328	
Other Parameters			
Electrode Length Loss cm	8.3 (Phase A)	4.8 (Phase B)	2.9 (Phase C)
Electrode Mass Loss (g)	241.0	357.5	190.5
Electrode Material		Copper	
Electrode Diameter		2.54 cm (1.0 in)	
Electrode Spacing		8.9 cm (3.5 in) on center	
Shorting Wire		2 – 24 AWG (0.511 mm diameter), single strand tinned copper	
Box Electrical Configuration		Neutral	
Generator Configuration		Neutral tied to ground via impedance	
Enclosure Breach		Bottom	
Enclosure Mass Loss (g)		110	

Fig. 48. Experiment OB04 pre-experiment (left) and post-experiment (right) electrodes. Phase sequence from left to right is C-B-A

Fig. 49. Experiment OB04 enclosure breach (Left – bottom side; Right – top side)

Fig. 50. Experiment OB04 electrode deflection post-experiment

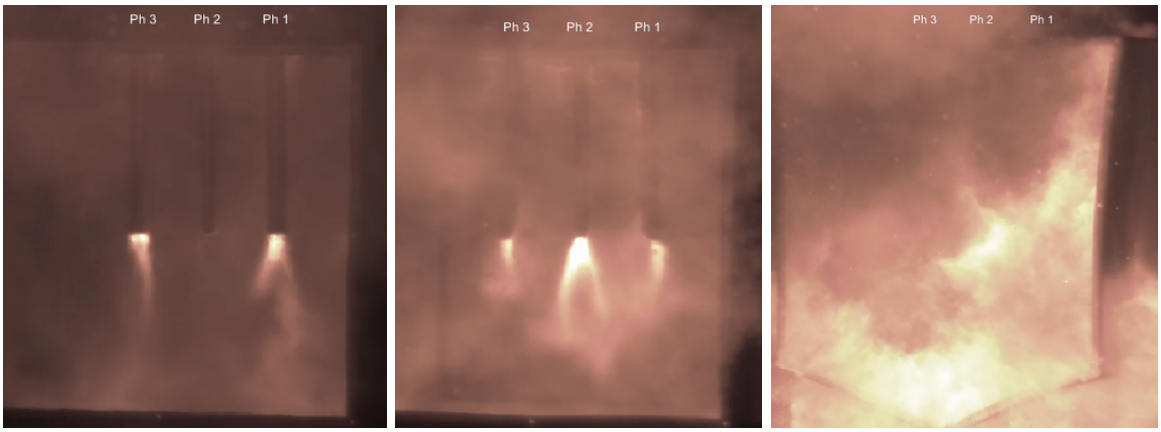

Fig. 51. Experiment OB04 visible video still shot during the arc (Left 0.09 s; Center 0.51 s; Right 1.08 s)

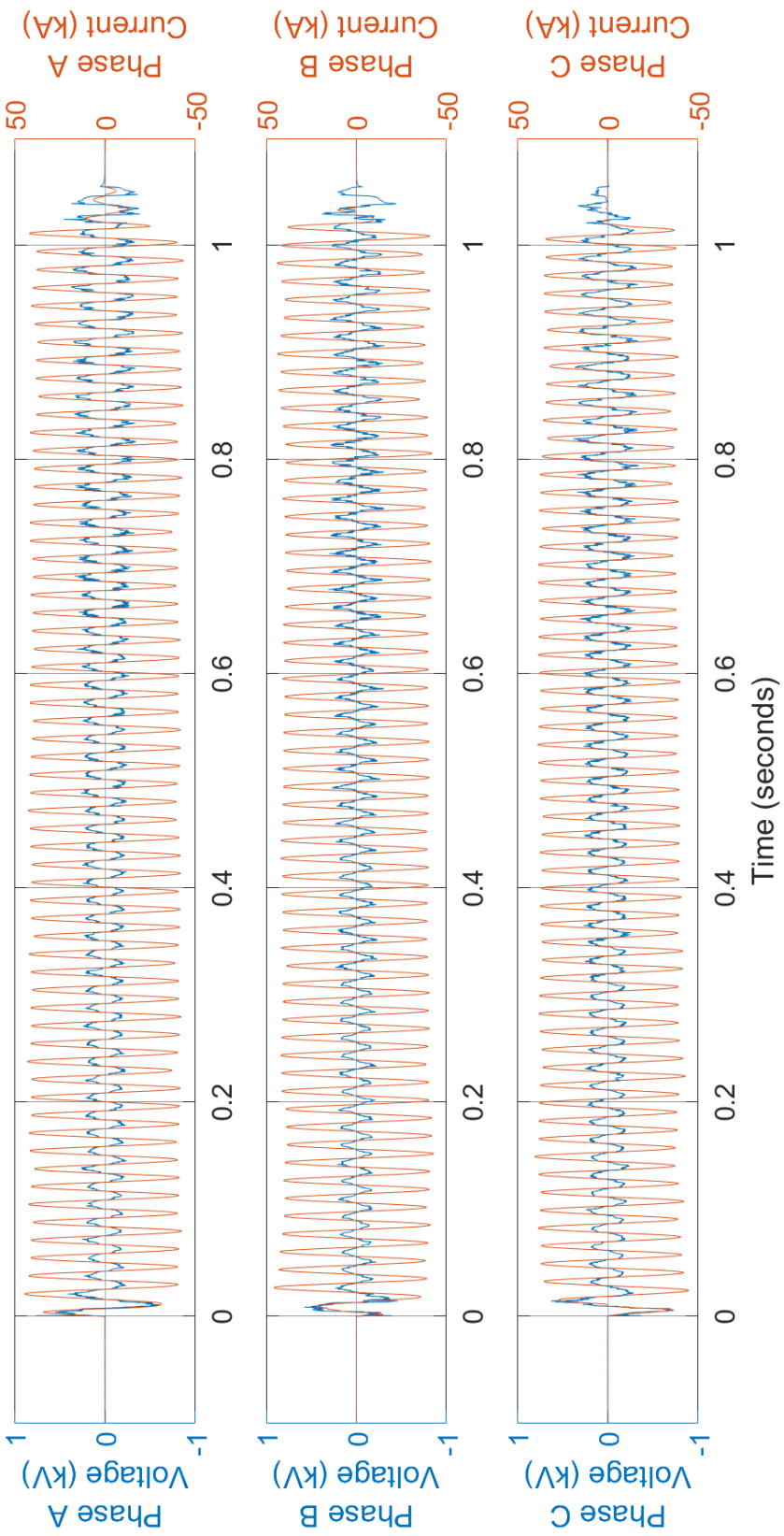

Fig. 52. Experiment OB04 voltage and current measurements

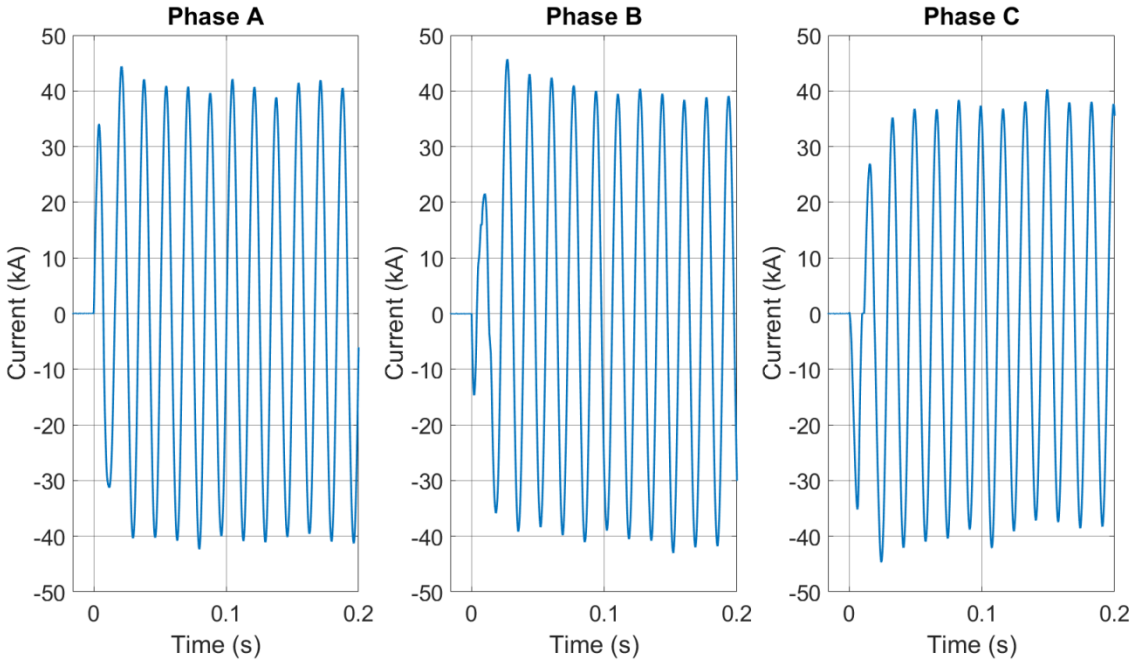

Fig. 53. Experiment OB01(b) transient current profiles

SNL used a radiometer to measure the incident energy during the experiment. The measurement specifics and results are presented in Table 17.

Table 17. Experiment OB04 radiometer measurements

Distance from Electrode (cm)	Thickness (mm)	ΔT (°C)	Calculated Incident Energy (MJ/m^2)	Calculated Energy (MJ)
182.9	3	10.6	0.11	4.63

Observations and Notes

The estimated mass loss from the enclosure is approximately 110 grams and a total breach opening on all sides of approximately 78 cm^2 (bottom opening of approximately 15 cm^2 and a top opening of approximately 63 cm^2).

3.1.6. Experiment ID: OB09

This experiment was performed on August 22, 2019. The electrical characteristics are presented in Table 18. Photos of Experiment OB09 are presented in Fig. 54 and Fig. 54, while the electrical measurements are presented in Fig. 56 and Fig. 57. Experiment OB09 used KEMA experiment circuit S02. The KEMA Experiment report identifies this experiment at 190822-7007.

Table 18. Experiment Parameters Experiment OB09

Electrical Parameter	Target	Actual	Other
Voltage (V_{L-L})	1 000	1 026	297 (Arc)
Current (A)	5 000	4 794	
Duration (ms)	2 000	2 010	
Energy (MJ)		2.242	
Other Parameters			
Electrode Length Loss (cm)	6.0 (Phase A)	7.6 (Phase B)	7.1 (Phase C)
Electrode Mass Loss (g)	61.5	77.0	74.0
Electrode Material		Copper	
Electrode Diameter		1.27 cm (0.5in)	
Electrode Spacing		8.9 cm (3.5 in) on center	
Shorting Wire		2 – 24 AWG (0.511 mm diameter), single strand tinned copper	
Box Electrical Configuration		Neutral	
Generator Configuration		Neutral not grounded	
Enclosure Breach		None	

Fig. 54. Experiment OB09 pre-experiment (left) and post-experiment (right) electrodes. Phase sequence from left-to-right is C-B-A.

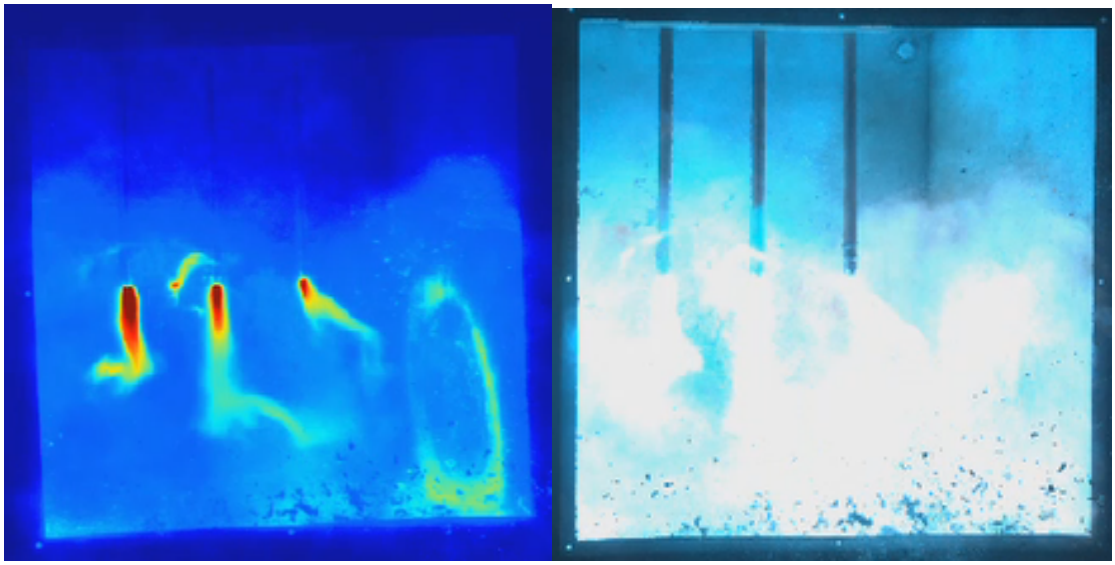

Fig. 55. Experiment OB09 thermal (left) and visible (right) video still shots during the arc (t = 0.06 s)

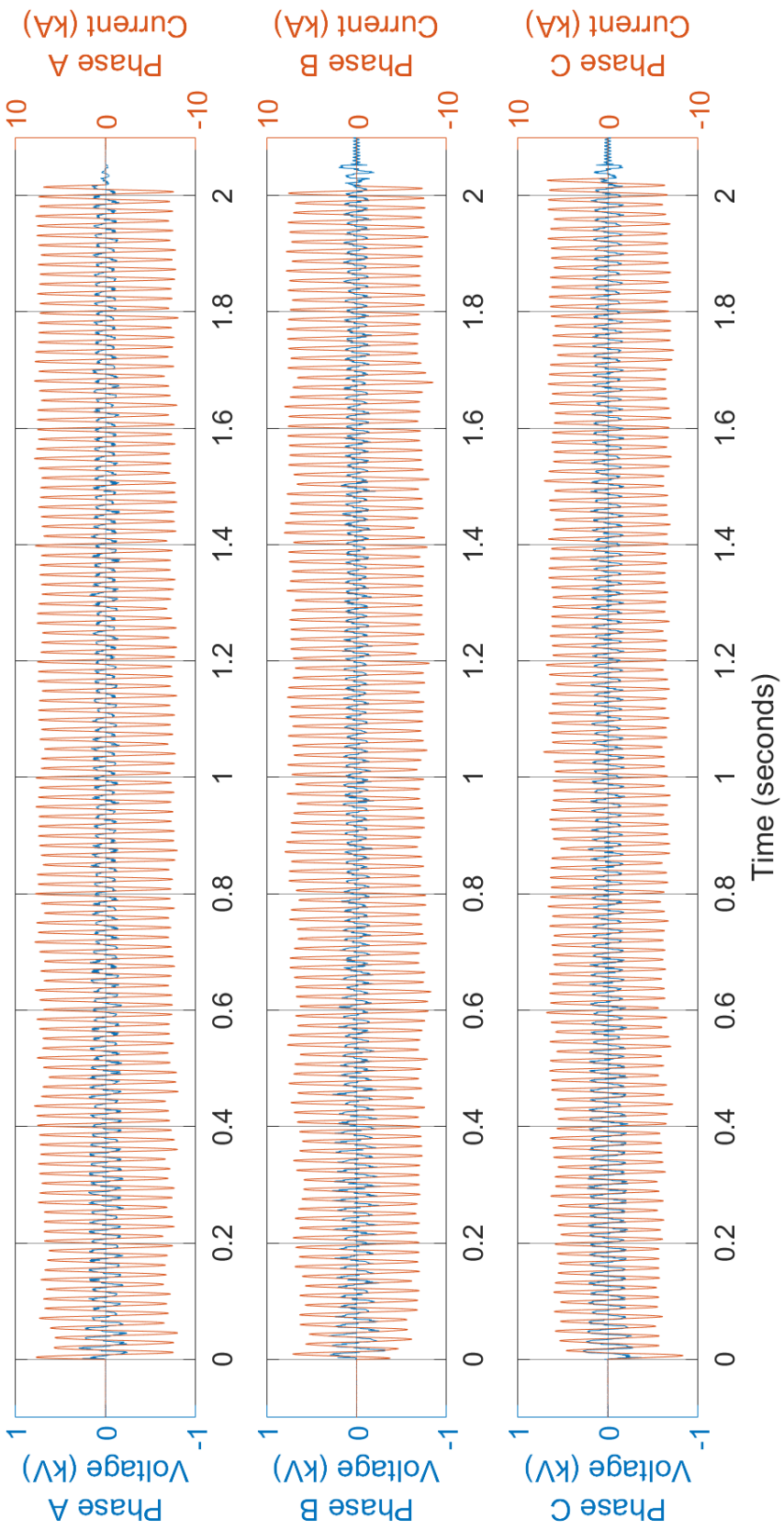

Fig. 56. Experiment OB09Voltage and current measurements

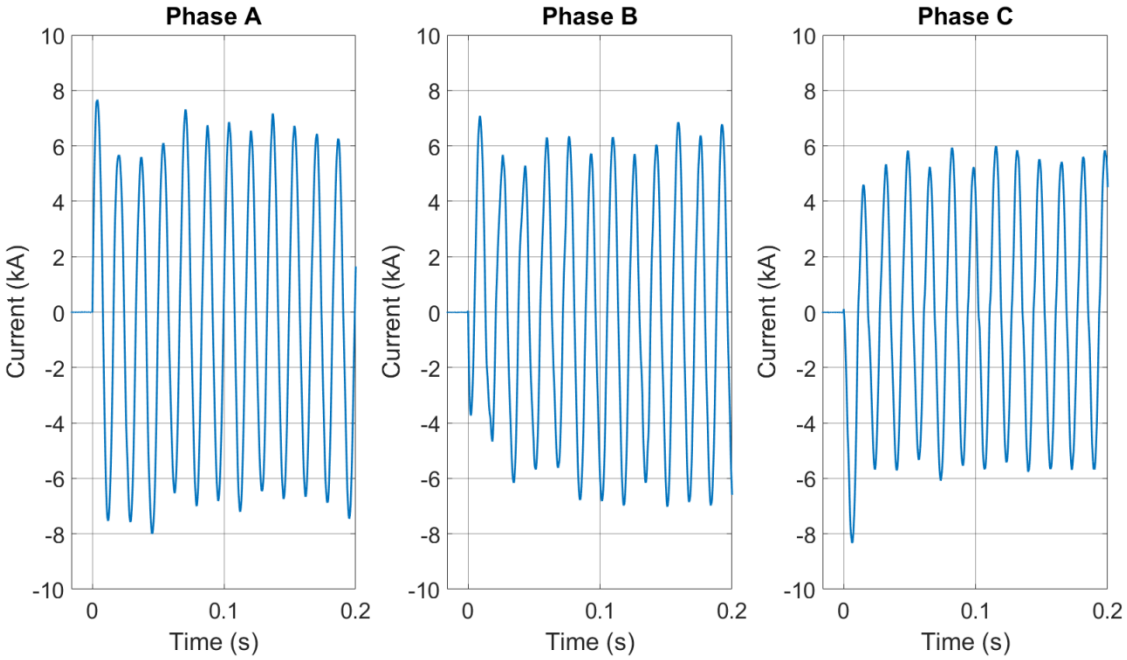

Fig. 57. Experiment OB09 transient current profiles

SNL used a radiometer to measure the incident energy during the experiment. The measurement specifics and results are presented in Table 19.

Table 19. Experiment OB09 radiometer measurement

Distance from Electrode (cm)	Thickness (mm)	ΔT (°C)	Calculated Incident Energy (MJ/m^2)	Calculated Energy (MJ)
182.9	3	3.6	0.04	1.57

SNL used the spectrometer during this experiment. The Iris was opened to 3 mm with the use of a 0.3 neutral density filter. The detector was positioned to focus immediately below the center copper electrode tip (Phase B). Spectra contained strong metallic features, and the intensity varied throughout the experiment. The spectra from this experiment are presented in Fig. 58.

The spectrum on the left is from the beginning of the experiment, and the spectrum on the right is near the end of the experiment. The intensity of the features decreases, likely due to the arc decay. Metallic copper features at 793.3 nm, and 809.3 nm are visible in both spectra. They dominate the later-time spectrum, Fig. 58 (right).

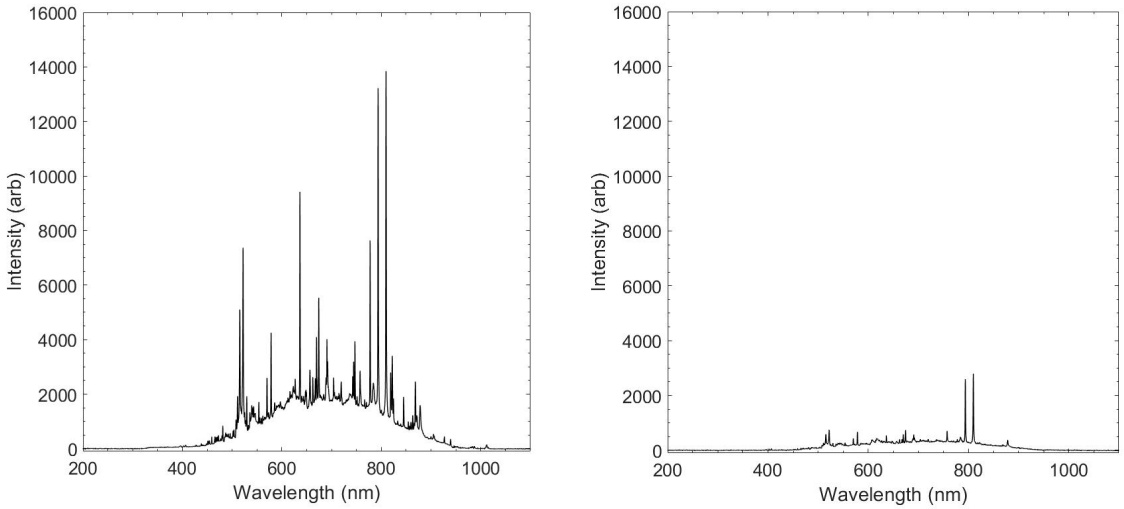

Fig. 58. Experiment OB09 Spectra

Observations and Notes

The steel enclosure did not breach.

3.2. Low-Voltage Experiment Results with Aluminum Electrodes

Experiments OB05 through OB08 and OB10 are presented in this subsection. All of these experiments used aluminum electrodes.

For each experiment, the following information is provided:

- Experiment specifications
- Electrode length and mass
- Photo of pre- and post-experiment configuration
- Photo of enclosure breach (if applicable)
- Voltage and current profile
- SNL Measurements (if applicable)
- Notes
- Observations

A summary of the low-voltage box experiments is presented at the end of this section.

3.2.1. Experiment ID: OB05

This experiment was performed on August 22, 2019. The electrical characteristics are presented in Table 20. Photos of Experiment OB05 are presented in Fig. 59, while the electrical measurements are presented in Fig. 61 and Fig. 62.

Table 20. Experiment OB05 experiment parameters

Electrical Parameter	Target	Actual	Other
Voltage (V_{L-L})	1 000	1 027	359 (Arc)
Current (A)	1 000	1 018	
Duration (ms)	2 000	2 010	
Energy (MJ)		0.796	
Other Parameters			
Electrode Length Loss (cm)	2.4 (Phase A)	3.0 (Phase B)	3.0 (Phase C)
Electrode Mass Loss (g)		Not measured	
Electrode Material			
Electrode Diameter		1.27 cm (0.5in)	
Electrode Spacing		8.9 cm (3.5 in) on center	
Shorting Wire		2 – 24 AWG (0.511 mm diameter), single strand tinned copper	
Box Electrical Configuration		Neutral	
Generator Configuration		Neutral not tied to ground	
Enclosure Breach		None	

Fig. 59. Experiment OB05 pre-experiment (left) and post-experiment (right) electrodes. Phase sequence from left-to-right is C-B-A.

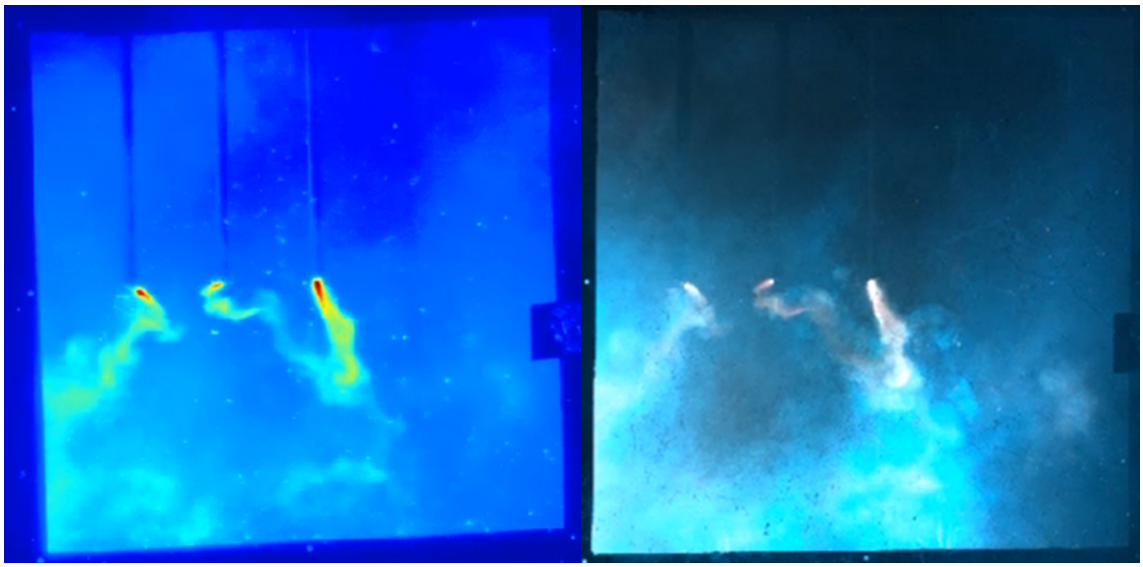

Fig. 60. Experiment OB02 thermal (left) and visible (right) video still shot during the arc (t = 0.33s)

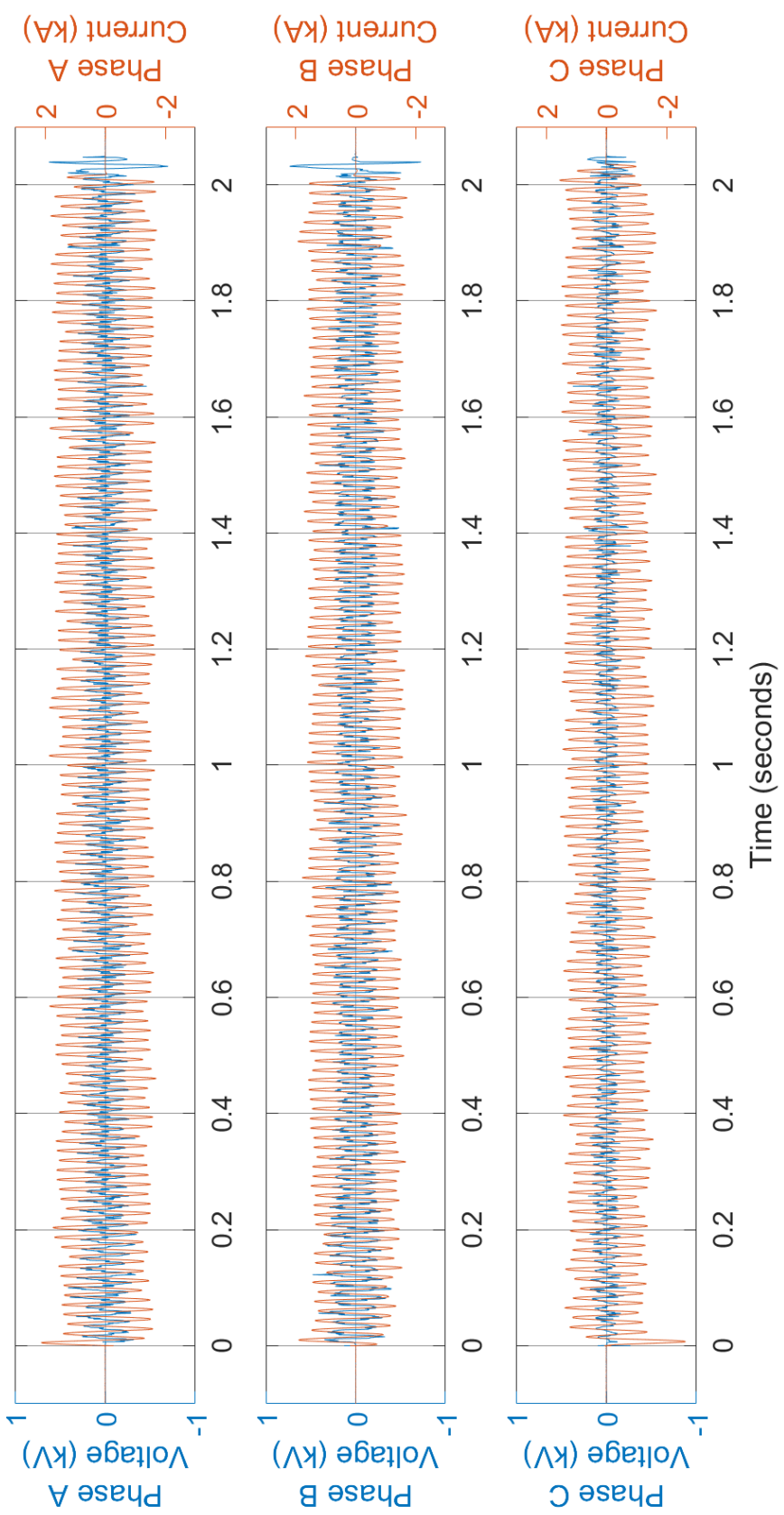

Fig. 61. Experiment OB05 voltage and current measurements

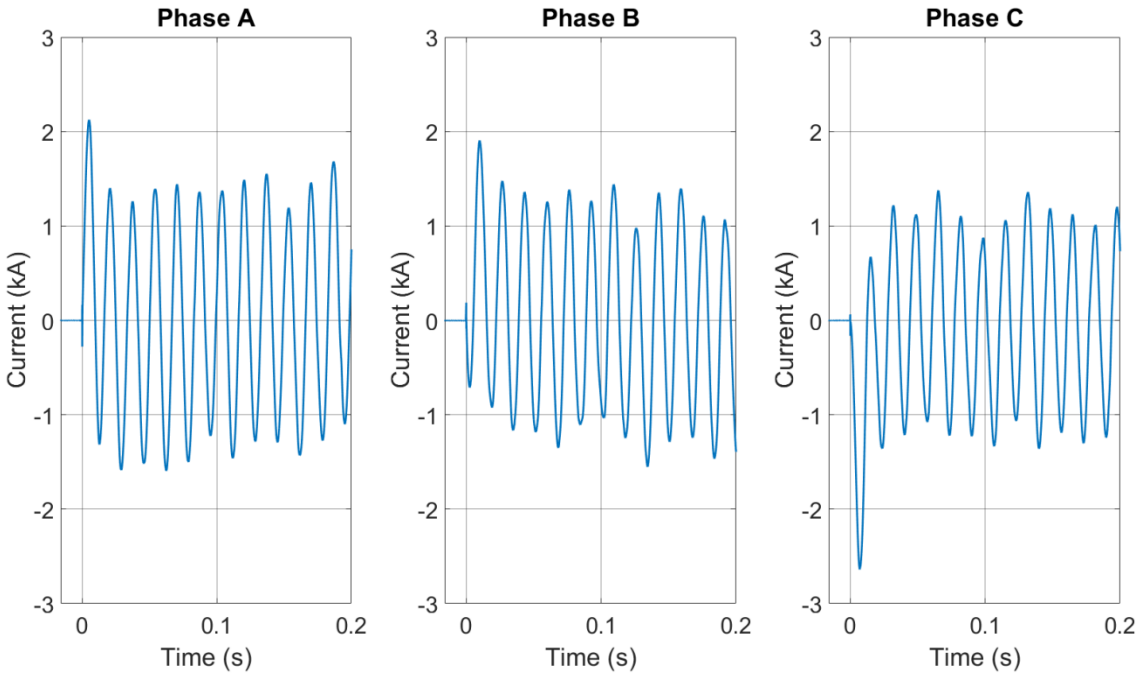

Fig. 62. Experiment OB05 transient current profiles

SNL used a radiometer to measure the incident energy during the experiment. The measurement specifics and results are presented in Table 21.

Table 21. Experiment OB05 radiometer measurement

Distance from Electrode (cm)	Thickness (mm)	ΔT (°C)	Calculated Incident Energy (MJ/m^2)	Calculated Energy (MJ)
45.7	1	88.7	0.31	0.81

SNL used the spectrometer during this experiment. The Iris was opened to 1 mm and a 0.3 neutral density optical filter was in place. The detector was positioned to focus immediately below the center electrode tip (Phase B). Spectra contained high baseline emission, as well as spectral features (Fig. 62).

Unlike the prior spectra in Experiments OB01a and OB01b, this spectrum contains emission from aluminum and reacting aluminum compounds. The sharp and narrow spectral features, like that at 400 nm, are indicative of atomic emission, but broader manifolds of emission, like those from 450 nm to 575 nm, are likely generated by molecular emission. These may be reacting aluminum molecules and radicals. With proper analysis, accounting for detector efficiency, nonlinearity, and background, these manifolds could be fit for temperature and compared to atomic aluminum emission from the plasma. However, that processing development was out of the scope of this project.

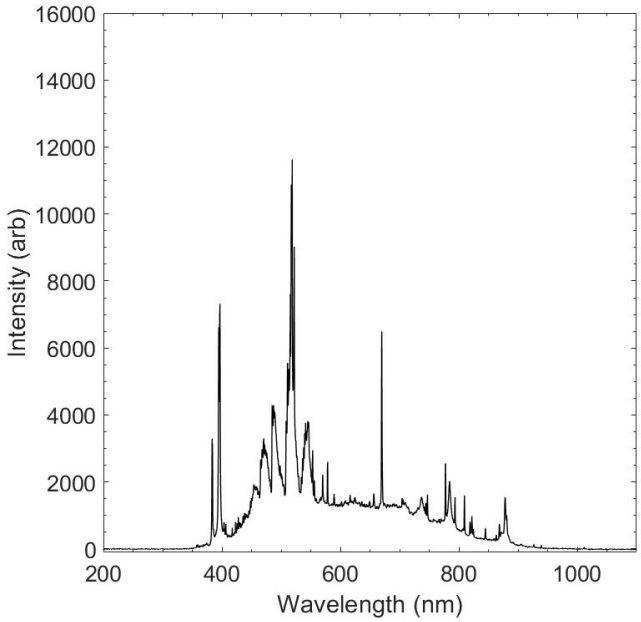

Fig. 63. Experiment OB05 Spectra

Observations and Notes

White aluminum oxide covered the electrodes and the interior of the steel enclosure. Due to the minimal mass loss of the electrodes, and scale accuracy, the mass loss was not measured.

3.2.2. Experiment ID: OB06

This experiment was performed on August 23, 2019. The electrical characteristics are presented in Table 22. Photos of Experiment OB06 are presented in Fig. 64 and Fig. 65, while the electrical measurements are presented in Fig. 66 and Fig. 67.

Table 22. Experiment OB06 experiment parameters

Electrical Parameter	Target	Actual	Other
Voltage (V_{L-L})	1 000	1 007	424 (Arc)
Current (A)	15 000	11 959	
Duration (ms)	2 000	2 020	
Energy (MJ)		12.591	
Other Parameters			
Electrode Length Loss (cm)	10.8 (Phase A)	15.9 (Phase B)	8.3 (Phase C)
Electrode Mass Loss (g)	264.5	263.0	212.5
Electrode Material		Aluminum	
Electrode Diameter		2.54 cm (1.0 in)	
Electrode Spacing		8.9 cm (3.5 in) on center	
Shorting Wire		2 – 24 AWG (0.511 mm diameter), single strand tinned copper	
Box Electrical Configuration		Neutral	
Generator Configuration		Neutral not tied to ground	
Enclosure Breach		Bottom, both sides and top	
Enclosure Mass Loss (g)		1 670	

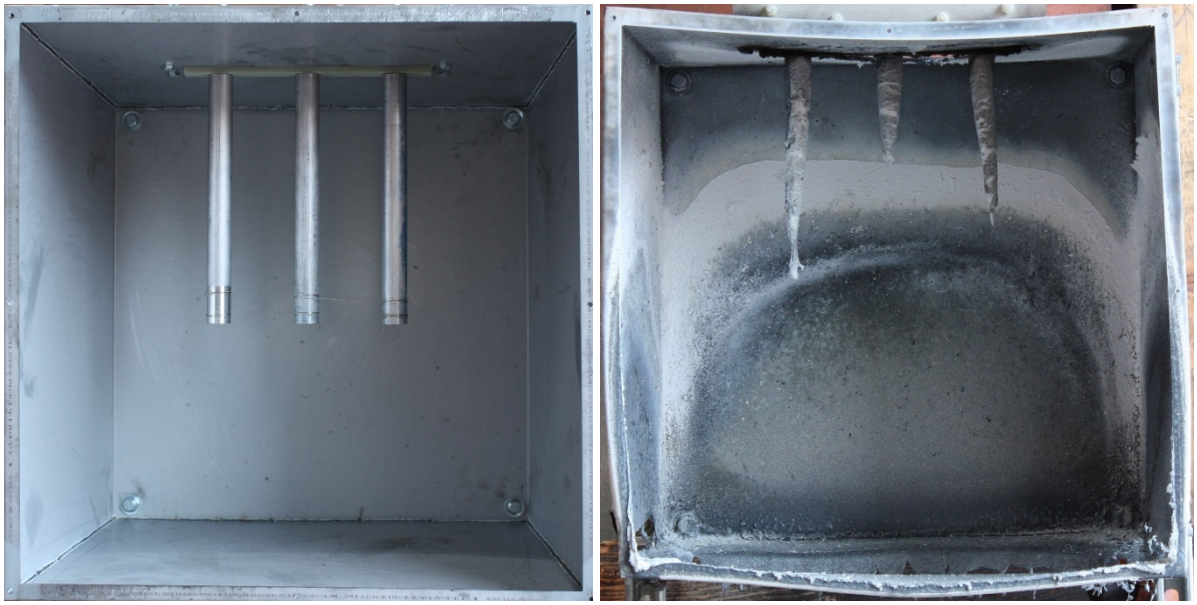

Fig. 64. Experiment OB06 pre-experiment (left) and post-experiment (right) electrodes. Phase sequence from left-to-right is C-B-A.

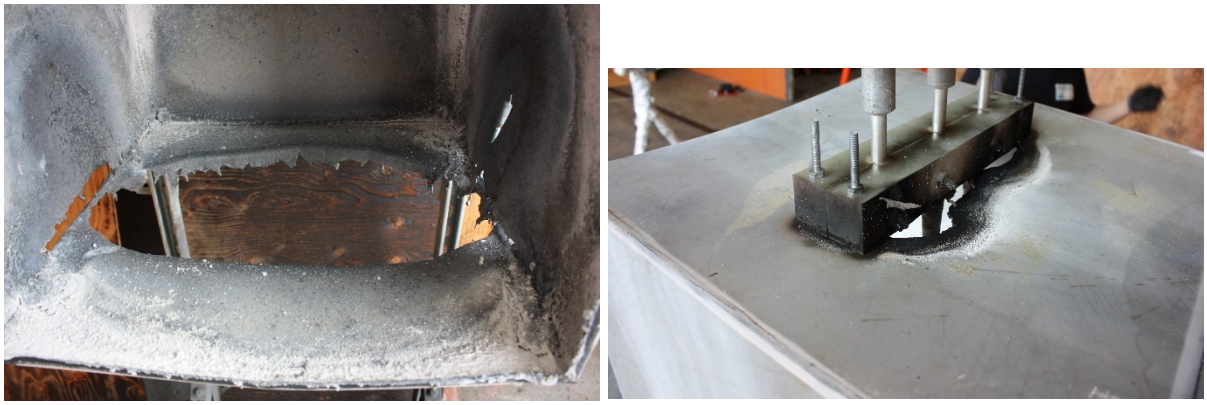

Fig. 65. Experiment OB06 enclosure breach (Left –bottom and sides; Right – rear top side)

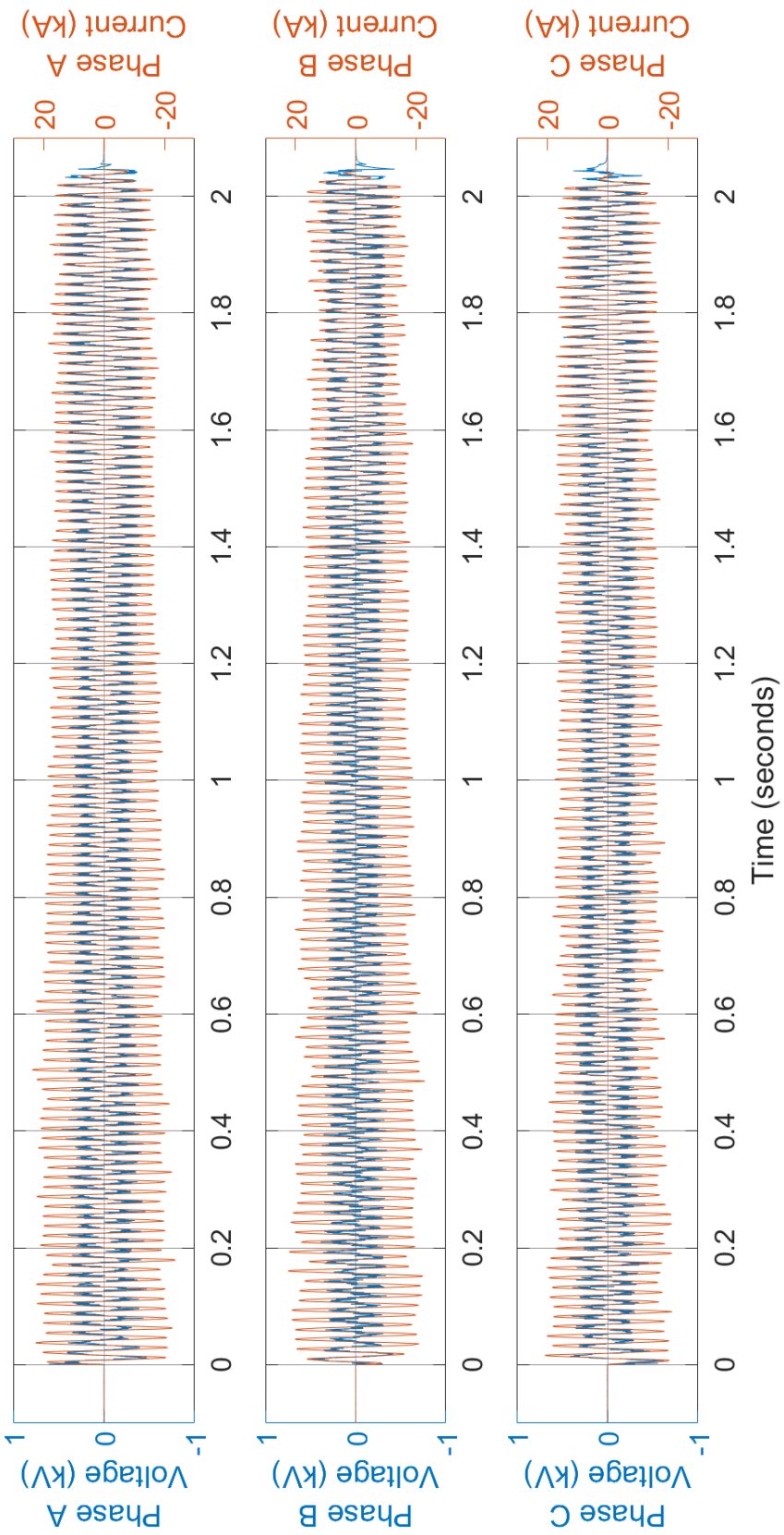

Fig. 66. Voltage and current measurements for Experiment OB06

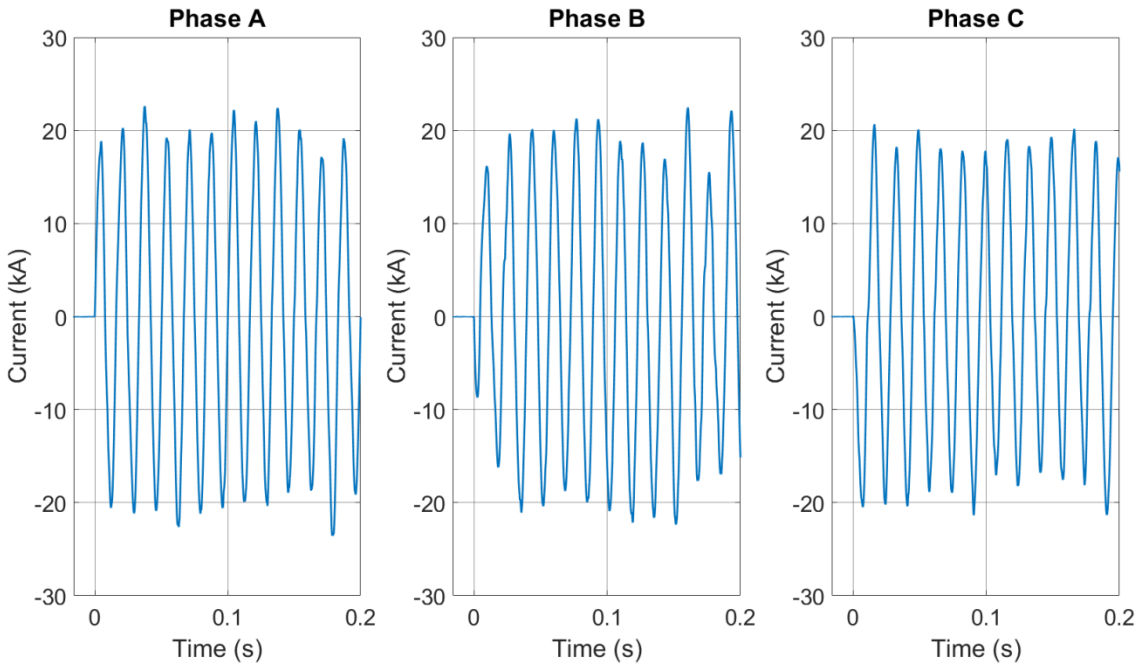

Fig. 67. Experiment OB06 transient current profiles

SNL used a radiometer to measure the incident energy during the experiment. The measurement specifics and results are presented in Table 23.

Table 23. Experiment OB06 radiometer measurement

Distance from Electrode (cm)	Thickness (mm)	ΔT (°C)	Calculated Incident Energy (MJ/m²)	Calculated Energy (MJ)
182.9	3	27.4	0.28	11.97

The SNL spectral emission measurement was attempted, but the neutral density filter placed in front of the detector attenuated the signal to the extent that no useful spectra were collected.

Observations and Notes

The estimated mass loss from the enclosure is approximately 1,670 grams and a total breach opening on all sides of approximately 1,189 cm^2. Bottom opening of approximately 1035 cm^2, left side approximately 40 cm^2, right side approximately 50 cm^2 and a top opening of approximately 64 cm^2.

3.2.3. Experiment ID: OB07

This experiment was performed on August 23, 2019. The electrical characteristics are presented in Table 24. Photos of Experiment OB07 are presented in Fig. 68 and Fig. 69, while the electrical measurements are presented in Fig. 71 through Fig. 72.

Table 24. Experiment OB07 experiment parameters

Electrical Parameter	Target	Actual	Other
Voltage (V_{L-L})	1 000	1 007	431 (arc)
Current (A)	15 000	12 952	
Duration (ms)	1 500	1 520	
Energy (MJ)		10.233	
Other Parameters			
Electrode Length Loss (cm)	7.0 (Phase A)	10.2 (Phase B)	5.7 (Phase C)
Electrode Mass Loss (g)	178	223	151
Electrode Material		Aluminum	
Electrode Diameter		2.54 cm (1.0 in)	
Electrode Spacing		8.9 cm (3.5 in) on center	
Shorting Wire		2 – 24 AWG (0.511 mm diameter), single strand tinned copper	
Box Electrical Configuration		Neutral	
Generator Configuration		Neutral not tied to ground	
Enclosure Breach		Bottom, both sides, and top	
Enclosure Mass Loss (g)		861	

Fig. 68. Experiment OB07 pre-experiment (left) and post-experiment (right) electrodes. Phase sequence from left-to-right is C-B-A.

Fig. 69. Experiment OB07 enclosure breach (Left – bottom and sides; Right – rear top side).

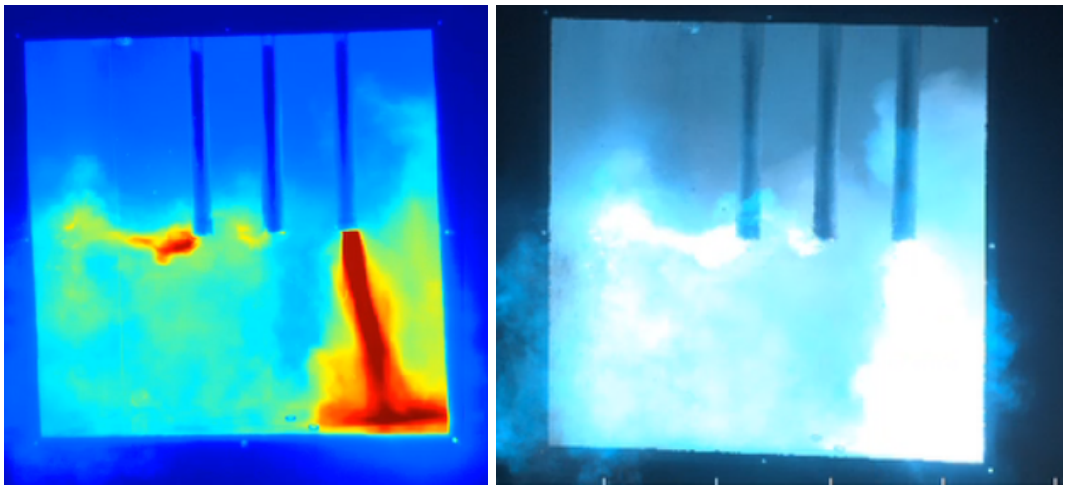

Fig. 70. Experiment OB07 thermal (left) and visible (right) video still shot during the arc (t = 0.06 s)

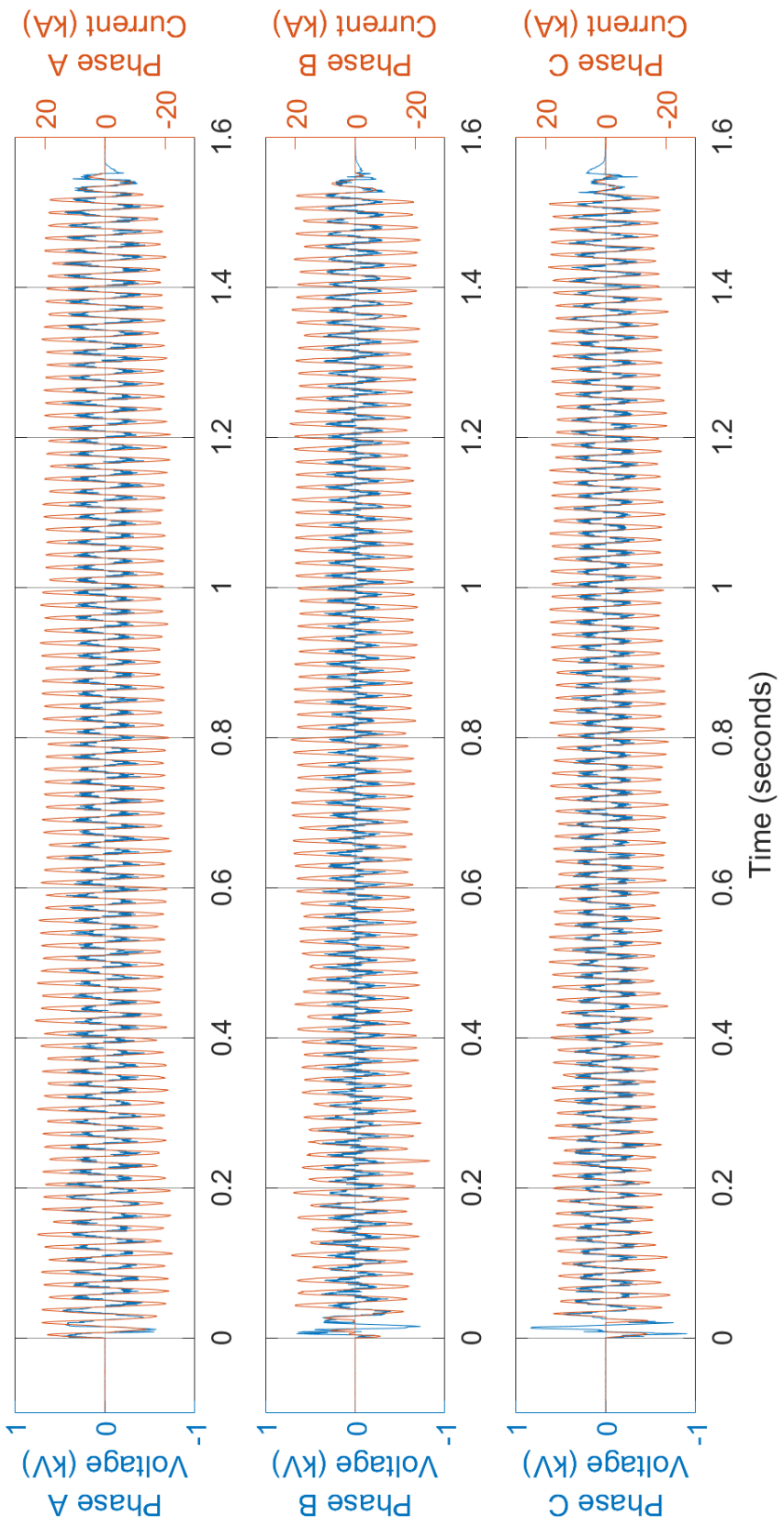

Fig. 71. Experiment OB07 voltage and current measurements

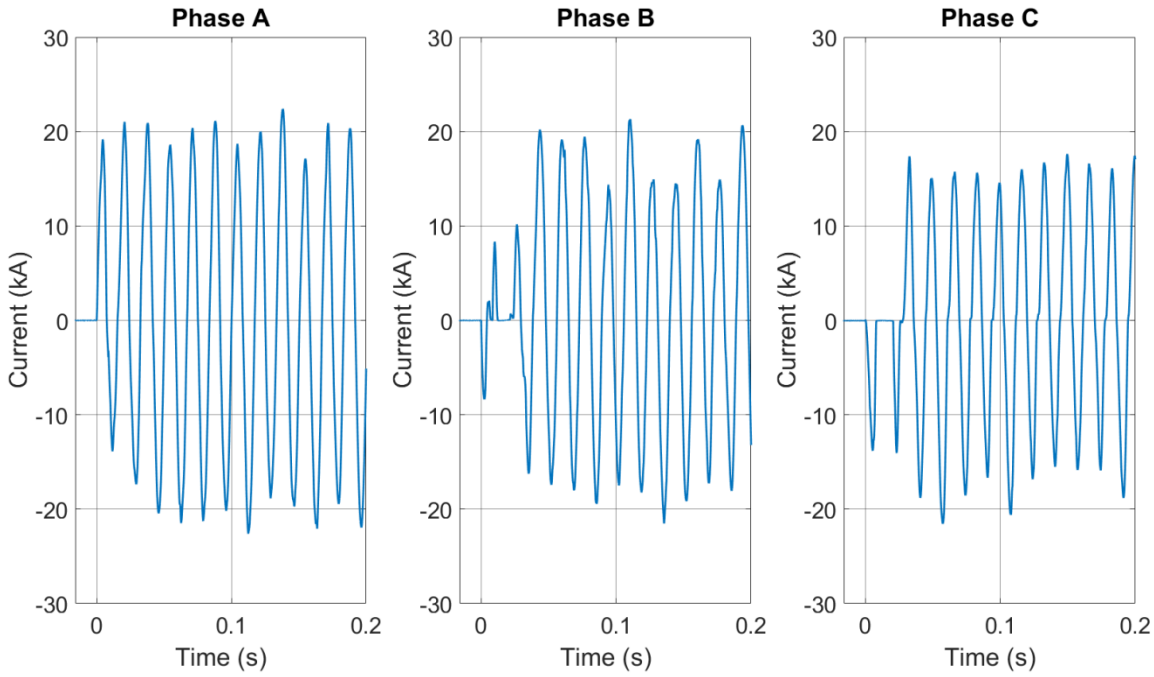

Fig. 72. Experiment OB07 transient current profiles

SNL used a radiometer to measure the incident energy during the experiment. The measurement specifics and results are presented in Table 25.

Table 25. Experiment OB07 radiometer measurement

Distance from Electrode (cm)	Thickness (mm)	ΔT (°C)	Calculated Incident Energy (MJ/m²)	Calculated Energy (MJ)
182.9	3	18.7	0.19	8.17

SNL used the spectrometer during this experiment. The Iris was opened to 1 mm with a 0.6 neutral density filter in place. The detector was positioned to focus approximately 7.6 cm (3 in) below the center copper electrode tip (Phase B). The spectrum from this experiment is presented in Fig. 73. Initial spectra contained metallic features, Fig. 73 (top), before transitioning to broadband emission, Fig. 73 (bottom left and bottom right).

The optical emission spectroscopy can be used to infer temperatures from the arc and from the surrounding environment. For this experiment, the spectrometer measurement volume was placed 3 inches below the central aluminum electrode to collect 'non metallic' spectra. A neutral density filter of OD = 0.6 was placed in front of the spectrometer. The broadband, gray body emission, can be assumed to follow a black body curve. The curve can be calibrated using a black body source and the same geometry as the experiment. If possible, it is a best practice to calibrate in-situ of the experiment, which was not possible for this series. The data in Fig. 73 are not corrected for detector nonlinearity, efficiency, or background – in the case of the top spectrum.

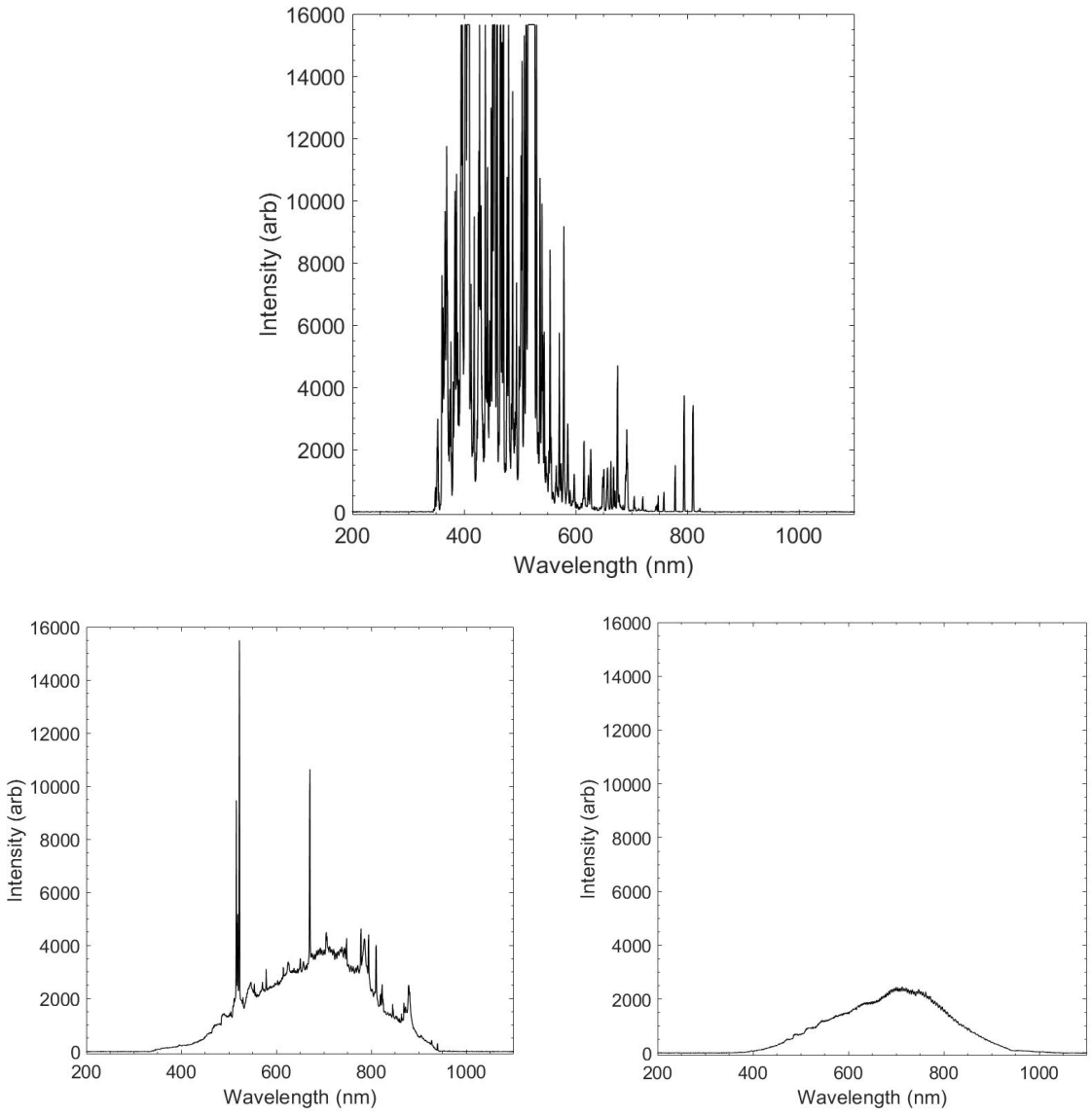

Fig. 73. Experiment OB07 spectral profiles from showing an early profile with spectral features (top), transition spectral features (bottom left), and a broadband emission spectrum (bottom right).

Observations and Notes

The estimated mass loss from the enclosure is approximately 861.4 grams and a total breach opening on all sides of approximately 613 cm^2 (bottom opening of approximately 549 cm^2, left side approximately 6 cm^2, right side approximately 19 cm^2 and a top opening of approximately 39 $cm^{2)}$.

3.2.4. Experiment ID: OB08

This experiment was performed on August 23, 2019. The electrical characteristics are presented in Table 26. Photos of Experiment OB08 are presented in Fig. 74 and Fig. 75. A photo of the post-experiment electrodes with comparative electrode at bottom is shown in Fig. 76. The electrical measurements are presented in Fig. 77 and Fig. 78.

Table 26. Experiment OB08 experiment parameters

Electrical Parameter	Target	Actual	Other
Voltage (V_{L-L})	1 000	1 062	748 (arc)
Current (A)	30 000	24 870	
Duration (ms)	1 000	1 020	
Energy (MJ)		19.57	
Other Parameters			
Electrode Length Loss (cm)	0.8 (Phase A)	0.8 (Phase B)	0.8 (Phase C)
Electrode Mass Loss (g)	210.0	216.0	170.5
Electrode Material		Aluminum	
Electrode Diameter		2.54 cm (1.0 in)	
Electrode Spacing		8.9 cm (3.5 in) on center	
Shorting Wire		2 – 24 AWG (0.511 mm diameter), single strand tinned copper	
Box Electrical Configuration		Neutral	
Generator Configuration		Neutral not tied to ground	
Enclosure Breach		Yes	
Enclosure Mass Loss (g)		72	

Fig. 74. Experiment OB08 pre-experiment (left) and post-experiment (right) electrodes. Phase sequence from left-to-right is C-B-A.

Fig. 75. Experiment OB08 enclosure breach (Left –bottom and sides; Right – rear top).

Fig. 76. Experiments OB08 aluminum electrodes post-experiment top three. (Bottom electrode is from other another experiment and included for comparison)

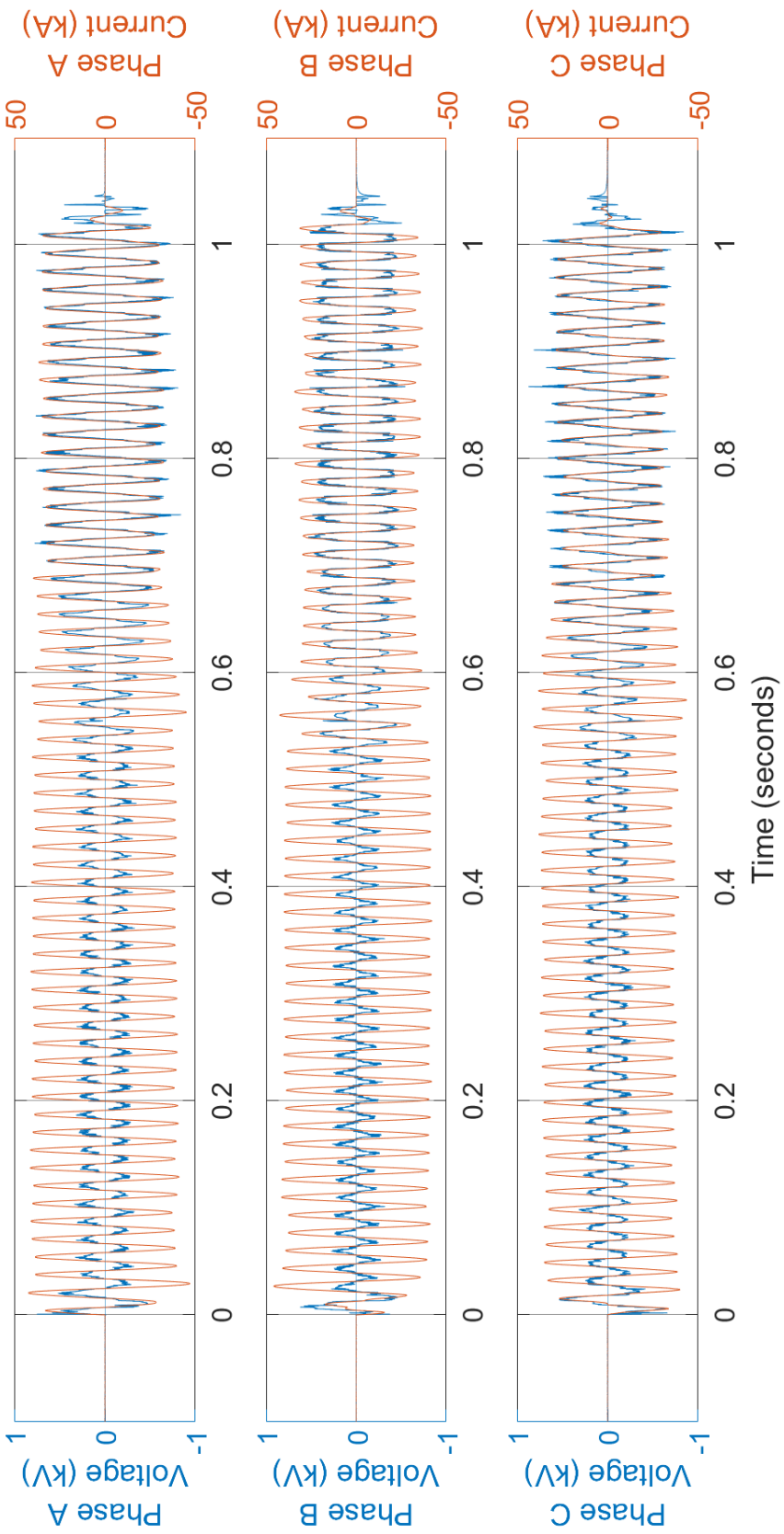

Fig. 77. Voltage and current measurements for Experiment OB08

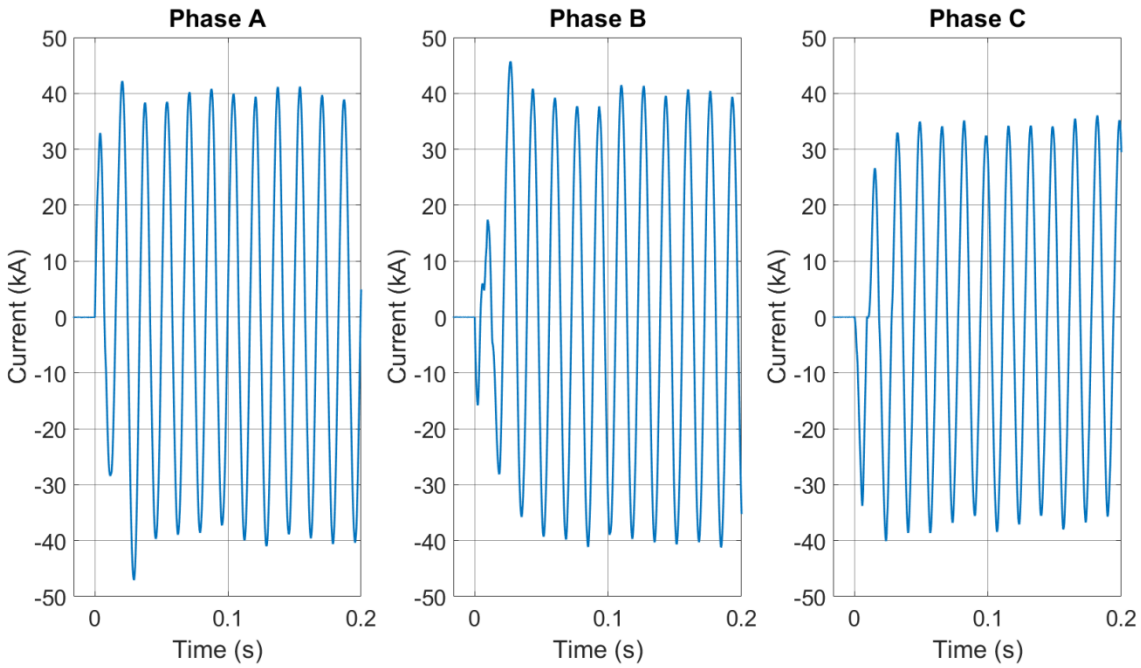

Fig. 78. Experiment OB08 transient current profiles

SNL used a radiometer to measure the incident energy during the experiment. The measurement specifics and results are presented in Table 27.

Table 27. Experiment OB08 radiometer measurement

Distance from Electrode (cm)	Thickness (mm)	ΔT (°C)	Calculated Incident Energy (MJ/m^2)	Calculated Energy (MJ)
182.9	3	37.1	0.39	16.2

SNL used the spectrometer during this experiment. The Iris was opened to 1 mm with a 0.6 neutral density filter in place. The detector was positioned to focus approximately 7.6 cm (3 in) below the center copper electrode tip (Phase B). This was to capture 'non-metallic' arc profiles. Broadband profiles varied throughout the experiments. The spectrum from this experiment is presented in Fig. 79.

These three spectra contain a few weak spectral features, but they are dominated by gray body emission. Because the material generated by the arc or from the surrounding environment was never characterized, the exact radiators are unknown. Likely, these spectra are dominated by smoke particulate matter.

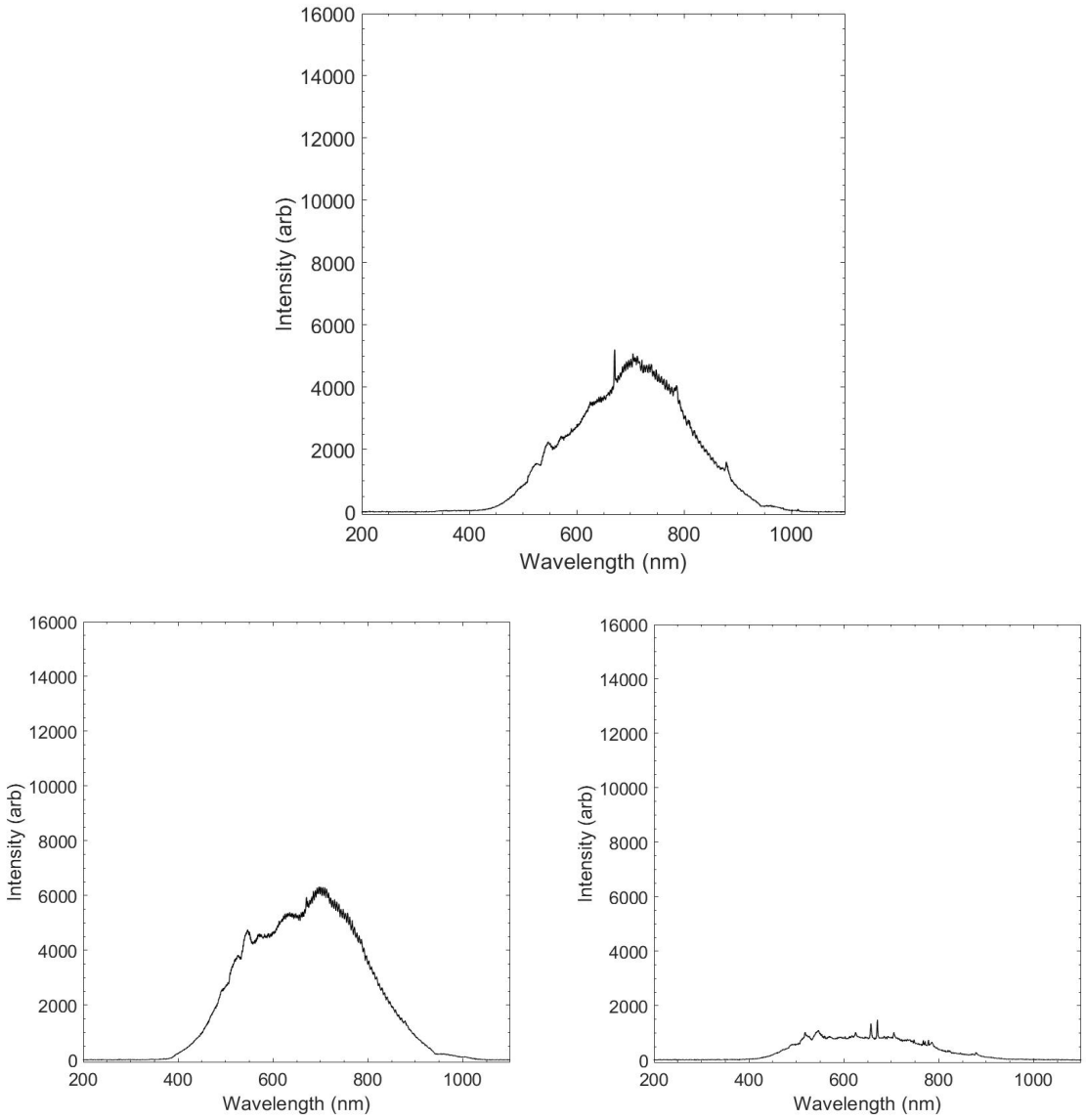

Fig. 79. Experiment OB08 spectra showing an early profile with spectral features (top), transition spectral features (bottom left), and a broadband emission spectra (bottom right).

Observations and Notes

The steel enclosure was breached. The Phase B electrode was ejected from the enclosure. The Phase A and C electrodes were deflected towards the steel box sides. All aluminum electrodes broke during experiment near the dog bone area at the rod holder. There is evidence from the thermal damage and examination of the rod top halves that the rods were arcing above the box for some time. The change in the electrical current and voltage waveform just prior to 0.6 s provides an indication of when the failure may have occurred.

The estimated mass loss from the enclosure is approximately 72 g and a total breach opening on all sides of approximately 51 cm^2. Bottom opening of approximately 40 cm^2 and a top opening of approximately 11 cm^2.

3.2.5. Experiment ID: OB10

This experiment was performed on August 22, 2019. The electrical characteristics are presented in Table 28. Photos of Experiment OB10 are presented in Fig. 80 and Fig. 81, while the electrical measurements are presented in Fig. 82 and Fig. 83.

Table 28. Experiment Parameters Experiment OB10

Electrical Parameter	**Target**	**Actual**	**Other**
Voltage (V_{L-L})	1 000	1 028	381 (arc)
Current (A)	5 000	4 869	
Duration (ms)	2 000	2 010	
Energy (MJ)		4.118	
Other Parameters			
Electrode Length Loss (cm)	9.8 (Phase A)	10.0 (Phase B)	5.4 (Phase C)
Electrode Mass Loss (g)	61	60	54
Electrode Material	Aluminum		
Electrode Diameter	1.27 cm (0.5in)		
Electrode Spacing	8.9 cm (3.5 in) on center		
Shorting Wire	2 – 24 AWG (0.511 mm diameter), single strand tinned copper		
Box Electrical Configuration	Neutral		
Generator Configuration	Neutral tied to ground via impedance		
Enclosure Breach	None		

Fig. 80. Experiment OB10 Pre-experiment (left) and Post-experiment (right) electrodes. Phase sequence left-to-right (C-B-A)

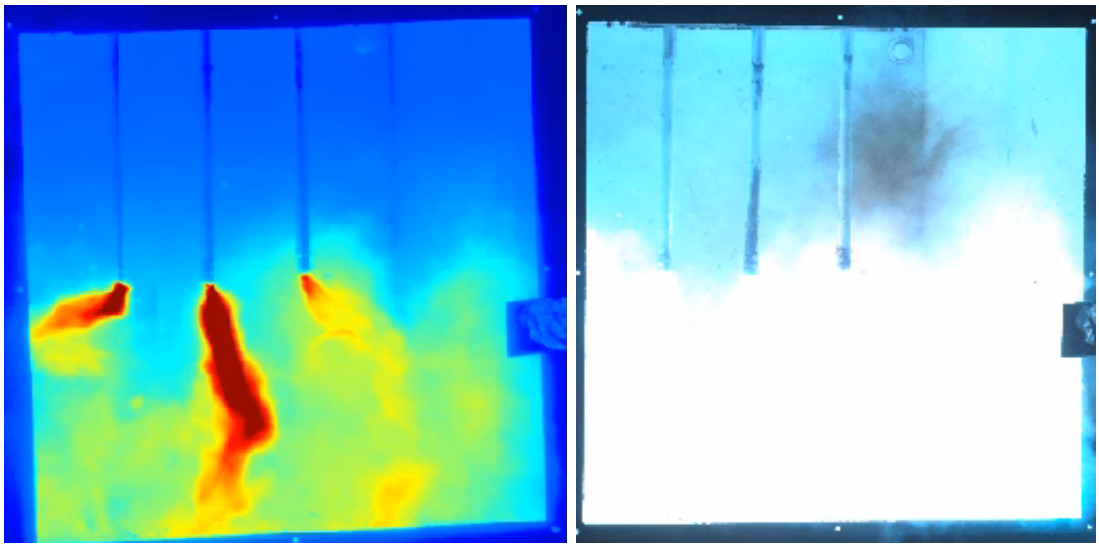

Fig. 81. Thermal (left) and Visible (right) video still shot during Experiment OB10 arc (t = 0.06s)

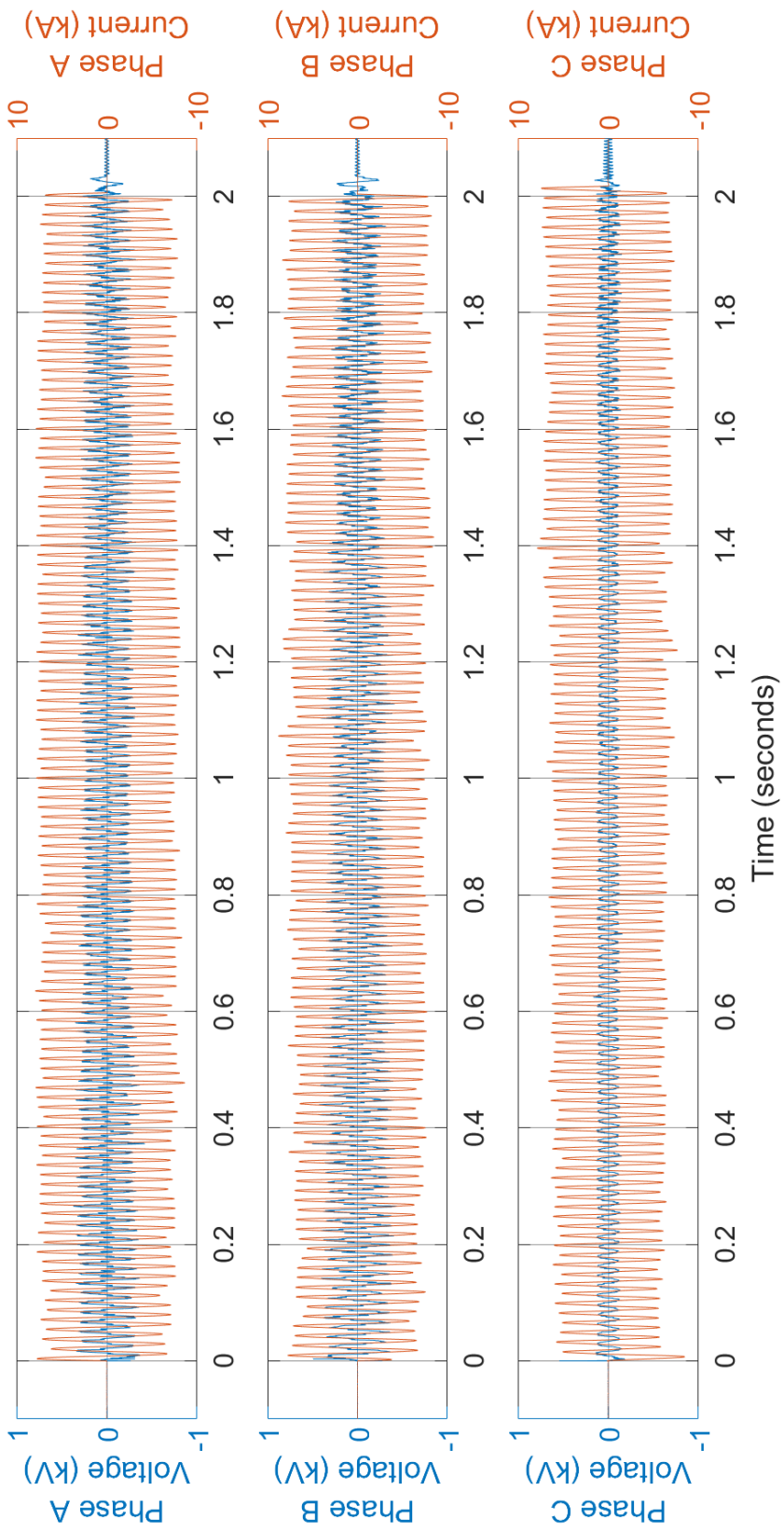

Fig. 82. Experiment OB10 voltage and current measurements

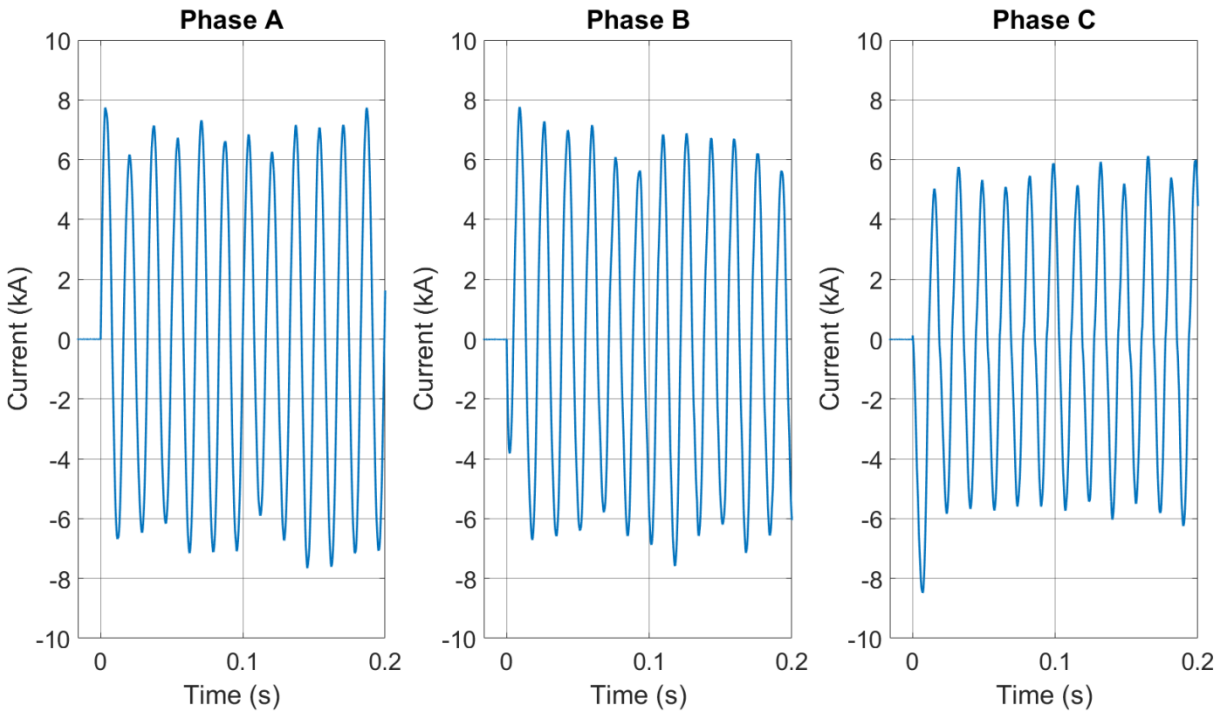

Fig. 83. Experiment OB10 transient current profiles

SNL used a radiometer to measure the incident energy during the experiment. The measurement specifics and results are presented in Table 29.

Table 29. Experiment OB10 radiometer measurement

Distance from Electrode (cm)	Thickness (mm)	ΔT (°C)	Calculated Incident Energy (MJ/m^2)	Calculated Energy (MJ)
45.7	1	423.4	1.47	3.85

SNL used the spectrometer during this experiment. The Iris was opened to 1 mm with a 0.6 neutral density optical density filter in place. The first several spectra saturated the detector, before the signal level decreased to a resolvable level. The signal level continued to decrease over the experiment. The detector was positioned to focus immediately below the center copper electrode tip (Phase B). The spectrum from this experiment is presented in Fig. 84.

The spectra intensity decreased for both the spectral features and the gray body emission throughout the experiment. These spectra have features from both atomic and molecular features, indicating emission from both metallic and reacting aluminum.

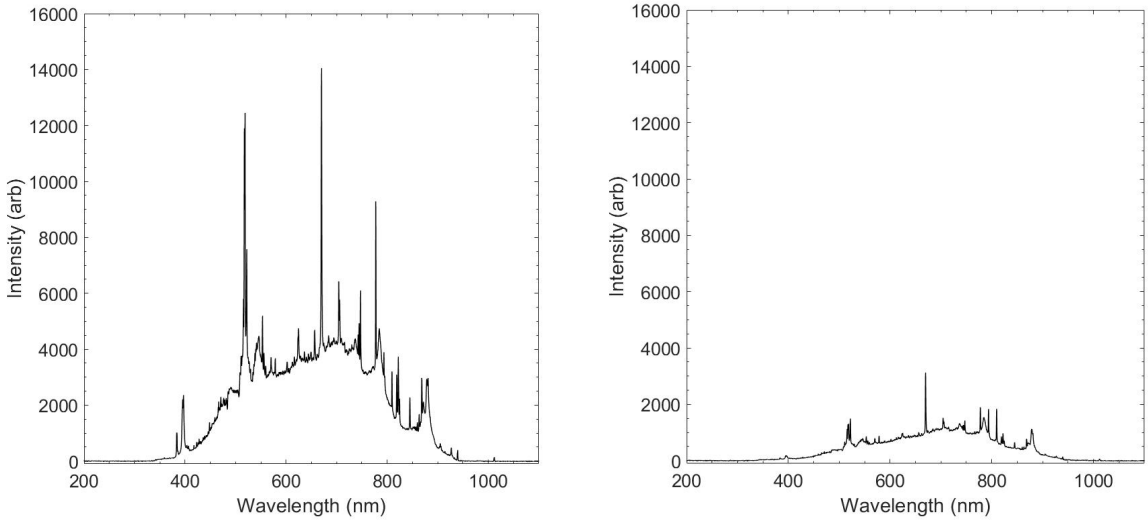

Fig. 84. Spectra taken during Experiment OB10 showing an early profile (left) and a late profile (right)

Observations and Notes

The electrodes were reused from Experiment OB05. The electrodes were shifted down following Experiment OB05 to ensure the bottom of the electrodes were at the center of the box.

3.3. Summary of Low-Voltage Box Experiments

Eleven low-voltage box experiments were performed at four different current levels and durations. The total electrical energy ranged from approximately 0.2 MJ to 20.2 MJ. Significant deflection of the electrodes was noted in the 30 kA experiments and those results should be used with caution.

With regard to mass loss, the aluminum electrodes experienced approximately 72% more mass loss than the copper electrodes when normalized to experiment arc energy. Given that the density of aluminum is slightly less than 1/3 that of copper (2.70 g/cm^3 versus 8.96 g/cm^3), aluminum electrodes lost almost twice (approximately 1.93 times) as much volume as copper for a given arc energy.

During these open box experiments, measurement devices recorded both the electrical energy (voltage and current) and calorimeter heat rise (ΔT in degrees C) of black 1mm (0.04 in) or 3mm (0.12 in) thick copper plate calorimeters, located a distance of 46 cm (18 in) or 183 cm (72 in) in front of the open boxes. To compare relative evolved energy collected on the calorimeters to electrical energy input, the equivalent radiated energy (radiated area* areal heat flux * time) indicated by the calorimeter was calculated and compared to the actual electrical energy (in MJ).

The evolved calorimeter energy in Table 31 and Fig. 85 was calculated as described in Section 2.4.4.1. This calculation assumes 100% absorption of incident radiation on the black copper calorimeter plates and either uniform arc radiation during the 1-3 second arc duration or similar spatial radiation for the Al and Cu arcs. Given measured ΔT values of 3.6 - 423 °C (38.5 - 793°F) and an expected thermocouple uncertainty of ± 1.2 °C (2.2 °F), the data shown in Fig. 85 appears well above uncertainties, and to show a significant difference in radiated energy as a function of metal electrode composition.

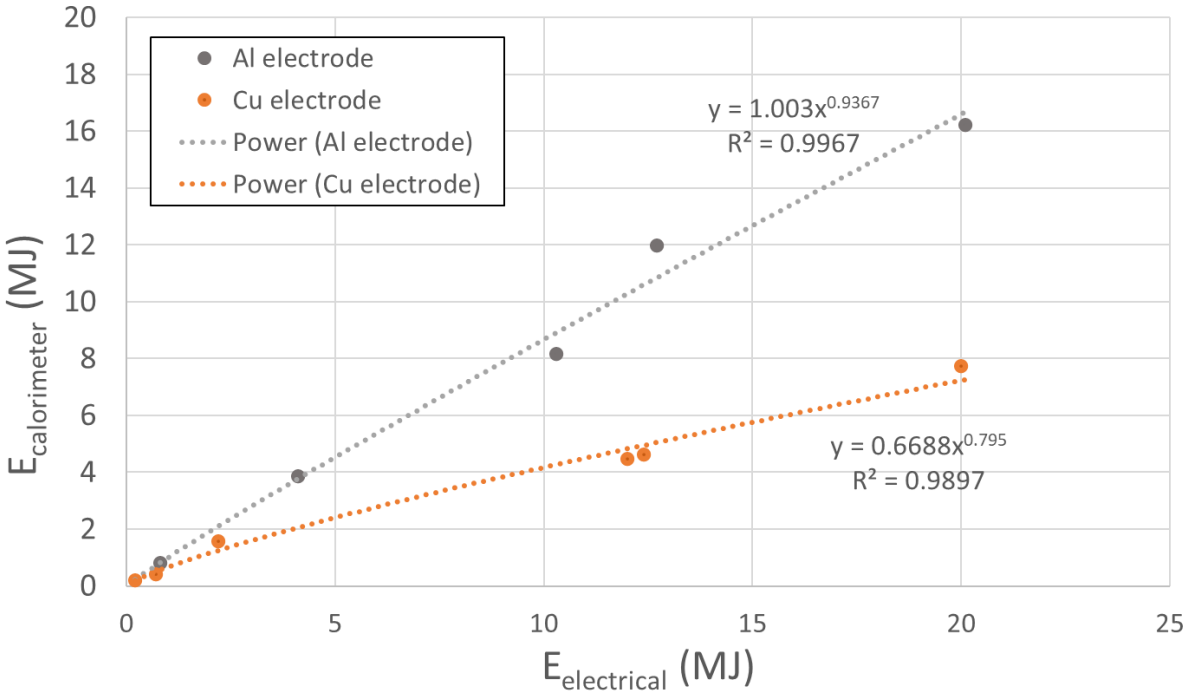

Fig. 85. Comparison of actual electrical energy input and calculated calorimeter energy, with power law fits indicated by dashed lines.

Table 30. Summary of low-voltage box experiments

EXPERIMENT			Rod Material		Rod Diameter (cm)		System Voltage (kV)			Current (kA)		Arc Duration (sec)		Energy (MJ)	Notes
#	Seq	Date	Al	Cu	1.3	2.5	Target	Actual	Arc	Target	Actual	Target	Actual	Actual	
OB01(a)	1	Aug 22		X	X		1.00	1.03	0.35	1.00	1.05	2.00	2.01	0.2	
OB01(b)	2	Aug 22		X	X		1.00	1.03	0.31	1.00	1.03	2.00	2.02	0.7	
OB02	9	Aug 30		X		X	1.00	1.01	0.27	15.00	14.02	2.00	2.02	12.0	
OB03	10	Aug 30		X		X	1.00	1.01	0.31	15.00	13.80	3.00	3.03	20.0	Duration changed from 4 seconds based on results from OB06, 07, and 02
OB04	11	Aug 30		X		X	1.00	1.06	0.28	30.00	27.79	1.00	1.03	12.4	
OB05	3	Aug 22	X		X		1.00	1.03	0.36	1.00	1.02	2.00	2.01	0.8	
OB06	6	Aug 23	X			X	1.00	1.01	0.42	15.00	11.96	2.00	2.02	12.7	
OB07	7	Aug 23	X			X	1.00	1.01	0.43	15.00	12.95	1.50	1.52	10.3	Duration changed from 4 seconds based on results from OB06
OB08	8	Aug 23	X			X	1.00	1.06	0.43	30.00	24.87	1.00	1.02	20.1	Phase 'B' electrode ejected, arcing outside box
OB09	5	Aug 22		X	X		1.00	1.03	0.30	5.00	4.79	2.00	2.01	2.2	Phase A voltage waveform not reported.
OB10	4	Aug 22	X		X		1.00	1.03	0.38	5.00	4.87	2.00	2.01	4.1	

Table 31. Low-voltage box experiment comparison of measured electrical energy and calculated energy from calorimeter heat rise

EXPERIMENT			Rod Material		Electrical Energy	Radiometer Calculated Energy	Radiometer Thickness	Distance	Radiometer ΔT
#	Seq	Date	Al	Cu	(MJ)	(MJ)	(mm)	(cm)	(°C)
OB01(a)	1	Aug 22		X	0.2	0.197	1	46	21.6
OB01(b)	2	Aug 22		X	0.7	0.410	1	46	45.1
OB02	9	Aug 30		X	12.0	4.456	3	183	10.2
OB03	10	Aug 30		X	20.0	7.733	3	183	17.7
OB04	11	Aug 30		X	12.4	4.631	3	183	10.6
OB05	3	Aug 22	X		0.8	0.807	1	46	88.7
OB06	6	Aug 23	X		12.7	11.970	3	183	27.4
OB07	7	Aug 23	X		10.3	8.170	3	183	18.7
OB08	8	Aug 23	X		20.1	16.208	3	183	37.1
OB09	5	Aug 22		X	2.2	1.573	3	183	3.6
OB10	4	Aug 22	X		4.1	3.854	1	46	423.4

4. Medium-Voltage Experiment Results

The experiments laboratory performed calibration runs to ensure that the power circuits selected met the experimental program needs. The calibrations were measured at a shorting bus within the laboratory's facility and the actual experiments conditions were slightly different because of the additional circuit length to the open box and that of the open box. The resulting calibrations experiments are presented in Table 32, with detail provided in the KEMA experiment report (Appendix B).

Table 32. Medium-Voltage circuit calibration.

Voltage (Volts)	Current Sym (kA)	Current Peak (kA)	Circuit
6,900	15.3	42.9	190916-9002
6,900	30.6	86.5	190916-9004

The calibration experiments were performed for about 10 cycles to ensure stabilization of the waveform. The duration of the arc during the actual experiments was determined by the ability to maintain the arc within the enclosure and the breaking of the circuit by the experiment laboratory's protective device(s). Provided that the arc did not prematurely extinguish prior to the desired arc time, the experiments laboratory ensured that the arc duration parameter was met by automatically triggering their protectives devices to open at the specified duration. Because there was a delay in the opening of the circuit (breaker opening time), the actual durations were longer than the desired durations. Table 7 present the experimental parameter variations planned for this series of experiments.

Table 33. Medium-voltage experiments planned nominal parameters

Experiment No. #	Rod Material		Bus size (cm)		System Voltage (kV)	Current (kA)	Duration (s)
	Al	Cu	7.6	10.2			
OBMV1	X			X	6.9	15.0	2
OBMV2	X			X	6.9	30.0	1
OBMV3	X			X	6.9	15.0	5
OBMV4		X	X		6.9	15.0	5
OBMV5		X	X		6.9	30.0	2

The following provides a quick summary of the experimental configuration and results for each medium-voltage open box experiment. The opportunity arose to perform medium-voltage open box experiments because the medium-voltage bus duct experiments were not being performed. The final experiment configurations were based on the availability of materials (enclosure and bus bars) and the parameters were chosen to allow for comparison between medium-voltage experiments and between medium-voltage and low-voltage experiments. Changes to the open box experimental durations were made based on observations and model predictions.

For each experiment, the following information is provided:

- Experiment specifications
- Electrode length and mass
- Photo of pre- and post-experiment configuration
- Photo of enclosure breach (if applicable)
- Photo of bus bars post-experiment
- Voltage and current profile
- SNL Measurements (if applicable)
- Notes
- Observations

A summary of the medium-voltage box experiments is presented at the end of this section.

4.1. Medium-voltage Experimental Results with Copper Electrodes

Two experiments were performed at medium-voltage in the box configuration with copper electrodes. These were Experiments OBMV04 and OBMV05. The results from these experiments are presented next.

4.1.1. Experiment ID: OBMV04

This experiment was performed on September 17, 2019. The electrical characteristics are presented in Table 34. Photos of Experiment OBMV04 are presented in Fig. 86 through Fig. **88** while the electrical measurements are presented in Fig. 89 through Fig. 91.

Table 34. Experiment OBMV04 experiment parameters

Electrical Parameter	Target	Actual	Other
Voltage (V_{L-L})	6 900	6 915	543 (arc)
Current (A)	15 000	14 330	
Duration (ms)	5 000	5 080	
Energy (MJ)		51.8	
Other Parameters			
Electrode Length Loss (cm)	12.4 (Phase A)	12.1 Phase B)	12.1 (Phase C)
Electrode Mass Loss (g)	1 066.0	1 104.0	1 082.0
Electrode Material		Copper	
Electrode Dimensions		1.27 cm (0.5in) x 7.6 cm (3.0in)	
Electrode Spacing		13 cm (5 in) on center	
Shorting Wire		2 – 24 AWG (0.511 mm diameter), single strand tinned copper	
Box Electrical Configuration		Neutral	
Generator Configuration		Neutral tied to ground via impedance	
Enclosure Breach		Sides, bottom, back	
Additional Cladding	Back	Sides	Bottom
Add. Cladding Thickness (cm)	0.29	0.18	0.18
Enclosure Mass Loss (g)		12 444	

Fig. 86. Experiment OBMV04 pre-experiment (left) and post-experiment (right) electrodes. Phase sequence from left to right is C-B-A.

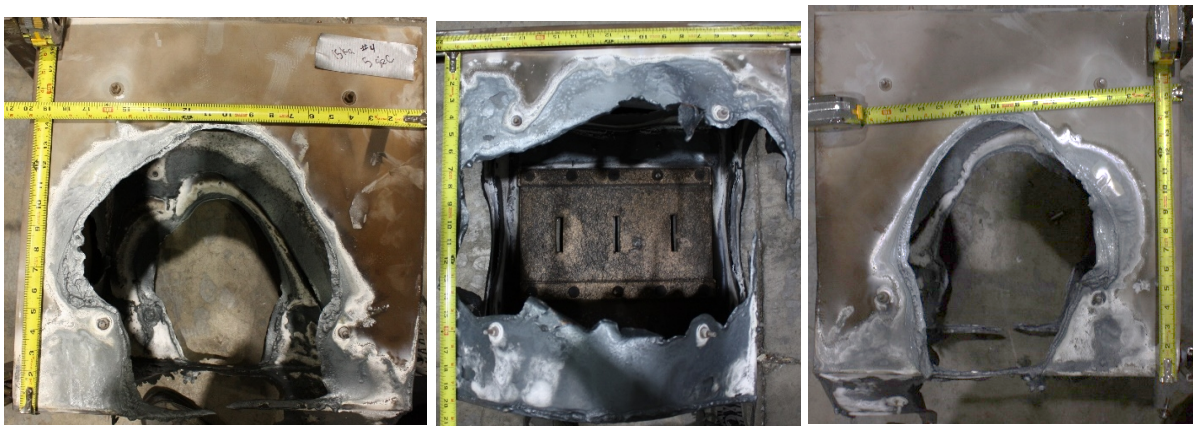

Fig. 87. Experiment OBMV4 enclosure breach (Left-to-right: Right side, back side, left side)

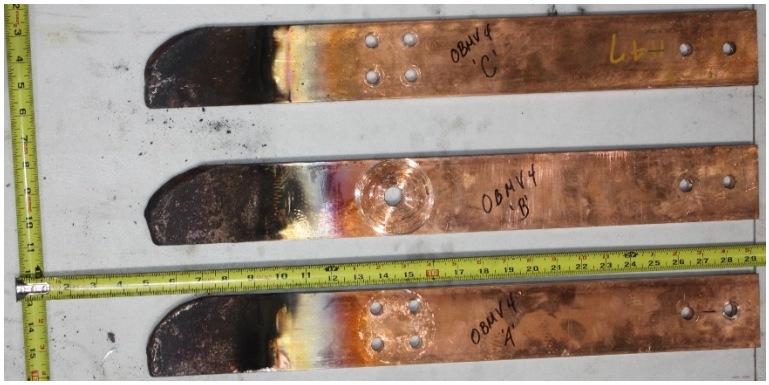

Fig. 88. Experiment OBMV4 electrode remanence post-experiment

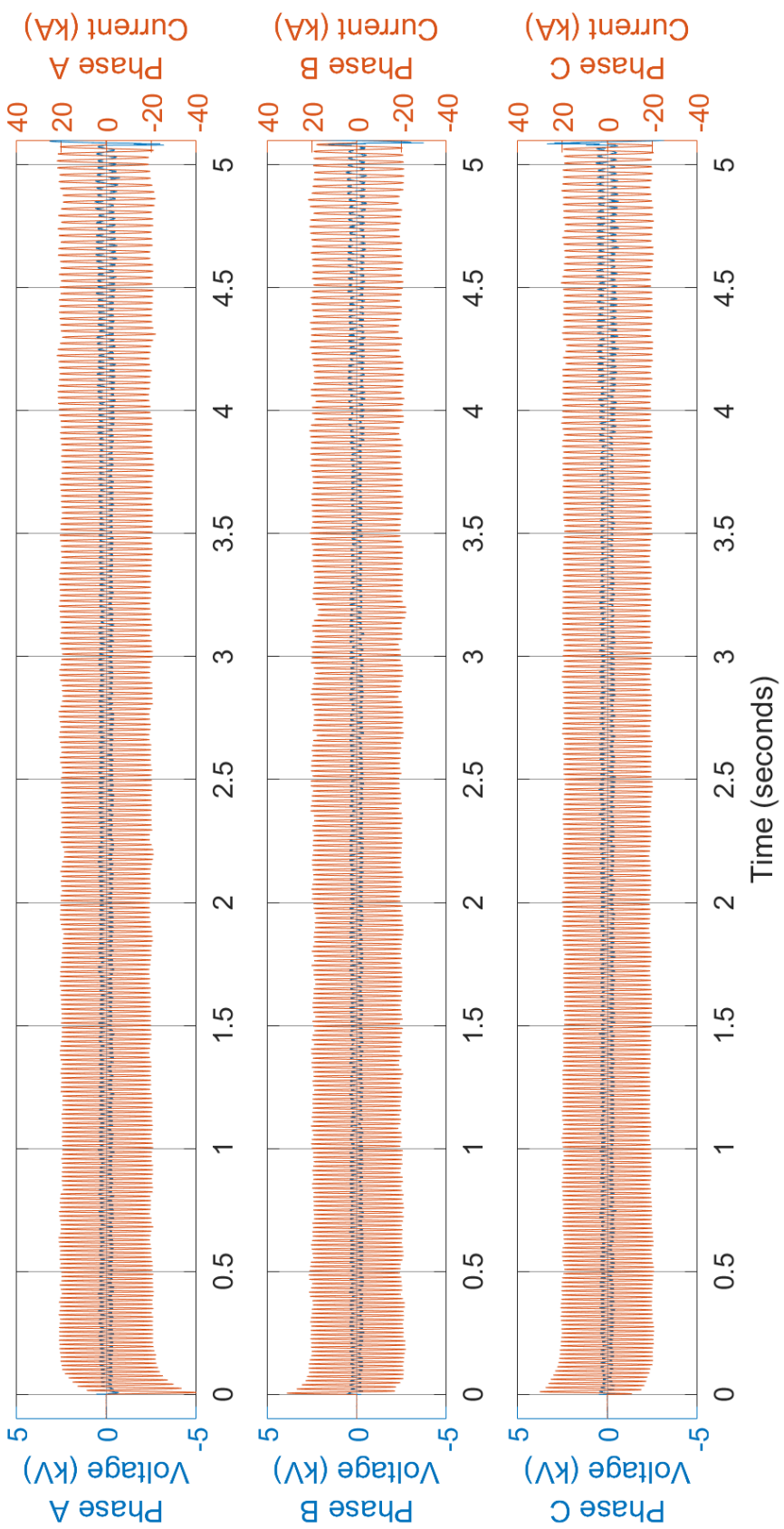

Fig. 89. Experiment OBMV04 voltage and current measurements

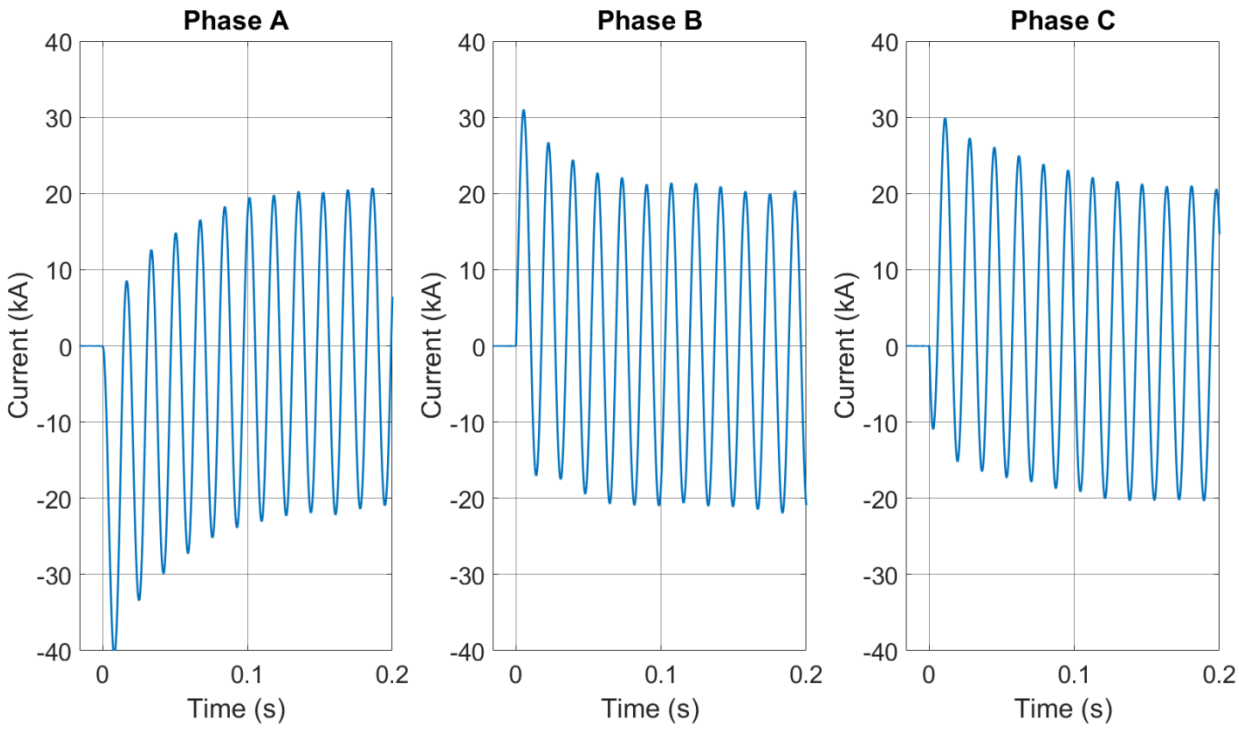

Fig. 90. Experiment OBMV04 transient current profiles

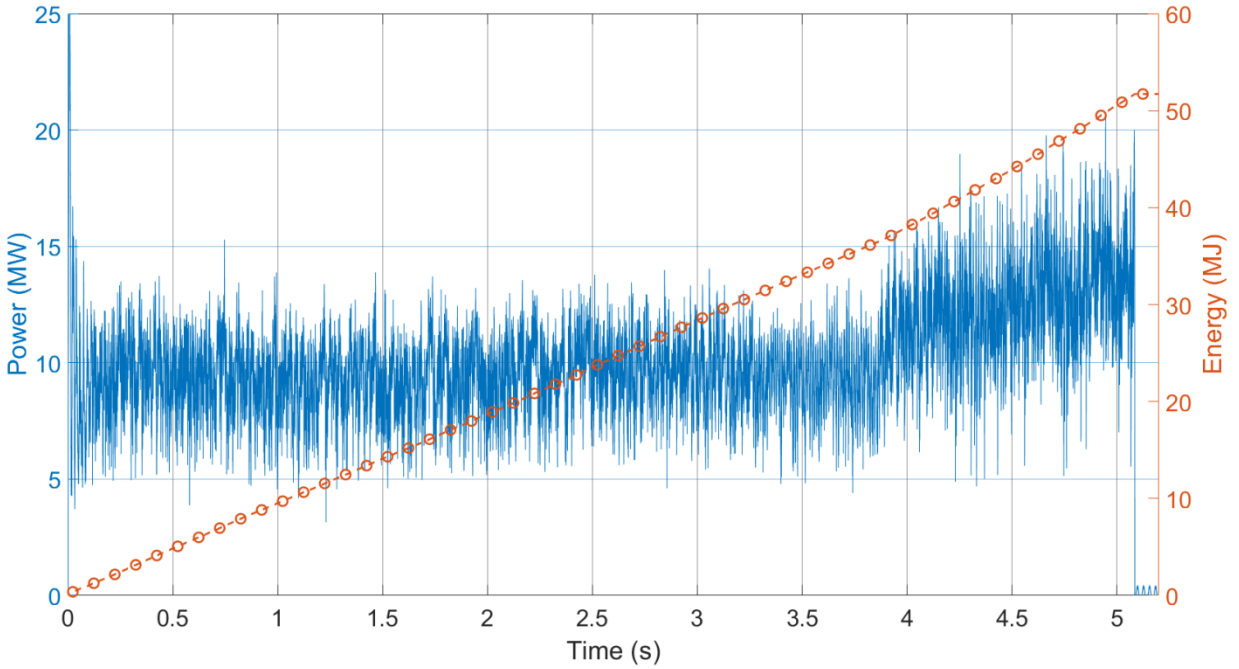

Fig. 91. Experiment OBMV04 power and energy profiles

A combination of thermal measurements devices including a plate thermometer, ASTM Slug Calorimeters, and thermal capacitance slugs (T_{cap}) were used in this experiment as described in Section 2.4.7. The resulting measured data is presented in Table 35.

Table 35. Experiment OBMV04 thermal measurements.

Location	Instrument (ID)	Max Heat Flux (kW/m^2) ± 1kW/m^2 or ± 5%	Average Heat Flux During Arc (kW/m^2) ± 1 kW/m^2 or ± 5%
Vertical	Plate Thermometer (2)	1 627	478
Location	**Instrument (ID)**	**Total Incident Energy (kJ/m^2) ± 1kJ/m^2 or ± 5%**	**Average Heat Flux During Arc (kW/m^2) ± 1 kW/m^2 or ± 5%**
Vertical	T_{cap} (1)	1 926	255
Horizontal	T_{cap} (3)	4 569	346
Horizontal	T_{cap} (4)	5 850	296
Location	**Instrument (ID)**	**Total Incident Energy (kJ/m^2) ± 18 kJ/m^2 or ± 4%**	**Time to Max Temperature (s) ± 3 %**
Vertical	ASTM (A)	1 137	6
Horizontal	ASTM (B)	2 575	8

Breakdown experiments: Prior to the HEAF, median breakdown voltage was 14 kV, resulting in a breakdown field of 28 kV/cm consistent with typical air breakdown strength of 25 kV/cm to 30 kV/cm. The breakdown voltage was also measured during the 5 second HEAF, and was observed to decrease to 12.3 kV, or approximately 24 kV/cm, with subsequent breakdowns occurring as low as 6.3 kV to 10 kV (12.6 kV/cm to 20 kV/cm). Again, this reduced holdoff strength appears real, but does not approach typical bus bar design electrical fields of 0.7 kV/cm to 1 kV/cm and would not be expected to result in propagating breakdown into nearby switchgear at these dielectric holdoff values.

Air conductivity measurements were taken during this experiment. Significant change in air conductance were observed at 4.27 m (14 ft) from the open box during the HEAF experiment. Air conductance values in the range of 1.6 E-5 mhos to 9 E-5 mhos (11 kohm to 62 kohm) were recorded; for the 0.5 cm (0.2 in) gap and 3.2 cm (1.25 in) radius sensor, this results in a conductivity of approximately 0.16 µS/cm to 9 µS/cm or 0.016 mS/m to 0.09 mS/m, similar to the conductivity of deionized water.

No EMI fields were detected above the ambient interference level trigger from this arc fault.

Observations and Notes

The estimated mass loss from the enclosure is approximately 12 444 grams and a total breach opening on all sides of approximately 2 796 cm^2 (bottom opening of approximately 1 224 cm^2, left side approximately 946 cm^2, and right side approximately 626 cm^2).

Burn through was observed on both sides, and bottom through all layers of cladding. The back side only had the internal cladding consumed.

4.1.2. Experiment ID: OBMV05

This experiment was performed on September 16, 2019. The electrical characteristics are presented in Table 36. Photos of Experiment OBMV05 are presented in Fig. 92 and Fig. 93, while the electrical measurements are presented in .Fig. 94 through Fig. 96.

Table 36. Experiment OBMV05 experiment parameters

Electrical Parameter	**Target**	**Actual**	**Other**
Voltage (V_{L-L})	6 900	6 917	405 (arc)
Current (A)	30 000	28 642	
Duration (ms)	2 000	2 320	
Energy (MJ)		43.5	
Other Parameters			
Electrode Length Loss (cm)	13.0 (Phase A)	12.7 (Phase B)	12.1 (Phase C)
Electrode Mass Loss (g)	1,009.5	1,142.0	1,064.0
Electrode Material	Copper		
Electrode Diameter	1.27 cm (0.5in) x 7.6 cm (3.0in)		
Electrode Spacing	13 cm (5 in) on center		
Shorting Wire	2 – 24 AWG (0.511 mm diameter), single strand tinned copper		
Box Electrical Configuration	Neutral		
Generator Configuration	Neutral tied to ground via impedance		
Enclosure Breach	Side and top		
Additional Cladding	Back	Left	Right	Bottom
Add. Cladding Thickness (cm)	0.29	0.18	0.29	0.18
Enclosure Mass Loss (g)	5 666			

Fig. 92. Experiment OB MV05 pre-experiment (top) and post-experiment (bottom). Phase sequence from left to right is C-B-A.

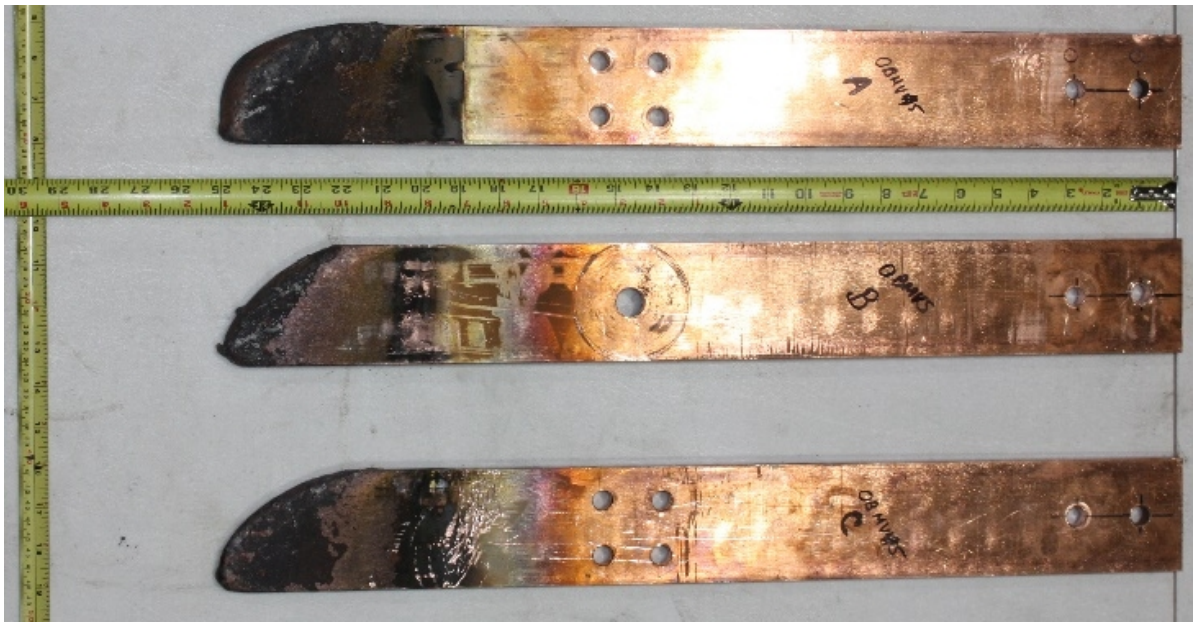

Fig. 93. Experiment OBMV5 copper electrodes post-experiment

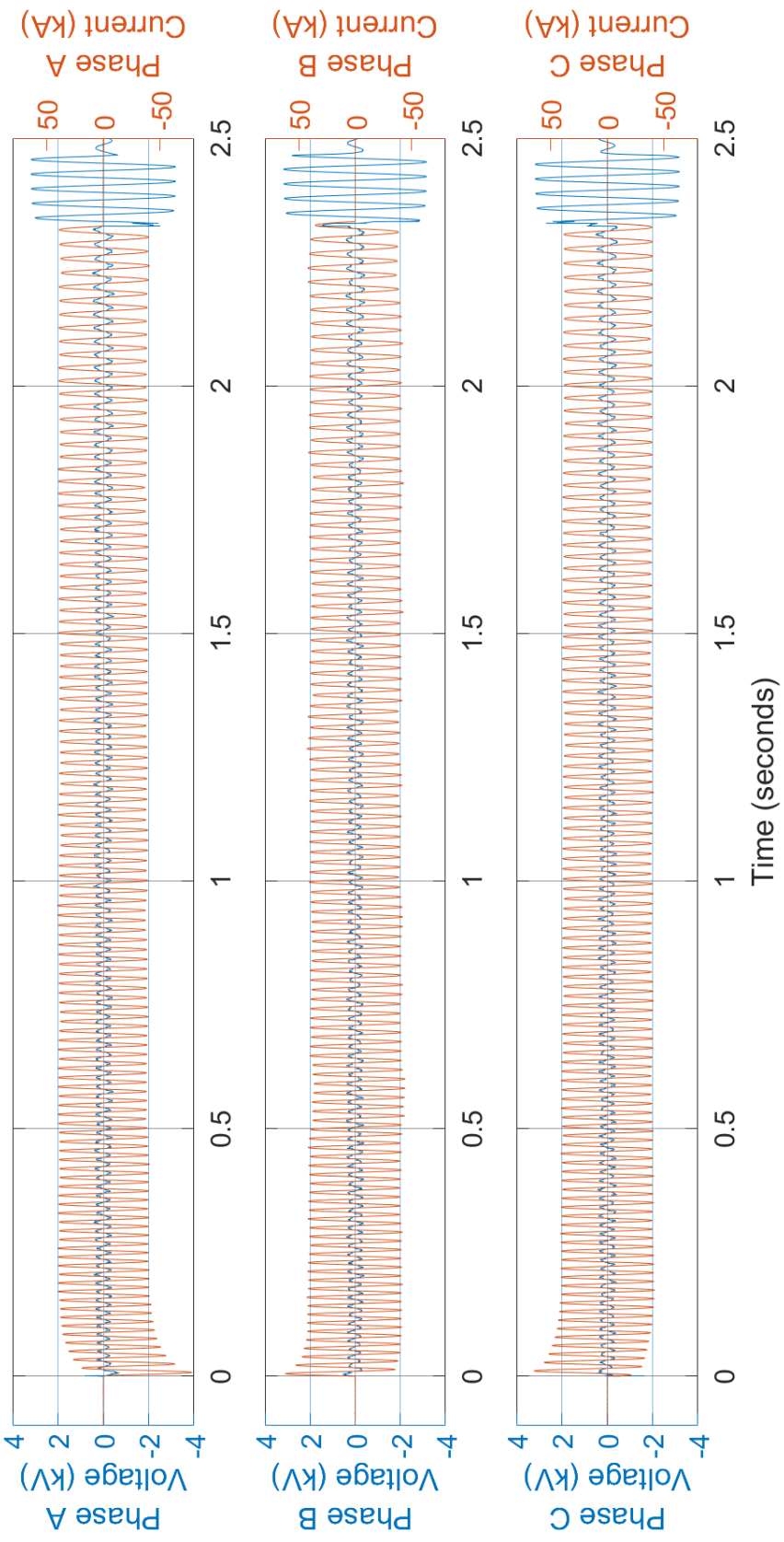

Fig. 94. Experiment OBMV05 voltage and current measurements.

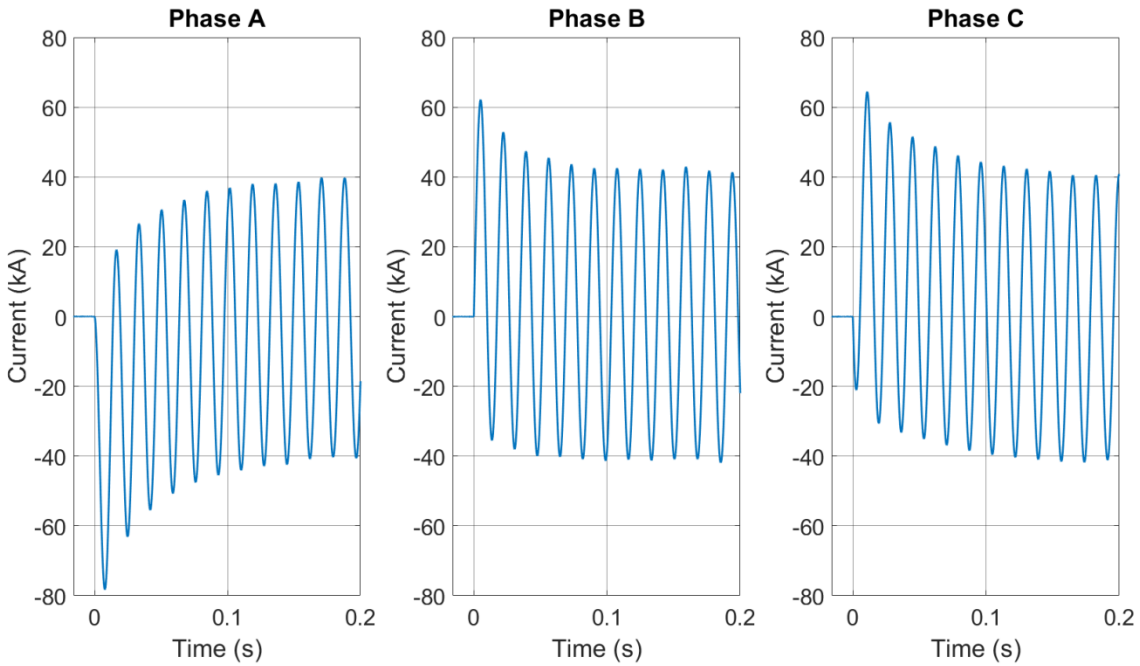

Fig. 95. Experiment OBMV05 transient current profiles

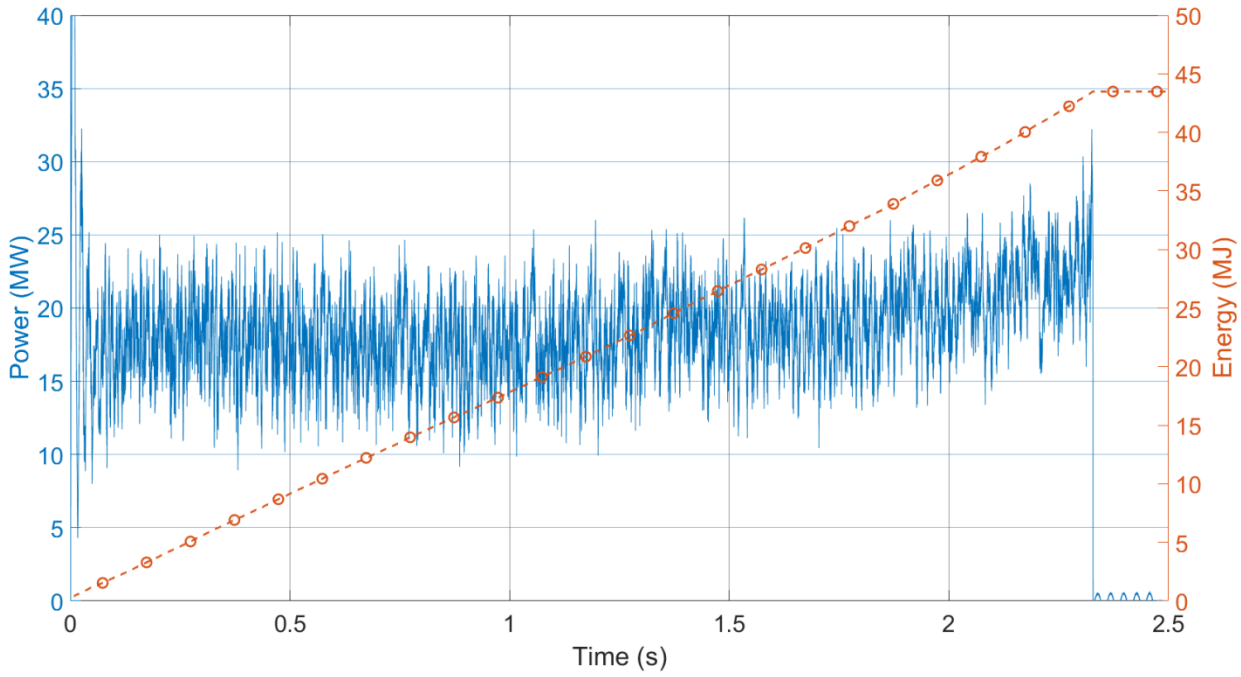

Fig. 96. Experiment OBMV05 power and energy profiles

A combination of thermal measurements devices including a plate thermometer, ASTM Slug Calorimeters, and thermal capacitance slugs (T_{cap}) were used in this experiment as described in Section 2.4.7. The resulting measured data is presented in Table 37.

Table 37. Experiment OBMV05 thermal measurements

Location	Instrument (ID)	Max Heat Flux (kW/m^2) ± 1kW/m^2 or ± 5%	Average Heat Flux During Arc (kW/m^2) ± 1 kW/m^2 or ± 5%
Vertical	Plate Thermometer (2)	3 636	1 486
Location	**Instrument (ID)**	**Total Incident Energy (kJ/m^2) ± 1kJ/m^2 or ± 5%**	**Average Heat Flux During Arc (kW/m^2) ± 1 kW/m^2 or ± 5%**
Vertical	T_{cap} (1)	2 816	723
Horizontal	T_{cap} (3)	1 215	97
Horizontal	T_{cap} (4)	1 161	74
Location	**Instrument (ID)**	**Total Energy (kJ/m^2) ± 18kJ/m^2 or ± 4%**	**Time (s) to Max Temperature ± 3%**
Vertical	ASTM (A)	471	4
Horizontal	ASTM (B)	2 157	34

SNL used the spectrometer during this experiment. The Iris was opened to 1 mm without the use of any optical density filter in place. The detector was positioned to focus immediately below the center copper electrode tip (Phase B). The spectrum from this experiment is presented in Fig. 97.

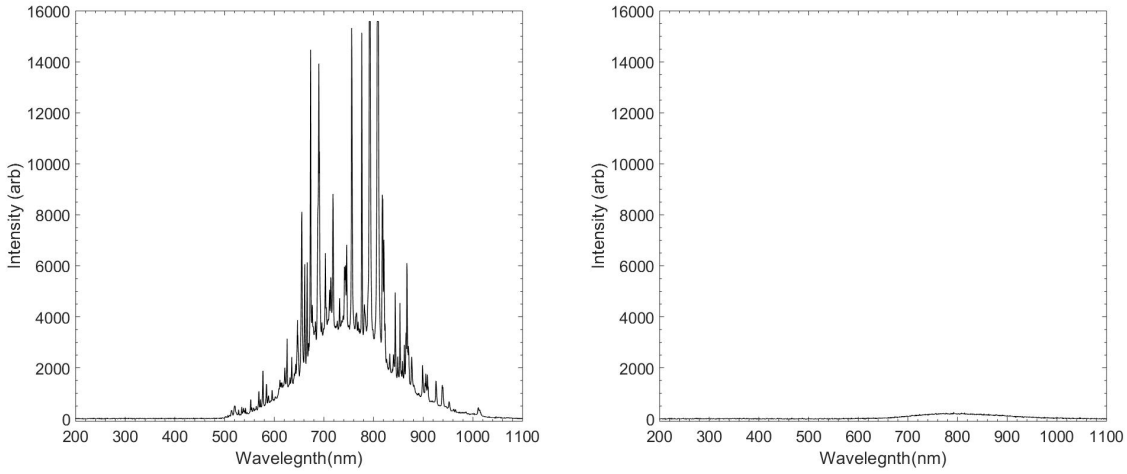

Fig. 97. Experiment OBMV05 spectrum

Breakdown Testing: Prior to the HEAF, median breakdown voltage was approximately 13.1 kV, resulting in a breakdown field of approximately 26 kV/cm consistent with typical air breakdown strength of 25 kV/cm to 30 kV/cm. Breakdown voltage was also measured

during the 2 s, 30 kA HEAF, and was observed to decrease to as low as 3.5 kV to 6.5 kV (8 kV/cm to 13 kV/cm) for three seconds, before recovering to greater than 10 kV. Again, this significantly reduced holdoff strength appears real, but did not approach typical bus bar design electrical fields of 0.7 kV/cm to 1 kV/cm, and would not be expected to result in propagating breakdown into nearby switchgear at these dielectric holdoff values.

Air conductivity measurements: During this large arc fault, large changes in air conductance were observed over the first second of the HEAF. Air conductance values as low as 3.6 E-3 mhos (277 ohms) were recorded; for the 0.5 cm (0.2 in) gap and 3.2 cm (1.25 in) radius sensor, this results in a conductivity of approximately 115 μS/cm or 0.011 S/m, similar to the conductivity of drinking water.

Ultimately damage (melting of the aluminum electrodes) occurred to the pie pan sensor, which was approximately 1.8 m (6.0 ft) from the front of the open box. Subsequent air conductivity experiments were conducted at approximately 3.0 m (10.0 ft) and 4.3 m (14 ft) distances using duplicate devices.

EMI measurements: No EMI fields were detected above the ambient interference level trigger from this arc fault.

Observations and Notes

Steel enclosure breached on both sides and at the top around the bar mounting block. The bottom was not breached but was deflected approximately 9.4 cm (3.7 in) at center of the front face opening.

The estimated mass loss from the enclosure was approximately 5 666 g and a total breach opening on all sides of approximately 711 cm^2 (bottom opening of approximately 13 cm^2, left side approximately 351 cm^2, right side approximately 98 cm^2 and a top opening of approximately 249 cm^2).

4.2. Medium-voltage Experiment Results with Aluminum Electrodes

Four experiments were performed at medium-voltage in the box configuration with aluminum electrodes. These were Experiments OBMV01 through OBMV03 and OBMV06. The results from these experiments are presented next.

4.2.1. Experiment ID: OBMV01

This experiment was performed on September 18, 2019. The electrical characteristics are presented in Table 38. Photos of Experiment OBMV01 are presented in Fig. 98 and Fig. 99, while the electrical measurements are presented in Fig. 100.

Table 38. Experiment OBMV01 experiment parameters

Electrical Parameter	Target	Actual	Other
Voltage (V_{L-L})	6 900	6 914	543 (arc)
Current (A)	15 000	14 280	
Duration (ms)	2 000	3 180	
Energy (MJ)		37.5	
Other Parameters			
Electrode Length Loss (cm)	10.8 (Phase A)	12.1 (Phase B)	10.5 (Phase C)
Electrode Mass Loss (g)	412.5	477.0	434.0
Electrode Material	Aluminum		
Electrode Dimensions	10.2 cm (4.0 in) x 1.27 cm (0.5 in)		
Electrode Spacing	13 cm (5 in) on center		
Shorting Wire	2 – 24 AWG (0.511 mm diameter), single strand tinned copper		
Box Electrical Configuration	Neutral		
Generator Configuration	Neutral tied to ground via impedance		
Enclosure Breach	Excessive		
Additional Cladding	None		
Enclosure Mass Loss (g)	10 168		

Fig. 98. Experiment OBMV01 pre-experiment (top) and post-experiment (bottom left – side, bottom center – back, bottom right - side). Phase sequence from left to right is C-B-A.

Fig. 99. Experiment OBMV1 electrode post-experiment

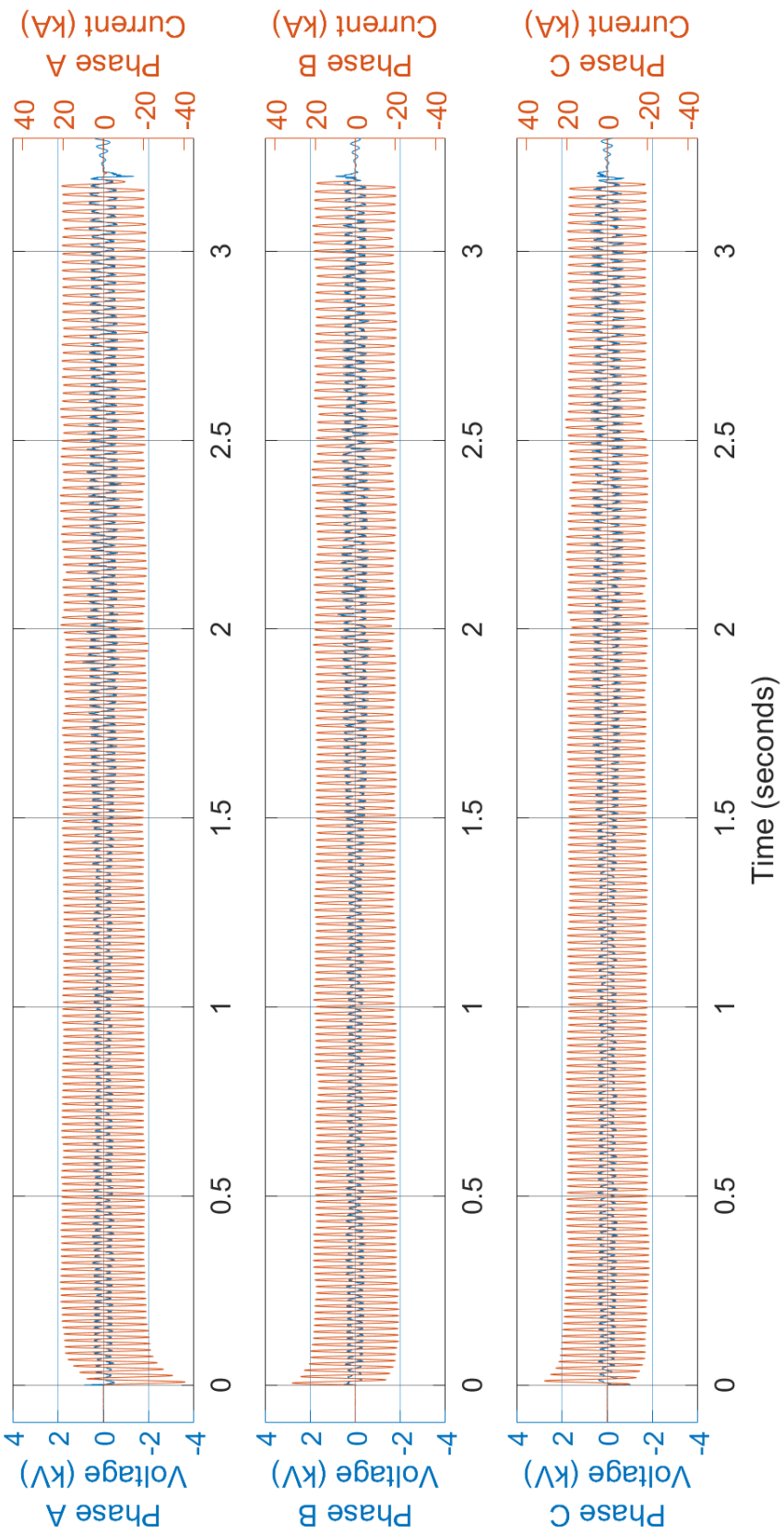

Fig. 100. Experiment OBMV01 voltage and current measurements

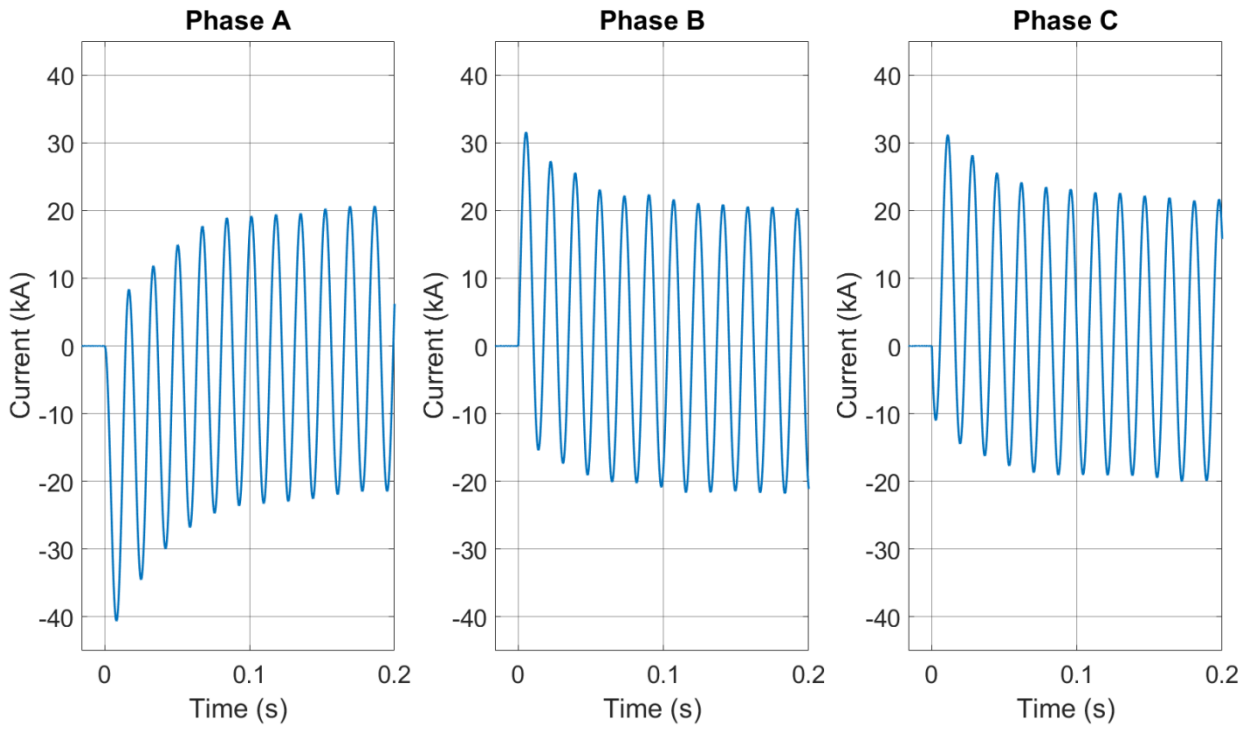

Fig. 101. Experiment OBMV01 transient current profiles

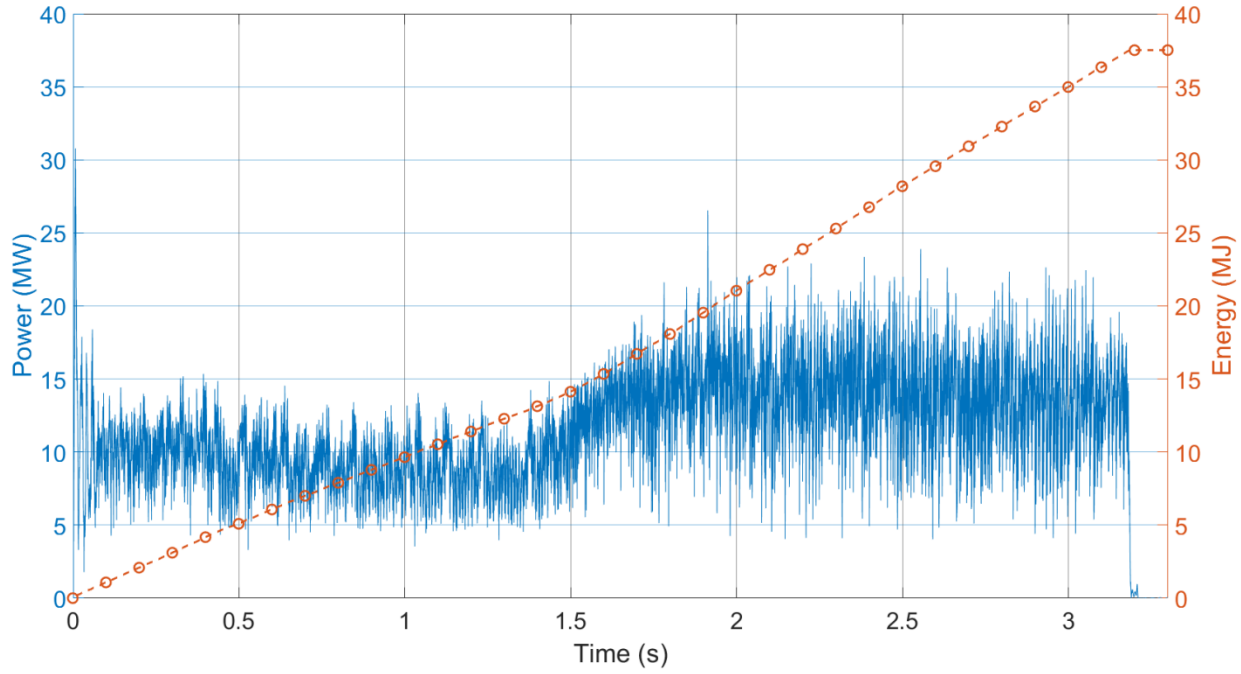

Fig. 102. Experiment OBMV01 power and energy profiles

A combination of thermal measurements devices including a plate thermometer, ASTM Slug Calorimeters, and thermal capacitance slugs (T_{cap}) were used in this experiment as described in Section 2.4.7. The resulting measured data is presented in Table 39.

Table 39. Experiment OBMV01 thermal measurements

Location	Instrument (ID)	Max Heat Flux (kW/m²) ± 1kW/m² or ± 5%	Average Heat Flux During Arc (kW/m²) ± 1 kW/m² or ± 5%	Notes
Vertical	Plate Thermometer (2)	414	250	
Location	**Instrument (ID)**	**Total Incident Energy (kJ/m²) ± 1kJ/m² or ± 5%**	**Average Heat Flux During Arc (kW/m²) ± 1 kW/m² or ± 5%**	**Notes**
Vertical	T_{cap} (1)	1 038	160	
Horizontal	T_{cap} (3)	7 000	1 357	
Horizontal	T_{cap} (4)	5 500	936	
Location	**Instrument (ID)**	**Total Energy (kJ/m²) ± 18kJ/m² or ± 4%**	**Time (s) to Max Temperature ± 3%**	**Notes**
Vertical	ASTM (A)	749	6	
Horizontal	ASTM (B)	No Data	No Data	Exposure exceeded device range

SNL used the spectrometer during this experiment. The spectrum from this experiment is presented in Fig. 103.

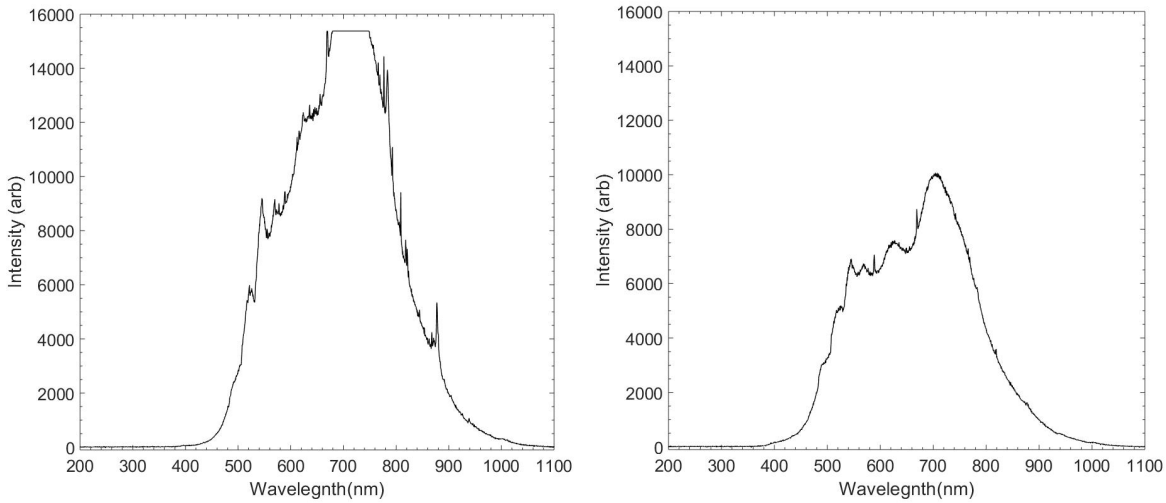

Fig. 103. Spectrum from Experiment OBMV01

Air breakdown experiments were not conducted during experiment OBMV1.

During this arc fault experiment, changes in air conductance were observed at 4.27 m (14 ft) distance from open box. A minimum air conductance value of 1.15 x10^{-4} mhos (10 kohm) and several events of 1.6 E-5 mhos (62.5 kohms) were recorded with an uncertainty of 9 E-6 mhos; for the 0.5mm (0.02 in) gap and 3.2 cm (1.25 in) radius sensor, this results in a maximum conductivity of approximately 1 μS/cm or 0.1 mS/m, similar to the conductivity of drinking water. Result from this test are presented in Fig. 104.

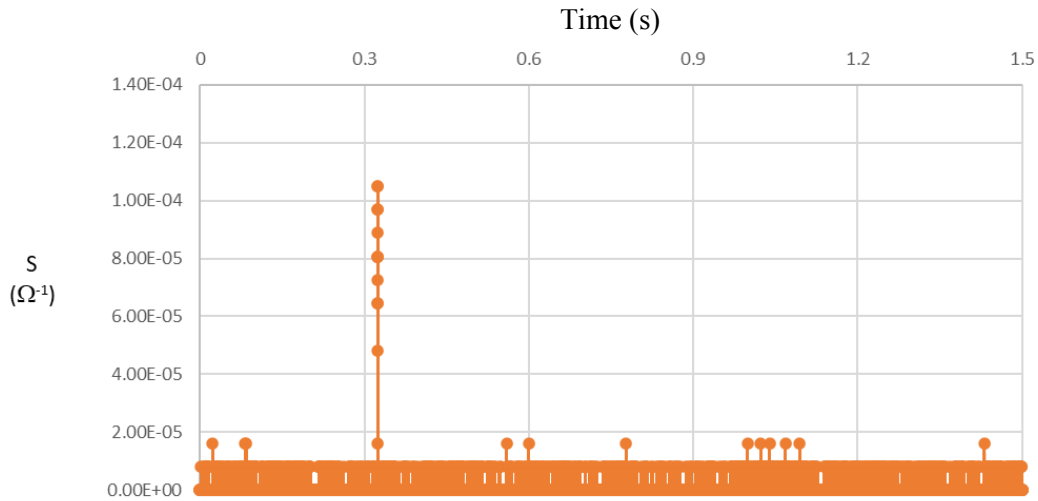

Fig. 104. Air Conductivity Measurement during OBMV01

No EMI fields were detected above the ambient interference level trigger from this arc fault.

Observations and Notes

The laboratories timer experienced a failure and the experiment lasted for 3 180 ms versus the planned 2 000ms. This resulted in an experiment that was 59% longer than planned. As such more of the enclosure was consumed than estimated during experiment planning phase which supported the use of single clad box. The additional duration resulted in little of the box remaining after the experiment and limited the usability of the results to evaluate enclosure burn thorough. However, conductor material loss and all other instrumentation worked as planned and provided usable data. Additional measures were taken by the laboratory to ensure that the timer failure did not occur in subsequent experiments. The experiment was re-run as OBMV6.

4.2.2. Experiment ID: OBMV02

This experiment was performed on September 17, 2019. The electrical characteristics are presented in Table 40. Photos of Experiment OB0 are presented in Fig. 105 through Fig. 107, while the electrical measurements are presented in Fig. 108 through Fig. 110.

Table 40. Experiment Parameters Experiment OBMV02

Electrical Parameter	**Target**	**Actual**	**Other**
Voltage (V_{L-L})	6,900	6,915	468 (arc)
Current (A)	30,000	29,143	
Duration (ms)	1,000	1,120	
Energy (MJ)		21.42	
Electrode Length Loss (cm)	5.7 (Phase A)	5.7 (Phase B)	7.0 (Phase C)
Electrode Mass Loss (g)	319.5	333.5	291.5
Other Parameters			
Electrode Material	Aluminum		
Electrode Dimensions	10.2 cm (4.0 in) x 1.27 cm (0.5 in)		
Electrode Spacing	13 cm (5 in) on center		
Shorting Wire	2 – 24 AWG (0.511 mm diameter), single strand tinned copper		
Box Electrical Configuration	Neutral		
Generator Configuration	Neutral tied to ground via impedance		
Enclosure Breach	No		
Additional Cladding	Back	Sides	Bottom
Add. Cladding Thickness (cm)	0.18	0.18	0.18
Enclosure Mass Loss (g)	982 (cladding only)		

Fig. 105. Experiment OBMV02 pre-experiment (left) and post-experiment (right) aluminum electrodes. Phase sequence from left to right is C-B-A.

Fig. 106. Experiment OBMV2 enclosure breach (Left-to-right: left side, bottom side, right side)

Fig. 107. Experiment OBMV2 aluminum electrodes post-experiment

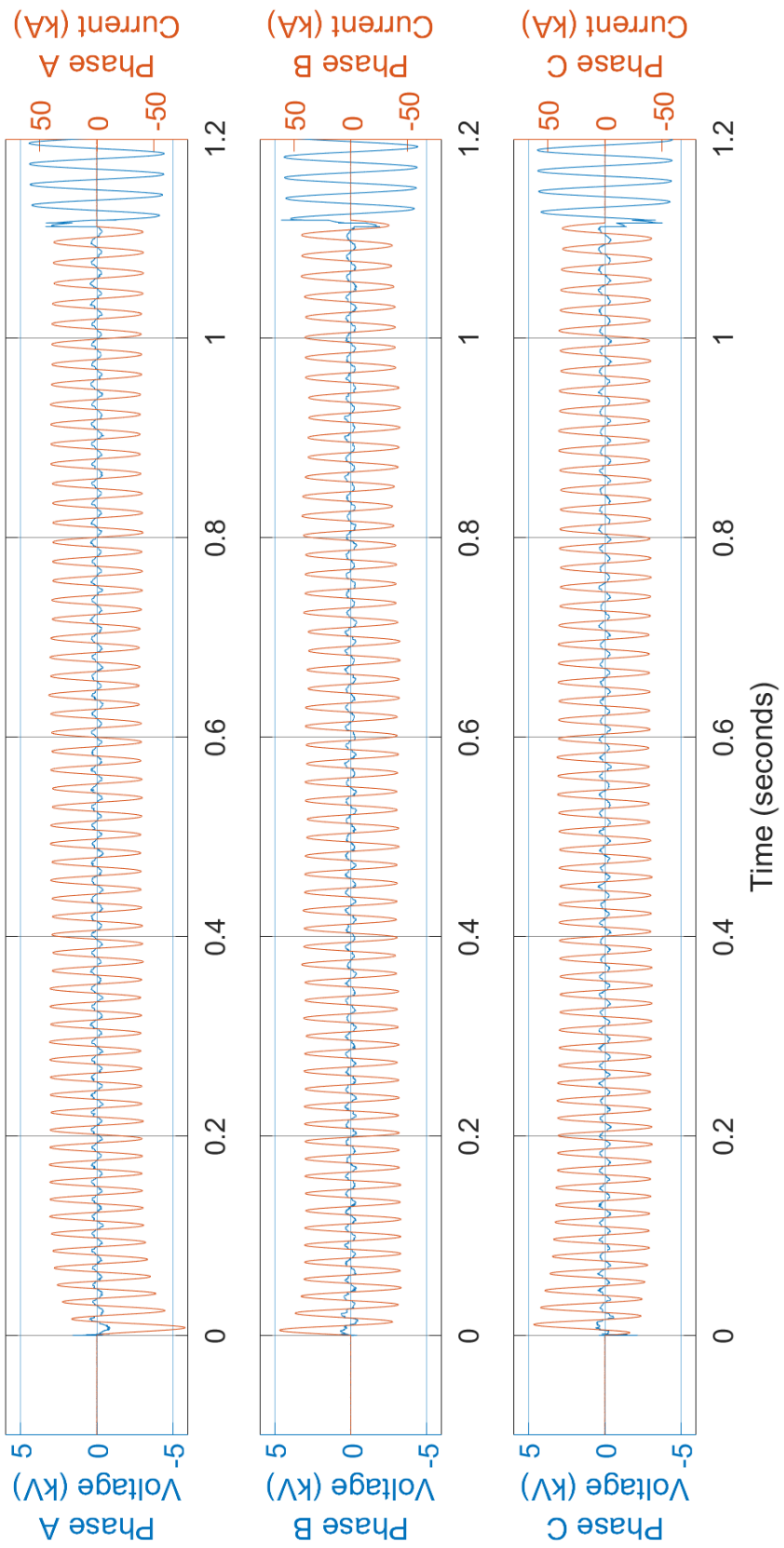

Fig. 108. Voltage and current measurements for Experiment OBMV02

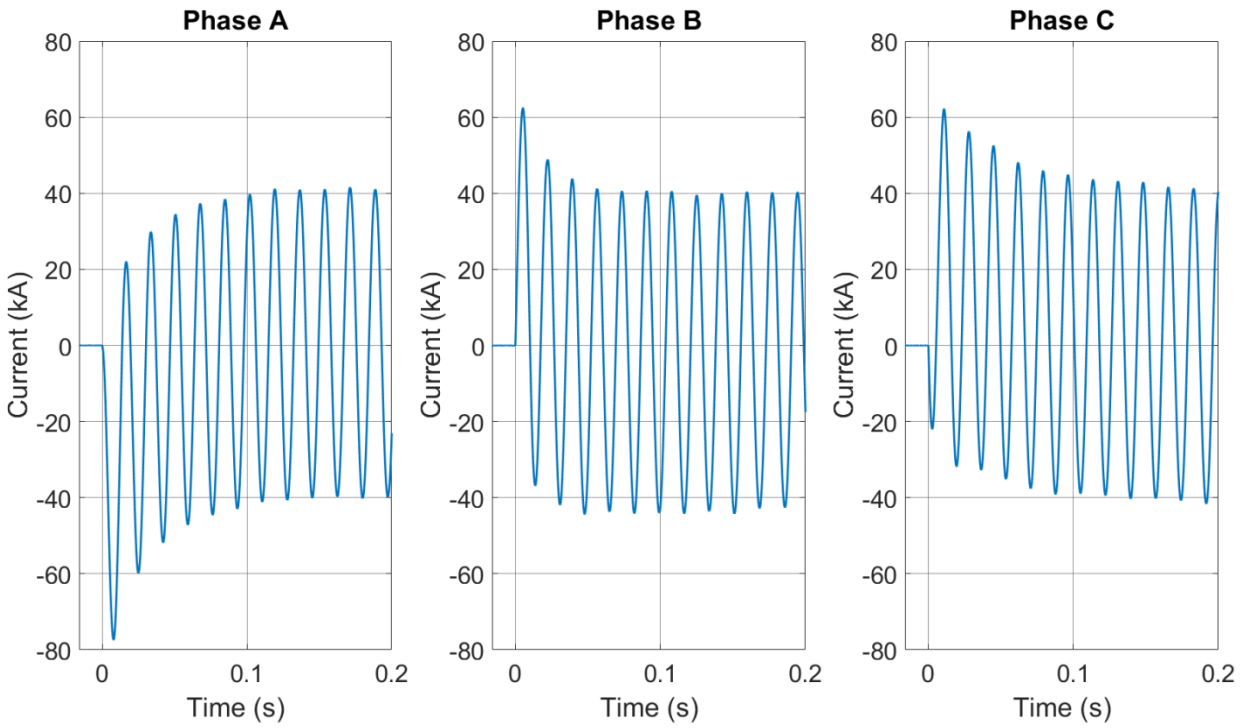

Fig. 109. Experiment OBMV02 transient current profiles

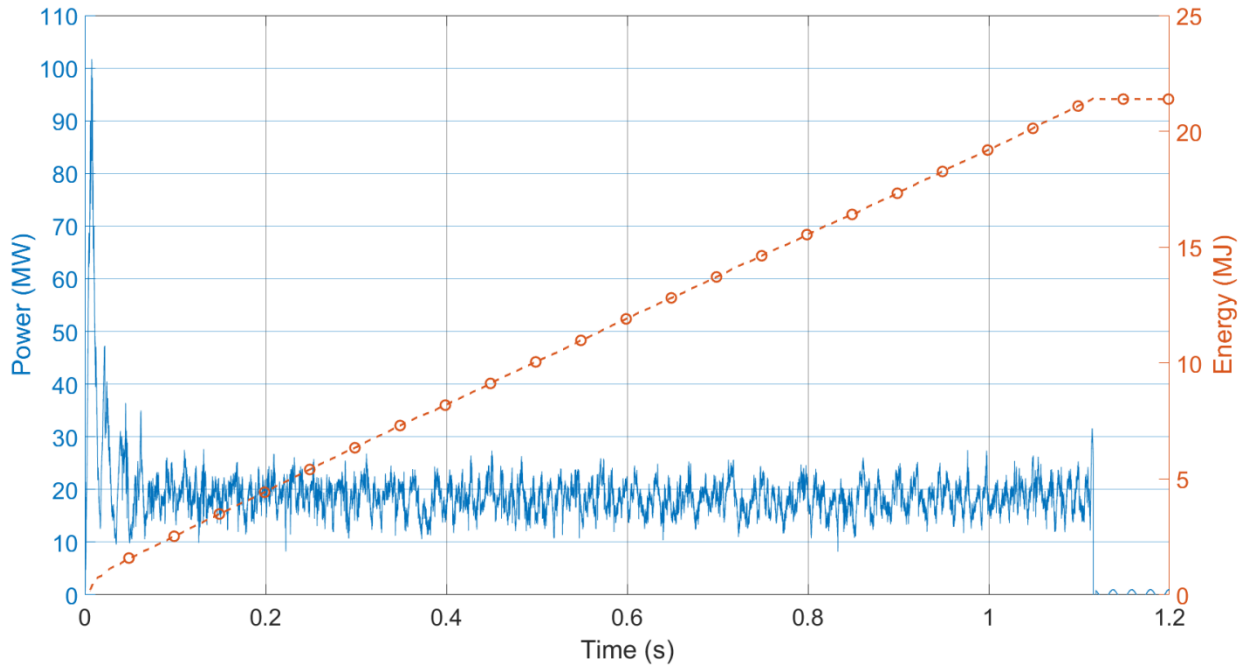

Fig. 110. Experiment OBMV02 power and energy profiles

A combination of thermal measurements devices including a plate thermometer, ASTM Slug Calorimeters, and thermal capacitance slugs (T_{cap}) were used in this experiment as described in Section 2.4.7. The resulting measured data is presented in Table 41.

Table 41. Experiment OBMV02 thermal measurements

Location	Instrument (ID)	Max Heat Flux (kW/m^2) ± 1kW/m^2 or ± 5%	Average Heat Flux During Arc (kW/m^2) ± 1 kW/m^2 or ± 5%	Notes
Vertical	Plate Thermometer (2)	3 817	1 835	
Location	**Instrument (ID)**	**Total Incident Energy (kJ/m^2) ± 1kJ/m^2 or ± 5%**	**Average Heat Flux During Arc (kW/m^2) ± 1 kW/m^2 or ± 5%**	**Notes**
Vertical	T_{cap} (1)	2 182	1 477	
Horizontal	T_{cap} (3)	532	286	
Horizontal	T_{cap} (4)	531	317	
Location	**Instrument (ID)**	**Total Incident Energy (kJ/m^2) ± 18kJ/m^2 or ± 4%**	**Time (s) to Max Temperature ± 3%**	**Notes**
Vertical	ASTM (A)	2 149	2	
Horizontal	ASTM (B)	No Data	No Data	Sensor non-functional

SNL used the spectrometer during this experiment. The spectrum from this experiment is presented in Fig. 111.

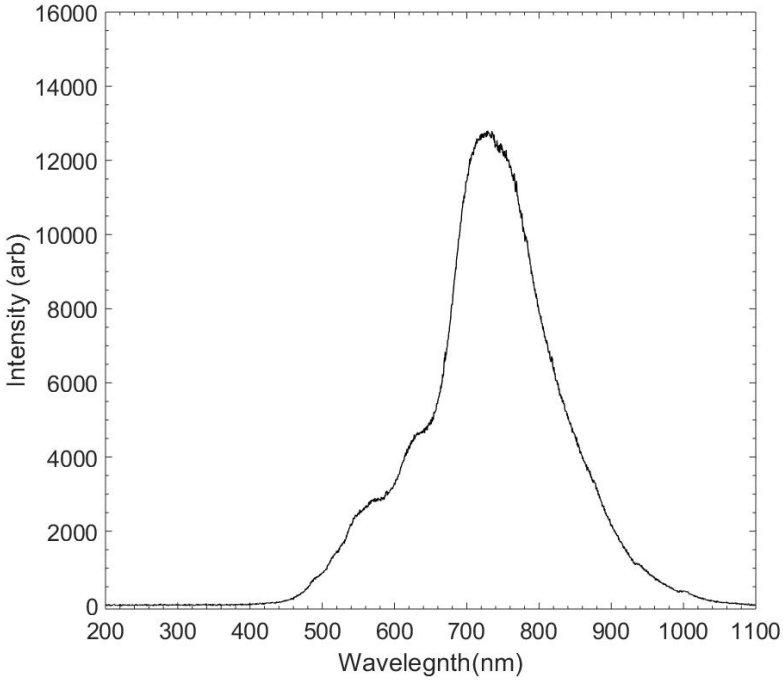

Fig. 111. Spectrum from Experiment OBMV02

High voltage breakdown experiments were conducted prior to, and during the arc fault experiment. Prior to the HEAF experiment, median breakdown voltage was measured at 15.1 kV and shown in Fig. 112, consistent with typical, air breakdown strength of 25 kV/cm to 30 kV/cm. Breakdown voltage was measured during the HEAF and was observed to decrease to 11.6 kV, or approximately 23 kV/cm as shown in Fig. 113. This decrease, while notable, does not approach typical bus bar electrical fields of 0.7 kV/cm to 1 kV/cm, and would not be expected to result in propagating breakdown into nearby switchgear at these dielectric holdoff values.

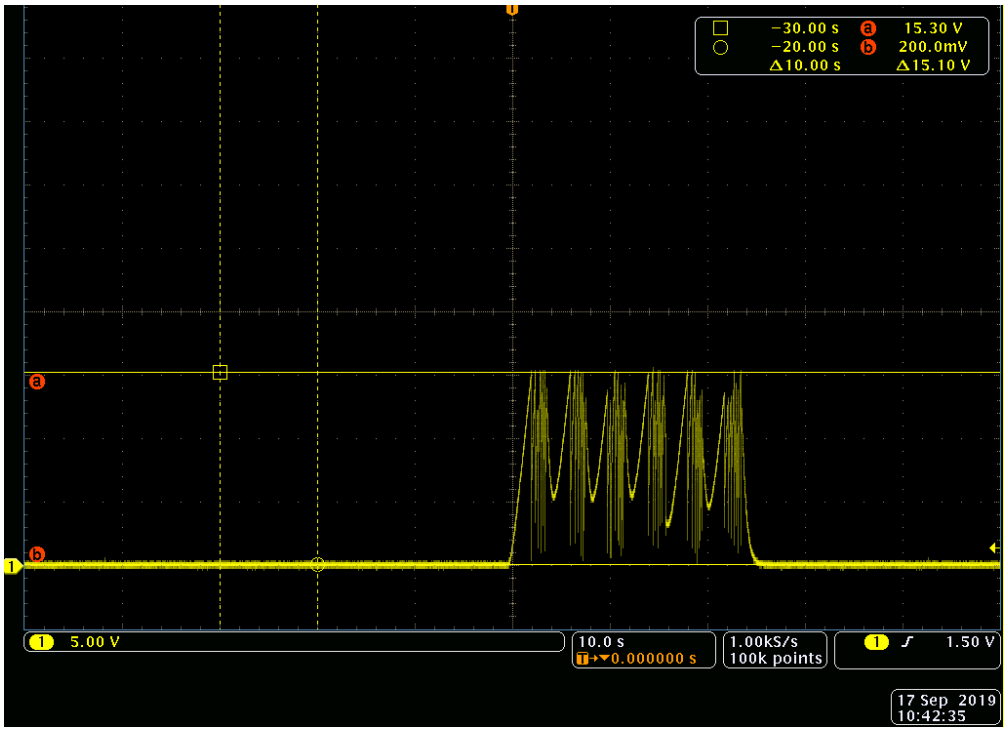

Fig. 112. Breakdown experiment prior to Experiment OBMV02, breakdown voltage indicated in kV.

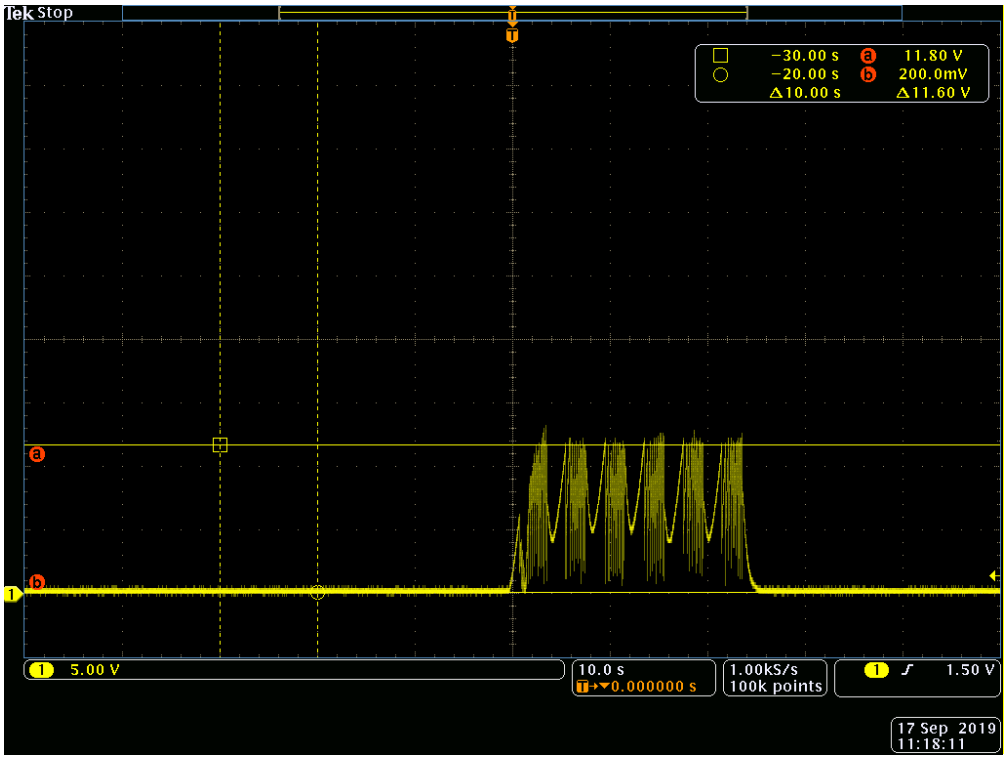

Fig. 113. Breakdown experiment during Experiment OBMV02, breakdown voltage indicated in kV.

During this arc fault experiment, changes in air conductance were observed at 3 m (10 ft) distance from open box. Air conductance values as low as 6 x10^{-4} mhos (1.6 kohm) were recorded with an uncertainty of 9 x10^{-9} mhos; for the 0.5mm (0.02 in) gap and 3.2 cm (1.25 in) radius sensor. These results are presented in and represent a conductivity of approximately 6 µS/cm or 0.6 mS/m, similar to the conductivity of drinking water.

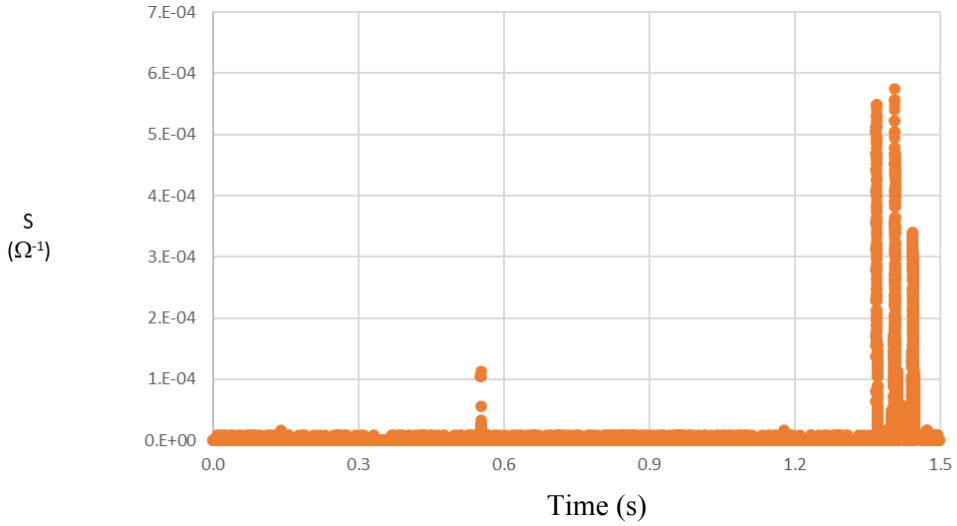

Fig. 114. Air conductance measurements during OBMV02 HEAF event

No EMI fields were detected above the ambient interference level trigger from this arc fault.

Observations and Notes

There was no breach of the outer box enclosure, the internal panels were removed. The estimated mass loss from the enclosure internal cladding is 982.2 grams and a total breach opening on all sides of 699 cm^2. Bottom opening of 71 cm^2, left side 334 cm^2, and right side 294 cm^2.

4.2.3. Experiment ID: OBMV03

This experiment was performed on September 18, 2019. The electrical characteristics are presented in **Table 42**. Photos of Experiment OBMV03 are presented in Fig. 115 through Fig. **117**, while the electrical measurements are presented in Fig. 118 through Fig. 120.

Table 42. Experiment Parameters Experiment OBMV03

Electrical Parameter	**Target**	**Actual**	**Other**
Voltage (V_{L-L})	6 900	6 918	475 (arc)
Current (A)	15 000	14 370	
Duration (ms)	5 000	5 050	
Energy (MJ)		55.7	
Electrode Length Loss (cm)	21.6 (Phase A)	22.2 Phase B)	22.2 (Phase C)
Electrode Mass Loss (g)	765.5	779.5	751.0
Other Parameters			
Electrode Material	Aluminum		
Electrode Dimensions	10.2 cm (4.0 in) x 1.27 cm (0.5 in)		
Electrode Spacing	13 cm (5 in) on center		
Shorting Wire	2 – 24 AWG (0.511 mm diameter), single strand tinned copper		
Box Electrical Configuration	Neutral		
Generator Configuration	Neutral tied to ground via impedance		
Enclosure Breach	Bottom, Sides, Top, Back (partial)		
Additional Cladding	Back	Left	Right	Bottom
Add. Cladding Thickness (cm)	0.29	0.18	0.29	0.18
Enclosure Mass Loss (g)	17 483			

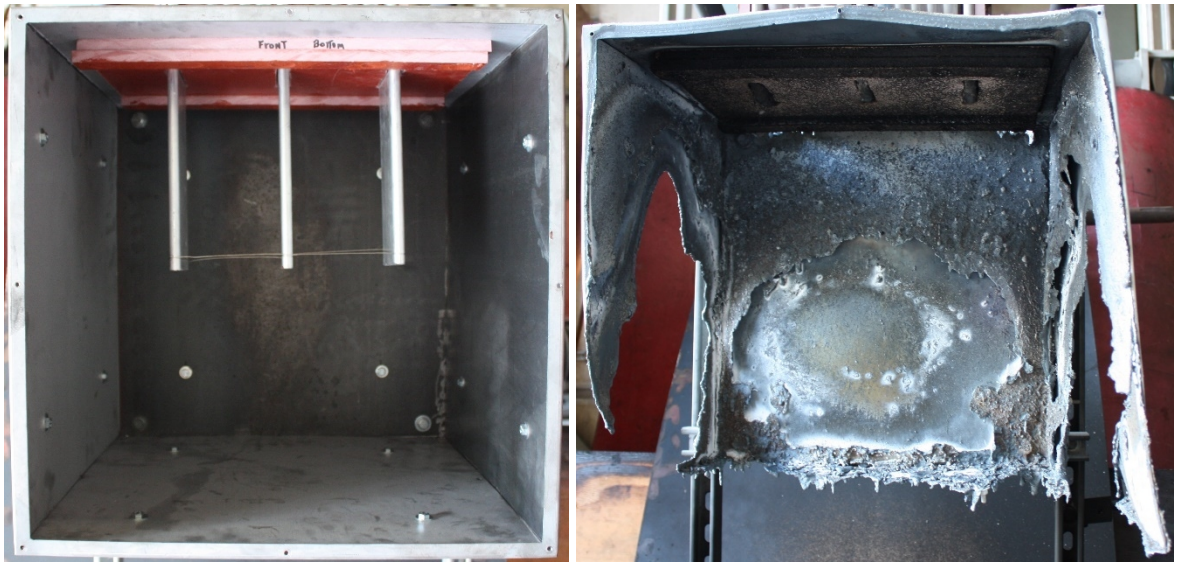

Fig. 115. Experiment OBMV03 pre-experiment (left) and post-experiment (right) electrodes. Phase sequence left to right is C-B-A.

Fig. 116. Experiment OBMV3 enclosure breach (left-to-right: Left side, back side, right side, top)

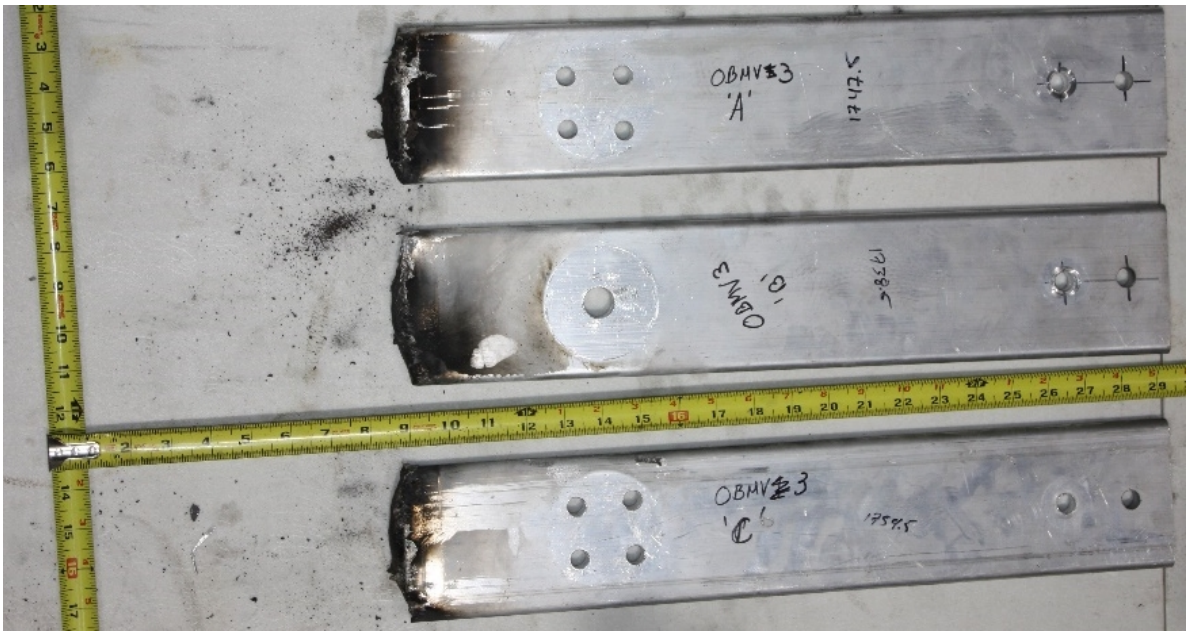

Fig. 117. Experiment OBMV03 aluminum electrode post-experiment

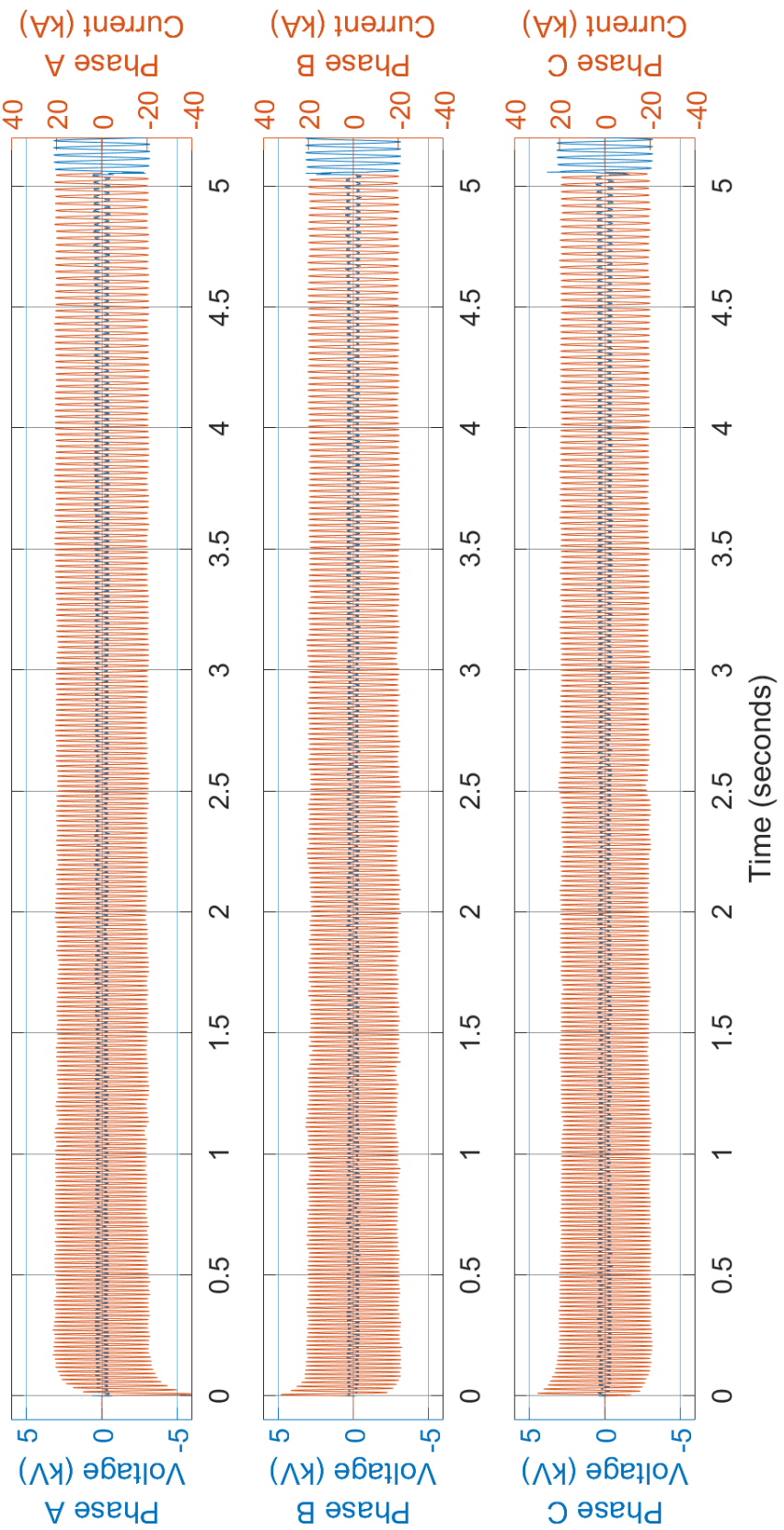

Fig. 118. Experiment OBMV03 voltage and current measurements

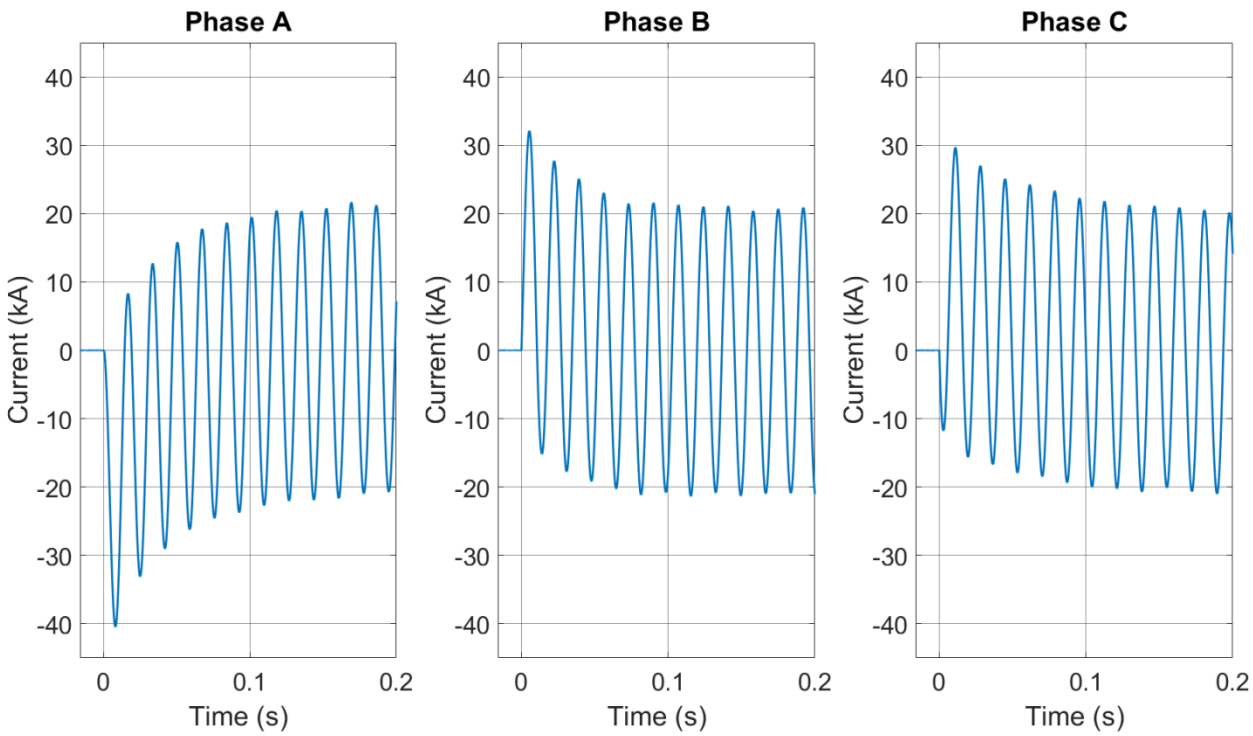

Fig. 119. Experiment OBMV03 transient current profiles

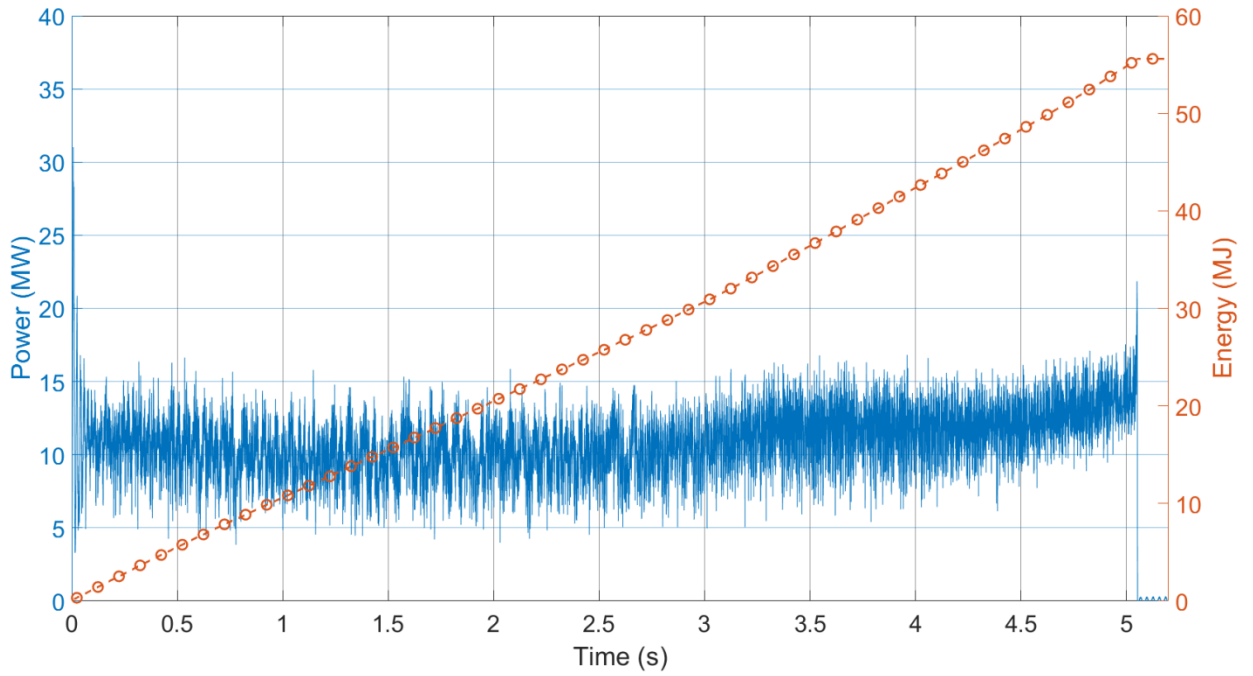

Fig. 120. Experiment OBMV03 power and energy profiles

A combination of thermal measurements devices including a plate thermometer, ASTM Slug Calorimeters, and thermal capacitance slugs (T_{cap}) were used in this experiment as described in Section 2.4.7. The resulting measured data is presented in Table 43.

Table 43. Experiment OBMV03 thermal measurements

Location	Instrument (ID)	Max Heat Flux (kW/m^2) ± 1kW/m^2 or ± 5%	Average Heat Flux During Arc (kW/m^2) ± 1 kW/m^2 or ± 5%	Notes
Vertical	Plate Thermometer (2)	716	369	
Location	**Instrument (ID)**	**Total Incident Energy (kJ/m^2) ± 1kJ/m^2 or ± 5%**	**Average Heat Flux During Arc (kW/m^2) ± 1 kW/m^2 or ± 5%**	**Notes**
Vertical	T_{cap} (1)	2 327	351	
Horizontal	T_{cap} (3)	8 385	1 032	
Horizontal	T_{cap} (4)	12 441	965	
Location	**Instrument (ID)**	**Total Incident Energy (kJ/m^2) ± 18kJ/m^2 or ± 4%**	**Time (s) to Max Temperature ± 3%**	**Notes**
Vertical	ASTM (A)	1 457	9	
Horizontal	ASTM (B)	No Data	No Data	Exposure exceeded device range

Prior to the HEAF, the median breakdown voltage was 15 kV, consistent with typical, air breakdown strength of 25 kV/cm to 30 kV/cm. Breakdown voltage was also measured during the HEAF experiment, and was observed to decrease to as low as 8.3 kV, or approximately 16 kV/cm. Again, this decrease does not approach typical bus bar design electrical fields of 0.7 kV/cm to 1 kV/cm, and would not be expected to result in propagating breakdown into nearby switchgear at these dielectric holdoff values.

Air conductance values in the range of 0.8 E-4 mhos to 6 E-4 mhos (1.6 kohm) were recorded; for the 0.5 mm (0.02 in) gap and 3.2 cm (1.25 in) radius sensor, this results in a conductivity of approximately 0.8 µS/cm to 6 µS/cm or 0.6 mS/m, similar to the conductivity of drinking water. The result from this test are presented in Fig. 121.

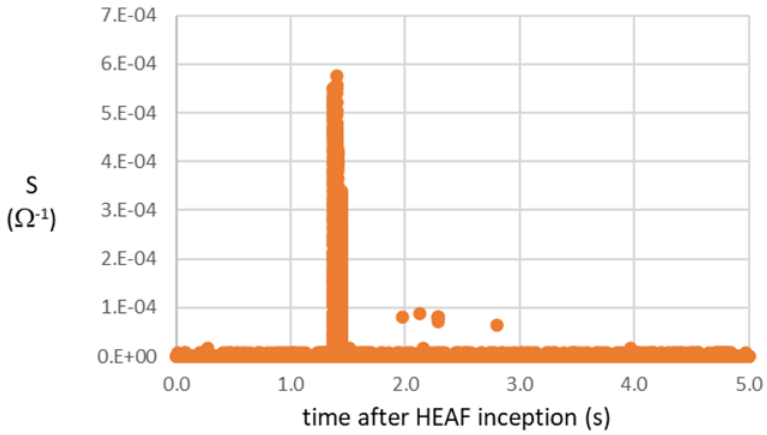

Fig. 121. Experiment OBMV03 air conductance measurement

SNL used the spectrometer during this experiment. The spectrum from this experiment is presented in Fig. 122.

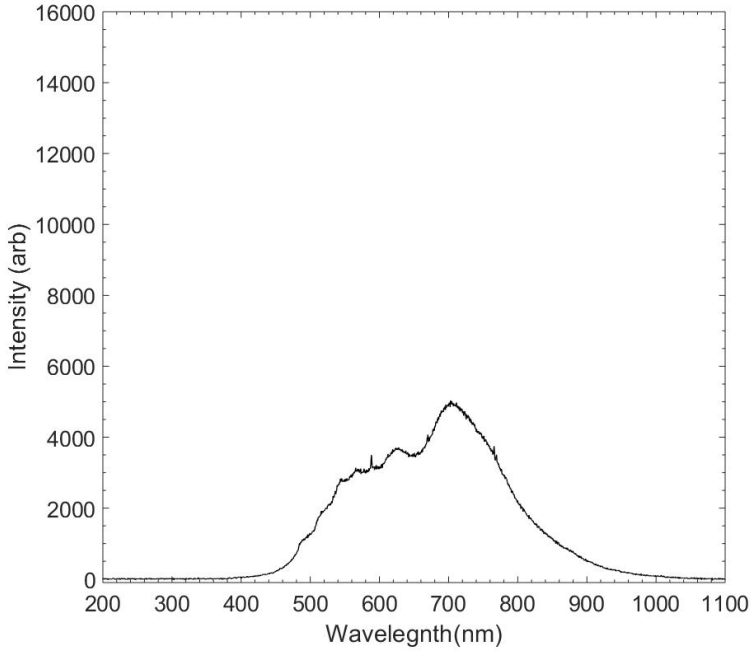

Fig. 122. Spectrum from Experiment OBMV03

Observations and Notes

The box burned through all sides except the back. The bottom of the box was completely consumed and large holes on both sides. The top behind the GPO3 insulative red board also experienced burn through.

The estimated mass loss from the enclosure is 17 483 grams and a total breach opening on all sides of 4 183 cm^2. Bottom was completely gone 2 080 cm^2 each, left side 1 309 cm^2, right side 684 cm^2 and top openings of 112 cm^2.

4.2.4. Experiment ID: OBMV06

This experiment was performed on September 18, 2019. The electrical characteristics are presented in Table 44. Photos of Experiment OBMV06 are presented in Fig. 123 through Fig. **125**, while the electrical measurements are presented in Fig. 126 through Fig. 128.

Table 44. Experiment Parameters Experiment OBMV06

Electrical Parameter	**Target**	**Actual**	**Other**
Voltage (V_{L-L})	6 900	6 913	493 (arc)
Current (A)	15 000	14 596	
Duration (ms)	2 000	2 050	
Energy (MJ)		22.72	
Other Parameters			
Electrode Length Loss (cm)	8.6 (Phase A)	8.9 (Phase B)	7.6 (Phase C)
Electrode Mass Loss (g)	252.0	252.0	223.0
Electrode Material	Aluminum		
Electrode Dimensions	7.6 cm (3.0 in) x 1.27 cm (0.5 in)		
Electrode Spacing	13 cm (5 in) on center		
Shorting Wire	2 – 24 AWG (0.511 mm diameter), single strand tinned copper		
Box Electrical Configuration	Neutral		
Generator Configuration	Neutral tied to ground via impedance		
Enclosure Breach	Bottom, sides, and back		
Additional Cladding	None		
Enclosure Mass Loss (g)	5 763		

Fig. 123. Experiment OBMV06 pre-experiment (left) and post-experiment (right) electrodes. Phase sequence from left to right is C-B-A.

Fig. 124. Experiment OBMV6 enclosure breach
(Left-to-right: left side, back side, bottom side, and right side)

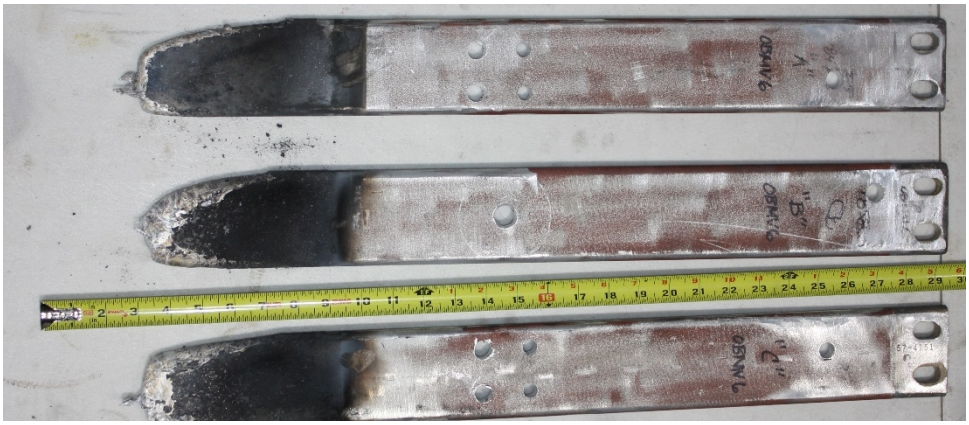

Fig. 125. Experiment OBMV06 aluminum electrodes post-experiment

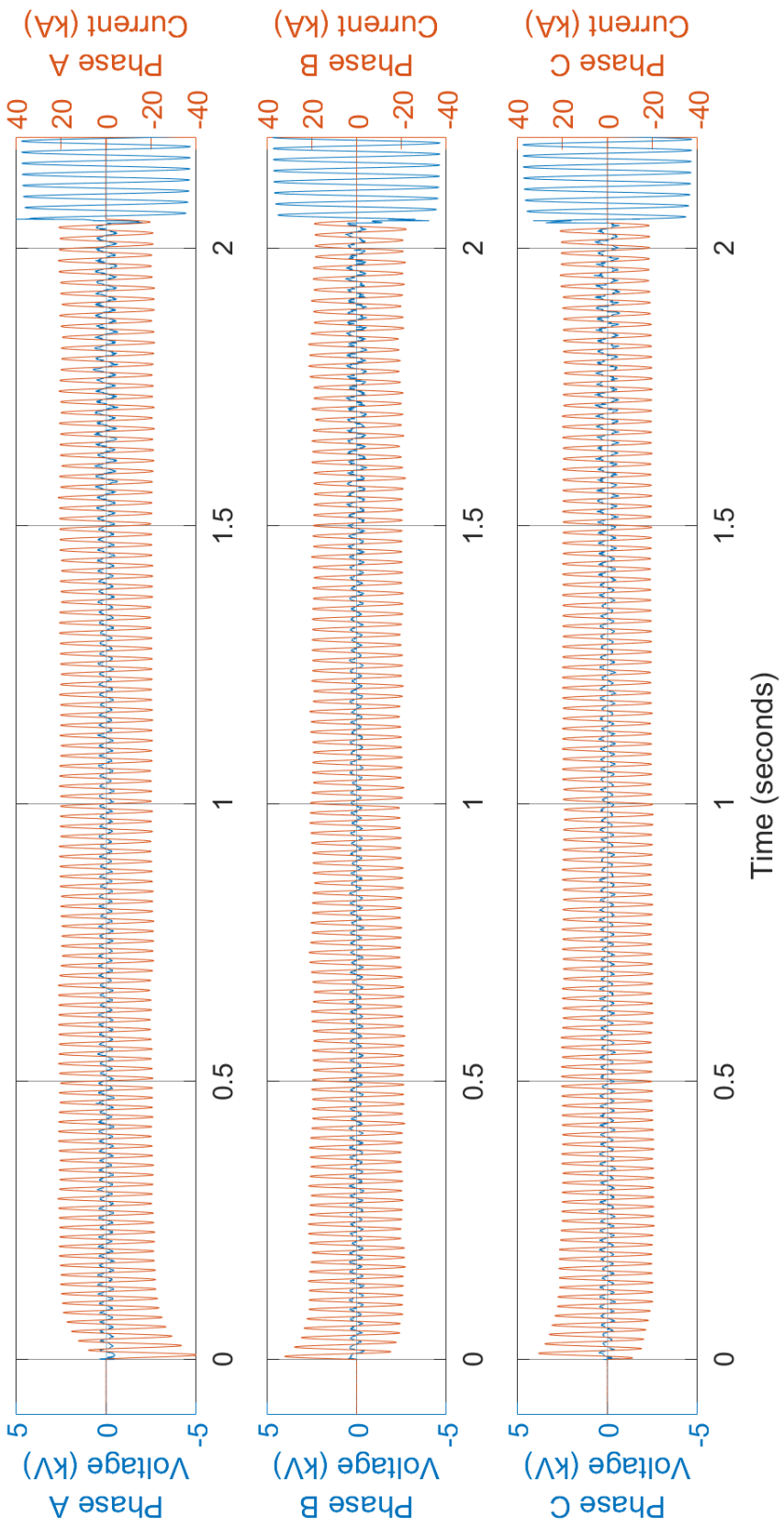

Fig. 126. Experiment OBMV06 voltage and current measurements

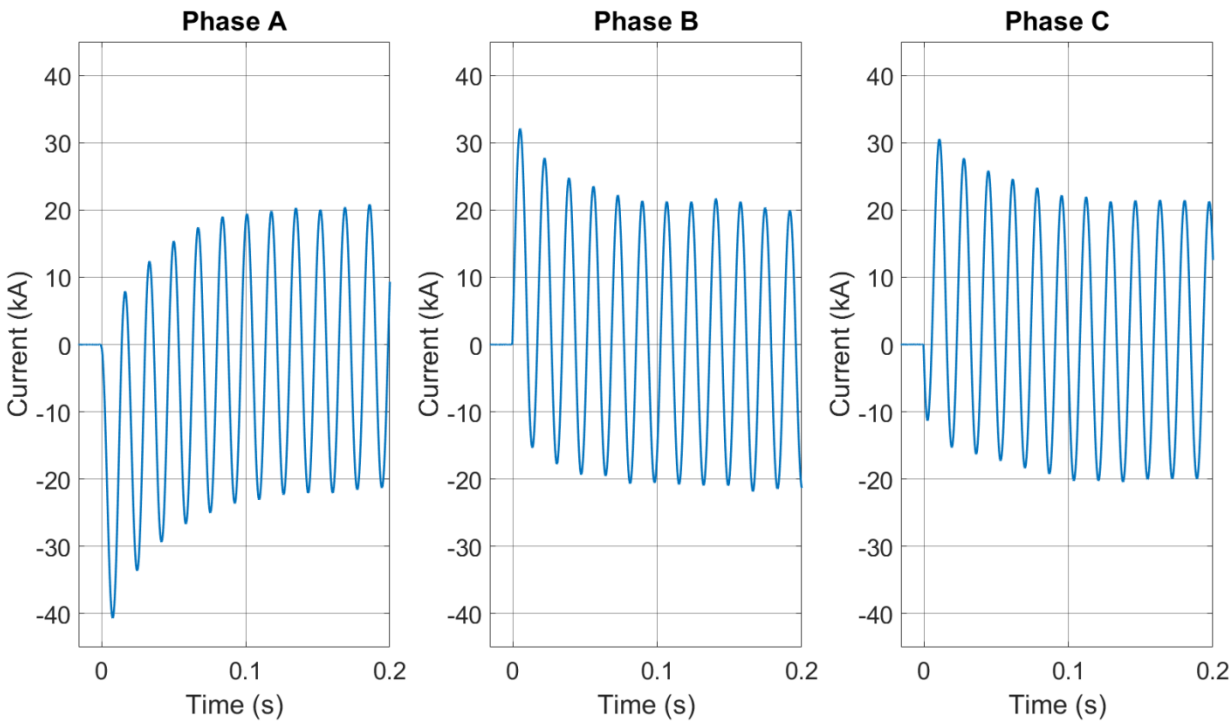

Fig. 127. Experiment OBMV06 transient current profiles

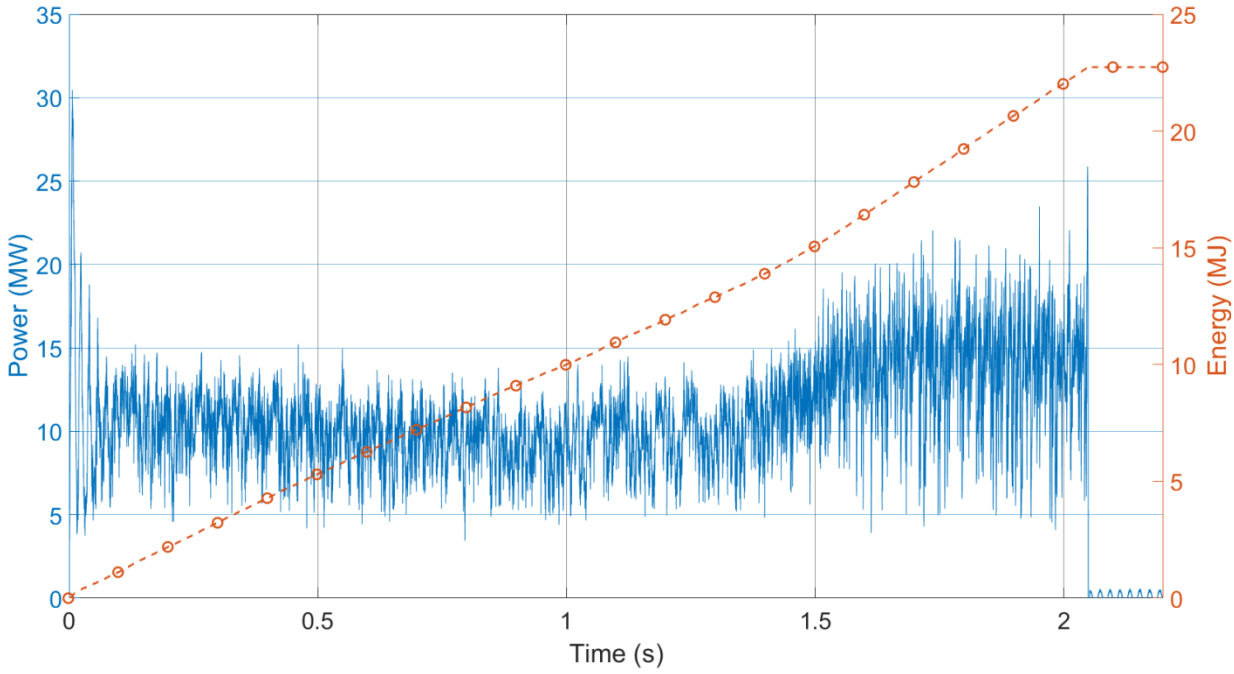

Fig. 128. Experiment OBMV06 power and energy profiles

A combination of thermal measurements devices including a plate thermometer, ASTM Slug Calorimeters, and thermal capacitance slugs (T_{cap}) were used in this experiment as described in Section 2.4.7. The resulting measured data is presented in Table 45.

Table 45. Experiment OBMV06 thermal measurements

Location	Instrument (ID)	Max Heat Flux (kW/m^2) ± 1kW/m^2 or ± 5%	Average Heat Flux During Arc (kW/m^2) ± 1 kW/m^2 or ± 5%	Notes
Vertical	Plate Thermometer (2)	445	236	
Location	**Instrument (ID)**	**Total Incident Energy (kJ/m^2) ± 1kJ/m^2 or ± 5%**	**Average Heat Flux During Arc (kW/m^2) ± 1 kW/m^2 or ± 5%**	**Notes**
Vertical	T_{cap} (1)	649	166	
Horizontal	T_{cap} (3)	2 893	849	
Horizontal	T_{cap} (4)	3 805	820	
Location	**Instrument (ID)**	**Total Incident Energy (kJ/m^2) ± 18kJ/m^2 or ± 4%**	**Time (s) to Max Temperature ± 3%**	**Notes**
Vertical	ASTM (A)	471	8	
Horizontal	ASTM (B)	2 157	4	

High-voltage breakdown experiments was conducted prior to and during the OBMV06 experiment. Prior to the HEAF, median breakdown voltage was 14.3 kV, consistent with typical air breakdown strength of 25 kV/cm to 30 kV/cm. Breakdown voltage was also measured during the HEAF, and was observed to decrease to as low as 11 kV, or approximately 22 kV/cm. This decrease does not approach typical bus bar electrical fields of 0.7 kV/cm to 1 kV/cm, and would not be expected to result in propagating breakdown into nearby switchgear at these dielectric holdoff values.

Air conductance experiments resulted in levels below minimum experiments resolution (conductance less than 1 E-6 mhos or resistance greater than 1 E+6 ohms).

Observations and Notes

The box sides were single clad. Due to the failure in Experiment OBMV01 and the experiments schedule, the 10 cm (4 in) by 1.3 cm (0.5in) aluminum bus bar electrodes used in OBMV01 through OBMV03 were not available. The options were to use two 10 cm (4 in) by 0.6 cm (0.25 in) rods per phase or to use 7.6 cm (3 in) by 1.3 cm (0.5 in) rods. The latter was selected to ensure homogeneity of the electrode and eliminate variations that the double bus bar per phase may have introduced.

4.3. Summary of Medium-Voltage Open Box Experiments

Six medium-voltage box experiments were performed at two different current levels and 3 different durations. The total arc energy among the experiments ranged from 22 to 59 MJ. The experiment results are summarized below in Table 46.

Table 46. Summary of Medium-Voltage Open Box Experiment Results

EXPERIMENT			Rod Material		Bar Diameter (cm)		System Voltage (kV)			Current (kA)		Arc Duration (sec)		Energy (MJ)	Notes
#	Seq	Date	Al	Cu	7.6	10.0	Target	Actual	Arc	Target	Actual	Target	Actual	Actual	
OBMV1	4	9/18	X			X	6.9	6.9	0.314	15	14.3	2.00	3.18	33.4	Lab timer failure. Experiment re-run under OBMV6
OBMV2	2	9/17	X			X	6.9	6.9	0.270	30	29.1	1.00	1.12	22.7	
OBMV3	5	9/18	X			X	6.9	6.9	0.274	15	14.4	5.00	5.05	58.6	
OBMV4	3	9/17		X	X		6.9	6.9	0.264	15	14.3	5.00	5.08	51.8	
OBMV5	1	9/16		X	X		6.9	6.9	0.234	30	28.6	2.00	2.32	43.6	
OBMV6	6	9/18	X		X		6.9	6.9	0.285	15	14.6	2.00	2.05	22.7	Aluminum rod dimensions were 3-in x ½-in

5. Summary and Conclusion

This section provides a brief summary and conclusions made from the series of experiments documented in this report.

5.1. Summary

A series of seventeen (17) arcing fault experiments were performed on an open box configuration. Each experiment consisted of a three-phase arcing fault initiated and sustained on aluminum or copper electrodes within the cubical box with one side open to the environment. The magnitude of the arc current and duration was varied at a nominal system voltage of either 1,000V or 6,900V. Electrical parameters are summarized in Table 47. Numerous measurements were made to characterize the environment surrounding the open box, including external heat flux, external incident energy, electric field strength, air conductivity, optical emission spectrum and mass loss. Photometric equipment was deployed to capture the event using a combination of devices to characterize the thermal environment, and event timing.

Table 47. Summary of low-voltage and medium-voltage experiment parameters

Experiment No.	Nominal Voltage (kV)	Current (kA)	Arc Duration (sec)	Energy (MJ)	Mass loss (g)	
					Enclosure	Electrodes
OB01(a)	1.00	1.05	2.01	0.201	None	24.5
OB01(b)	1.00	1.03	2.02	0.736	None	
OB02	1.00	14.02	2.02	11.989	386	762.5
OB03	1.00	13.80	3.03	19.886	1,799	1,327.5
OB04	1.00	27.79	1.03	12.328	110	789.0
OB05	1.00	1.02	2.01	0.796	None	See OB10
OB06	1.00	11.96	2.02	12.591	1,670	740.0
OB07	1.00	12.95	1.52	10.233	861	552.0
OB08	1.00	24.87	1.02	19.570	72*	596.5*
OB09	1.00	4.79	2.01	2.242	None	212.5
OB10	1.00	4.87	2.01	4.118	None	175.0
OBMV1	6.9	14.3	3.18	37.5	10,168	1,323.5
OBMV2	6.9	29.1	1.12	21.42	982	944.5
OBMV3	6.9	14.4	5.05	55.7	17,483	2,296.0
OBMV4	6.9	14.3	5.08	51.8	12,444	3,252.0
OBMV5	6.9	28.6	2.32	43.5	5,666	3,215.5
OBMV6	6.9	14.6	2.05	22.7	5,763	727.0

* electrode failure

5.2. Conclusions

This series of experiments provide valuable information related to the characteristics of the electrical arc and potential hazards, including:

- Thermal energy measurements which provide direct comparison between aluminum and copper electrodes. Low-voltage results shown in Section 3.3.
- Mass loss data was collected for the electrodes and the steel enclosure. This information can be subsequently used to evaluate or develop prediction models to support hazard modeling.
    - For the electrodes, more mass was lost for copper electrodes then aluminum when normalized to an equivalent electrical experimental energy.
    - For the steel enclosure, more steel mass was lost during the aluminum electrode experiments versus the copper electrode experiments when normalized to an equivalent electrical experimental energy.
- Air conductivity and breakdown strength measurements were made during a number of experiments. For the experimental conditions and locations investigated, the results indicated that a conductive cloud was unlikely to cause equipment arc over at the measurement locations. This conclusion may not hold for locations closer to the source.
- Surface conductivity measurement of HEAF byproduct surface deposition showed a decrease in resistance. For the experimental conditions and locations investigated, the result indicated that an impact on plant safety equipment is not likely. The impact of surface deposition, however, is highly dependent on the design, configuration, location and sensitivity of the equipment.
- For the experimental conditions and locations investigated, the electromagnetic interference measurements showed that the EMI signature was small and not likely to impact sensitive plant equipment.

Acknowledgments

Funding for this work was provided by the U.S. Nuclear Regulatory Commission, Office of Research. This report was developed jointly between the National Institute of Standards and Technology (NIST), Sandia National Laboratories, and the U.S. Nuclear Regulatory Commission.

References

[1] NRC RIL 2021-10, NIST TN 2188, SNL SAND2021-12049 R, Report on High Energy Arcing Fault Experiments, Experimental Results from Medium Voltage Electrical Enclosures, U.S. Nuclear Regulatory Commission, Washington, DC, National Institute of Standards and Technology, Gaithersburg, MD, Sandia National Laboratories, Albuquerque, NM, November 2021.

[2] NRC Information Notice 2017-04: High Energy Arcing Faults in Electrical Equipment Containing Aluminum Components, US NRC, Washington, DC, August 2017.

[3] OECD Fire Project – Topical Report No. 1, Analysis of High Energy Arcing Faults (HEAF) Fire Events, Nuclear Energy Agency Committee on the Safety of Nuclear Installations, Organization for Economic Cooperation and Development, June 2013.

[4] EPRI/NRC-RES Fire PRA Methodology for Nuclear Power Facilities, Volume 2: Detailed Methodology. Electric Power Research Institute (EPRI), Palo Alto, CA, and U.S. Nuclear Regulatory Commission, Office of Nuclear Regulatory Research (RES), Rockville, MD: 2005, EPRI TR-1011989 and NUREG/CR-6850.

[5] Fire Probabilistic Risk Assessment Methods Enhancements: Supplement 1 to NUREG/CR-6850 and EPRI 1011989, EPRI, Palo Alto, CA, and NRC, Washington, DC.: December 2009.

[6] NEA HEAF Project – TOPICAL REPORT No. 1, Experimental Results from the International High Energy Arcing Fault (HEAF) Research Program – Phase 1 Experiments 2014 to 2016, Nuclear Energy Agency Committee on The Safety of Nuclear Installations, 2017

[7] Memorandum from Mark Henry Salley, to Thomas H. Boyce, Regarding submittal of possible generic issue concerning the damage caused by high energy arc faults in electrical equipment containing aluminum components, ADAMS Accession No. ML16126A096, May 2016.

[8] Memorandum from Joseph Giitter to Michael F. Weber, regarding Results of Generic Issue Review Panel Screening Evaluation for Proposed Generic Issue PRE-GI-018, 'High Energy Arcing Faults involving Aluminum,' ADAMS Accession No. ML16349A027, July 15, 2017.

[9] Memorandum from Michael Franovich and Michael Cheok to Raymond V. Furstenau, regarding Assessment Plan for Pre-GI-018, Proposed Generic Issue on High Energy Arc Faults Involving Aluminum, ADAMS Accession No. ML18172A189, August 22, 2018.

[10] An International Phenomena Identification and Ranking Table (PIRT) Expert Elicitation Exercise for High Energy Arcing Faults (HEAFs), US NRC, Washington, DC, NUREG-2218, January 2018.

[11] Memorandum from Raymond V. Fustenau to Andrea D. Veil, regarding Closure of Proposed Generic Issue Pre-GI-018, 'High-Energy Arc Faults Involving Aluminum,' ADAMS Accession No. ML21237A360, August 31, 2021.

[12] K. Armijo and P. Clem, et. al., "Electrical Arc Fault Particle Size Characterization," Sandia Report SAND 2019-11145, September 2019.

[13] Tambakuchi, A., et. al., *NRC HEAF Tests, Imaging and Measurement Methodology Report,* SAND2021-12086 R, Sandia National Laboratories, September 2018.

[14] Lafarge, T. and Possolo, A, "The NIST Uncertainty Machine," NCLSI Measure J. Meas. Sci., Vol. 10, No. 3, pp.20-27, September 2015.

[15] SAND202-5747 C, Characterization of DC Arc-Plasmas Generated by High-Voltage Photovoltaic Power Systems; Winters, Caroline, Cruz-Cabrera, Alvaro Augusto, Armijo, Kenneth Miguel, Sandia National Laboratories, June 2020.
[16] RIL 2021-09, SAND2021-11327, HEAF Cable Fragility at the Solar Furnace at the National Solar Thermal Test Facility, Experimental Results, U.S. Nuclear Regulatory Commission, Washington, DC, Sandia National Laboratories, Albuquerque, NM, September 2021.
[17] Putorti, A., Melly, M., Bareham, S., and Praydis Jr., J., "Characterizing the Thermal Effects of High Energy Arc Faults." 23rd International Conference on Structural Mechanics in Reactor Technology (SMiRT 23) – 14th International Post-Conference Seminar on "FIRE SAFETY IN NUCLEAR POWER PLANTS AND INSTALLATIONS," Salford, UK, August 17-18, 2015, http://www.grs.de/en/publications/grs-a-3845.
[18] Ingason, H. and Wickstrom, U., "Measuring incident radiant heat flux using the plate thermometer," *Fire Safety Journal*, Vol. 42, No. 2, 2007, pp. 161-166.
[19] Taylor, B.N. and Kuyatt, C.E., "Guidelines for evaluating and expressing the uncertainty of NIST measurement results," NIST Technical Note 1297, National Institute of Standards and Technology, Gaithersburg, MD, USA, 1994.
[20] Joint Committee for Guides in Metrology. Evaluation of measurement data – Guide to the expression of uncertainty in measurement, Sèvres, France: International Bureau of Weights and Measures (BIPM), URL www.bipm.org/en/publications/guides/gum.html, BIPM, IEC, IFCC, ILAC, ISO, IUPAC, IUPAP and OIML, JCGM 100:2008, GUM 1995 with minor corrections (2008).
[21] Joint Committee for Guides in Metrology. International vocabulary of metrology – Basic and general concepts and associated terms (VIM), Sèvres, France: International Bureau of Weights and Measures (BIPM), 3rd ed., URL www.bipm.org/en/publications/guides/vim.html, BIPM, IEC, IFCC, ILAC, ISO, IUPAC, IUPAP and OIML, JCGM 200:2012 (2008 version with minor corrections) (2012).
[22] McGrattan, K., Hostikka, S., McDermott, R., Floyd, J., Weinschenk, C., Overholt, K., Fire Dynamics Simulator, Technical Reference Guide. National Institute of Standards and Technology, Gaithersburg, MD, USA, and VTT Technical Research Centre of Finland, Espoo, Finland, sixth edition, September 2013. Vol. 1: Mathematical Model; Vol. 2: Verification Guide; Vol. 3: Validation Guide; Vol. 4: Configuration Management Plan.
[23] ASTM Standard F1959 / F1959M-14, 2014, "Standard Experiment Method for Determining the Arc Rating of Materials for Clothing," ASTM International, West Conshohocken, PA, 2014.
[24] ASTM Standard E457-08, "Standard Test Method for Measuring Heat-Transfer Rate Using a Thermal Capacitance (Slug) Calorimeter," ASTM International, West Conshohocken, PA, 2008.
[25] Prodyn Technologies Electric Field Sensors, D-Dot Free Field-Radial Output Data Sheet, https://www.prodyntech.com/wp-content/uploads/2021/01/AD-Series-Free-Field-D-Dot-Data-Sheet.jpg, Albuquerque, NM, site accessed November 2021.
[26] MIL-STD-461G, 11 December 2015 Department of Defense Interface Standard Requirements for the Control of Electromagnetic Interference Characteristics of Subsystems and Equipment, Table XI RS103 limits p. 145 and Figure RS105-1 RS 105 limit for all applications p. 155.

[27] EPRI TR-102323, Revision 3, Guidelines for Electromagnetic Interference Testing of Power Plant Equipment, https://www.osti.gov/servlets/purl/837279, Electric Power Research Institute, Palo Alto, CA, November 2004.
[28] Tektronix Mixed Domain Oscilloscopes, MDO4000C Series Datasheet, Tektronix, Beaverton, OR, https://www.tek.com site accessed November 2021.
[29] NFPA 70, National Electric Code, 2020 Edition, National Fire Protection Association, Quincy, MA, 2020.
[30] ASTM D2477, Standard Test Method for Dielectric Breakdown Voltage and Dielectric Strength of Insulating Gases at Commercial Power Frequencies, ASTM International, West Conshohocken, PA, 2020.
[31] IEEE 1584, Guide for Performing Arc-Flash Hazard Calculations, Institute of Electrical and Electronic Engineers, New York, NY, 2018.

Appendix A: Engineering Drawings

This appendix provides detailed drawings and information on experiment facility, experiment object, and instrumentation.

A.1 Experiments Facility

Drawings of the experiments facility are presented in Fig. 129 through Fig. 134.

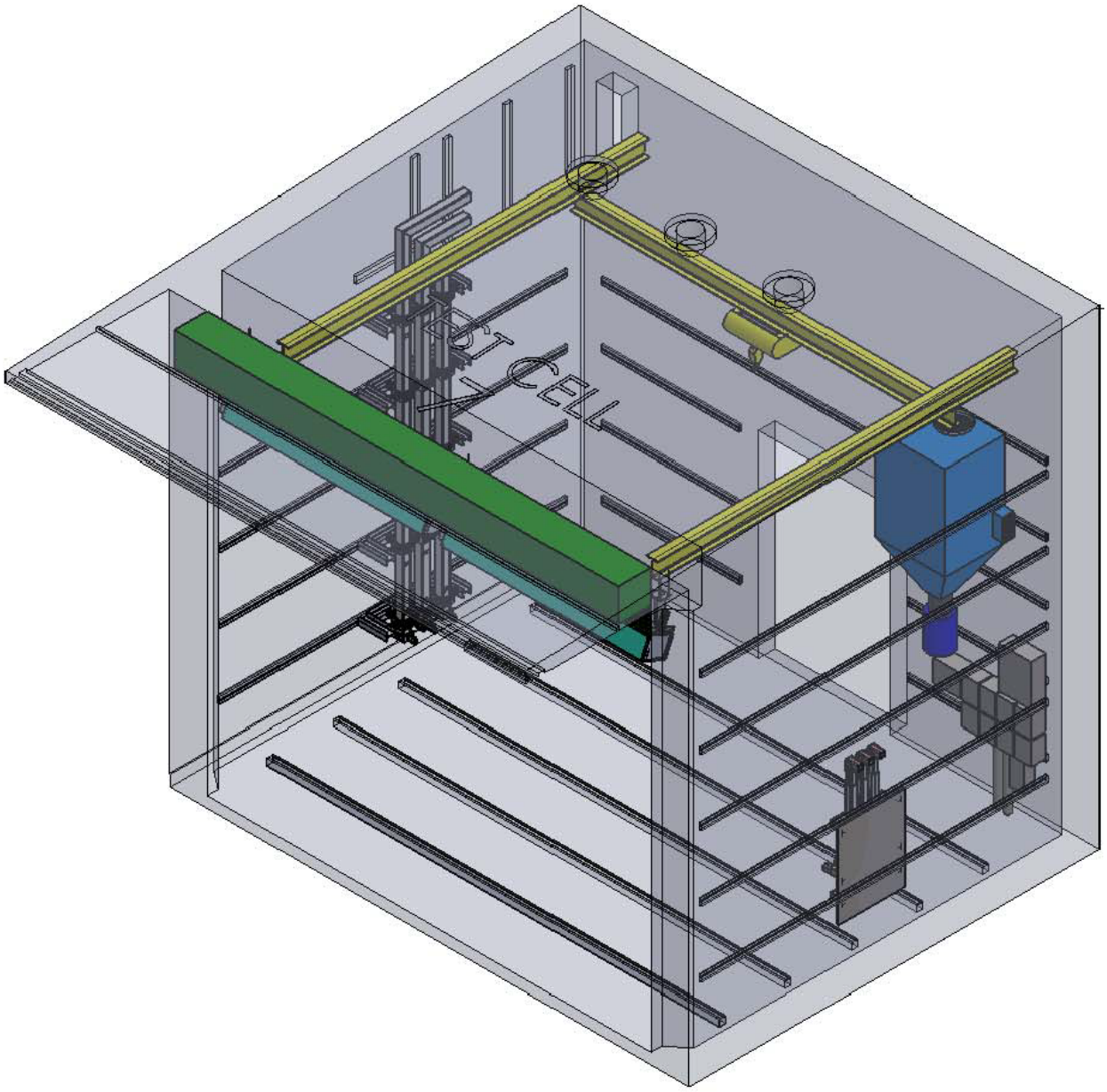

Fig. 129. Isometric drawing of Experiment Cell #7

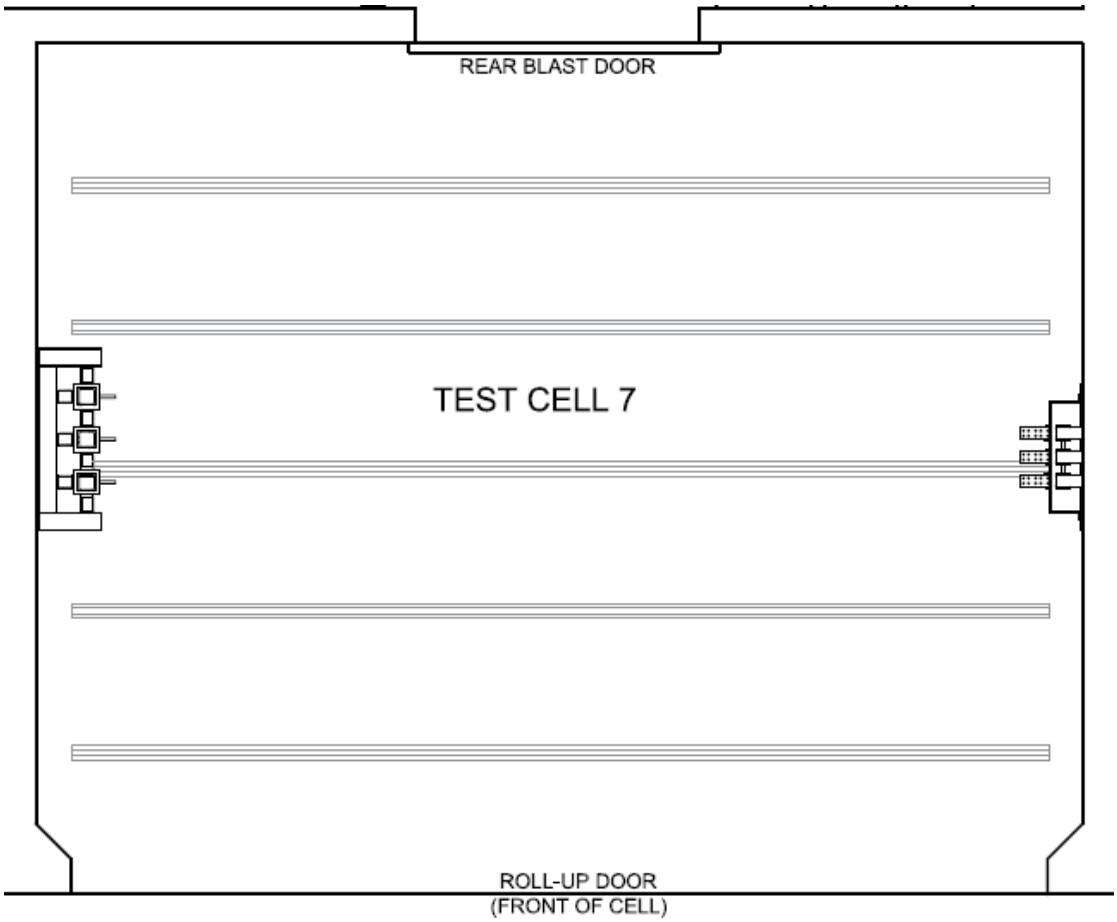

Fig. 130. Plan view of experiment cell #7.
Low-voltage power connections located on right side of drawing.

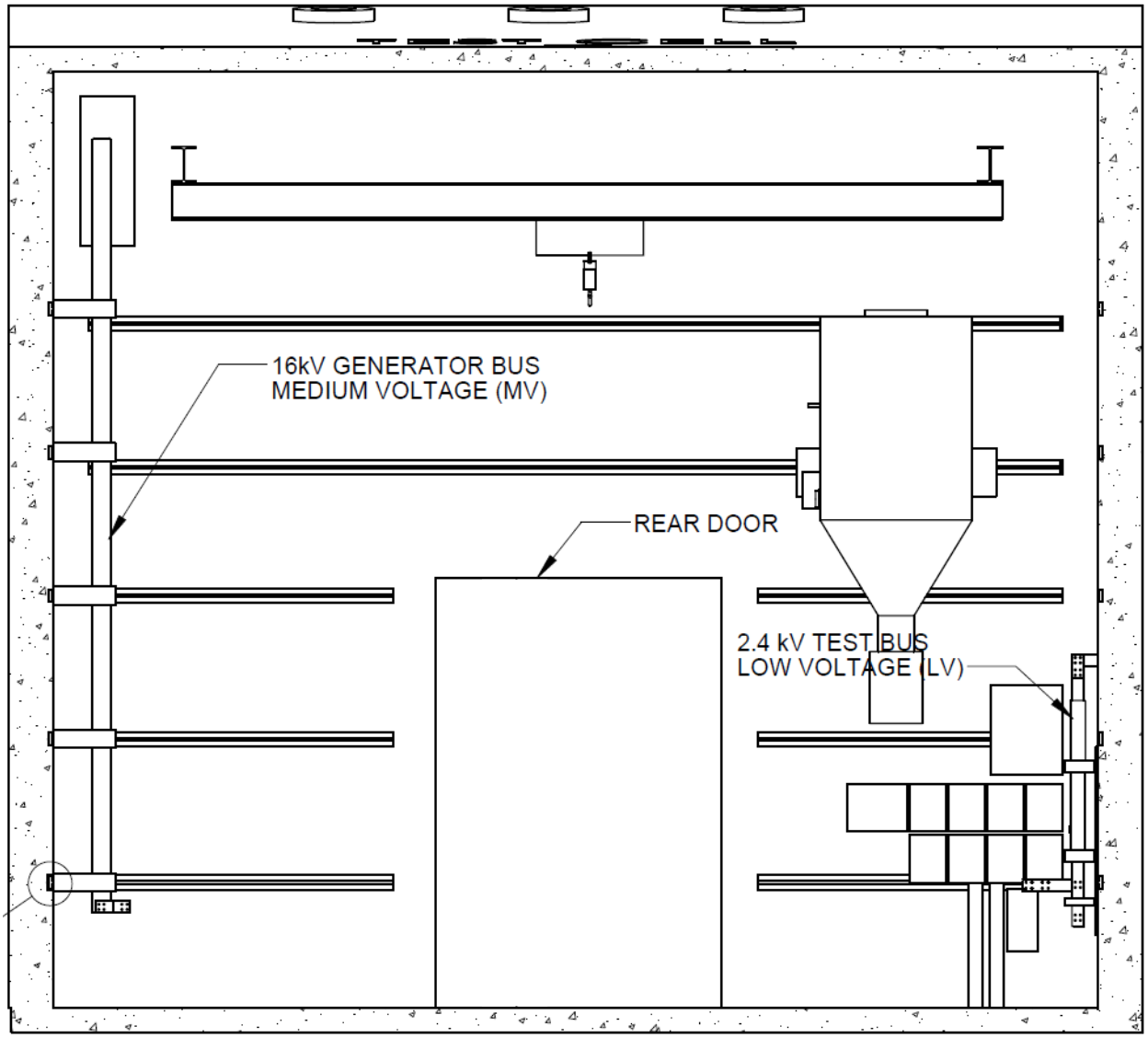

Fig. 131. Elevation view of Experiment Cell #7.
Low-voltage power connections located on right side of drawing.

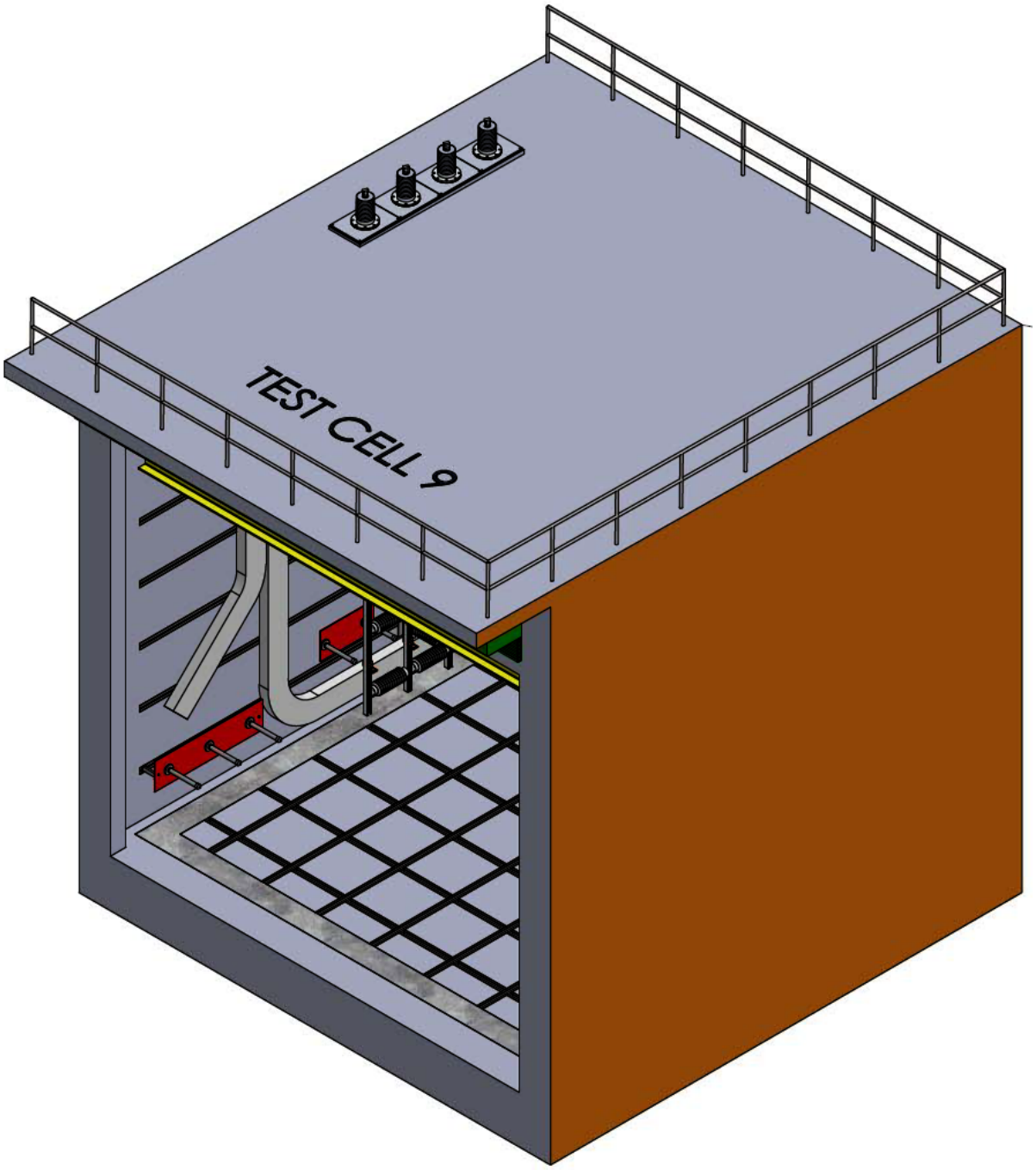

Fig. 132. Isometric drawing of experiment cell #9

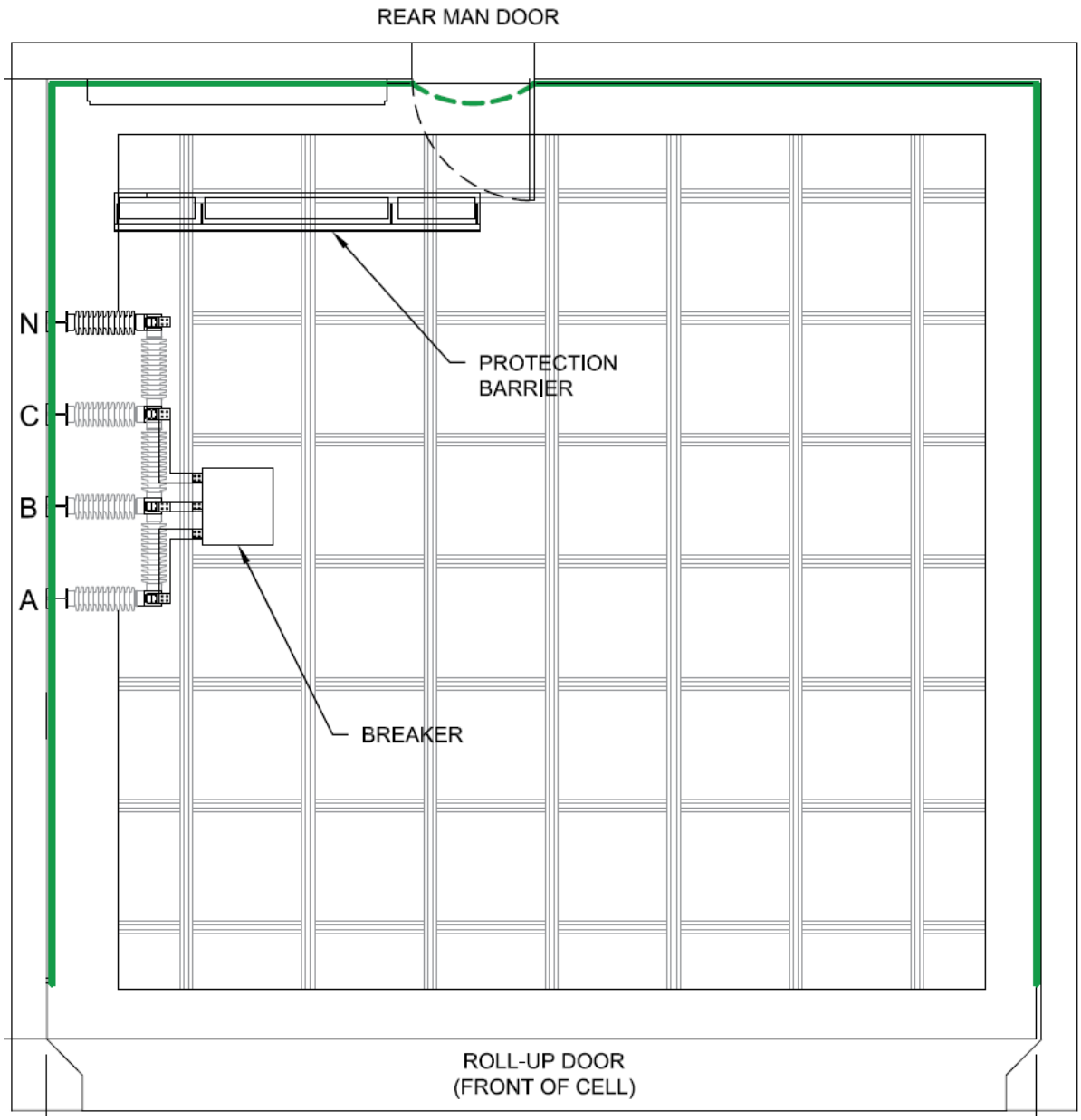

Fig. 133. Plan view of experiment cell #9.

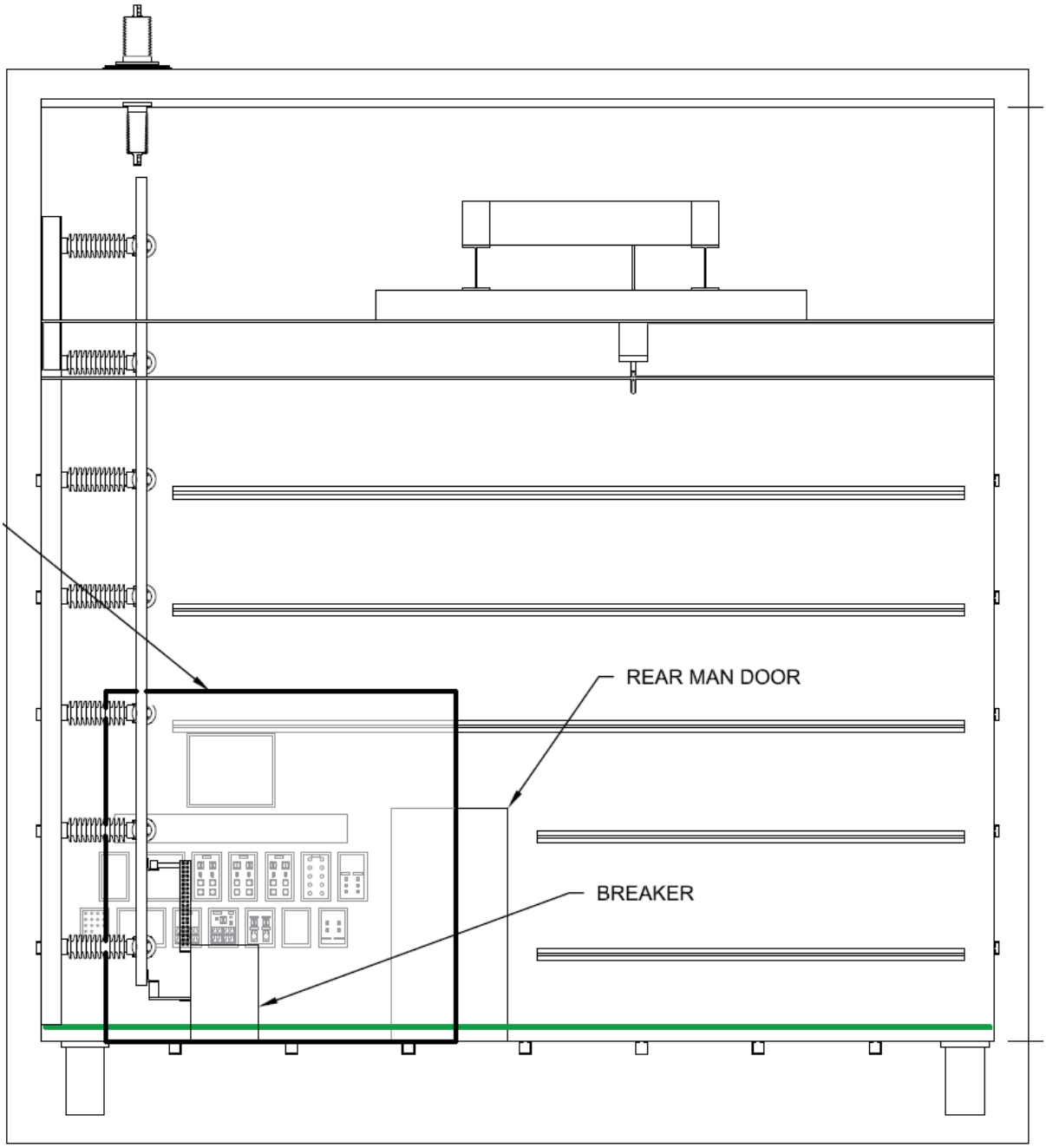

Fig. 134. Elevation view of experiment cell #9. Breaker shown in drawing is part of KEMA protection system and is not the open box.

A.2 Support Drawings

SNL manufactured three phase electrode holders for the low-voltage box experiments. The drawing of this component is presented below.

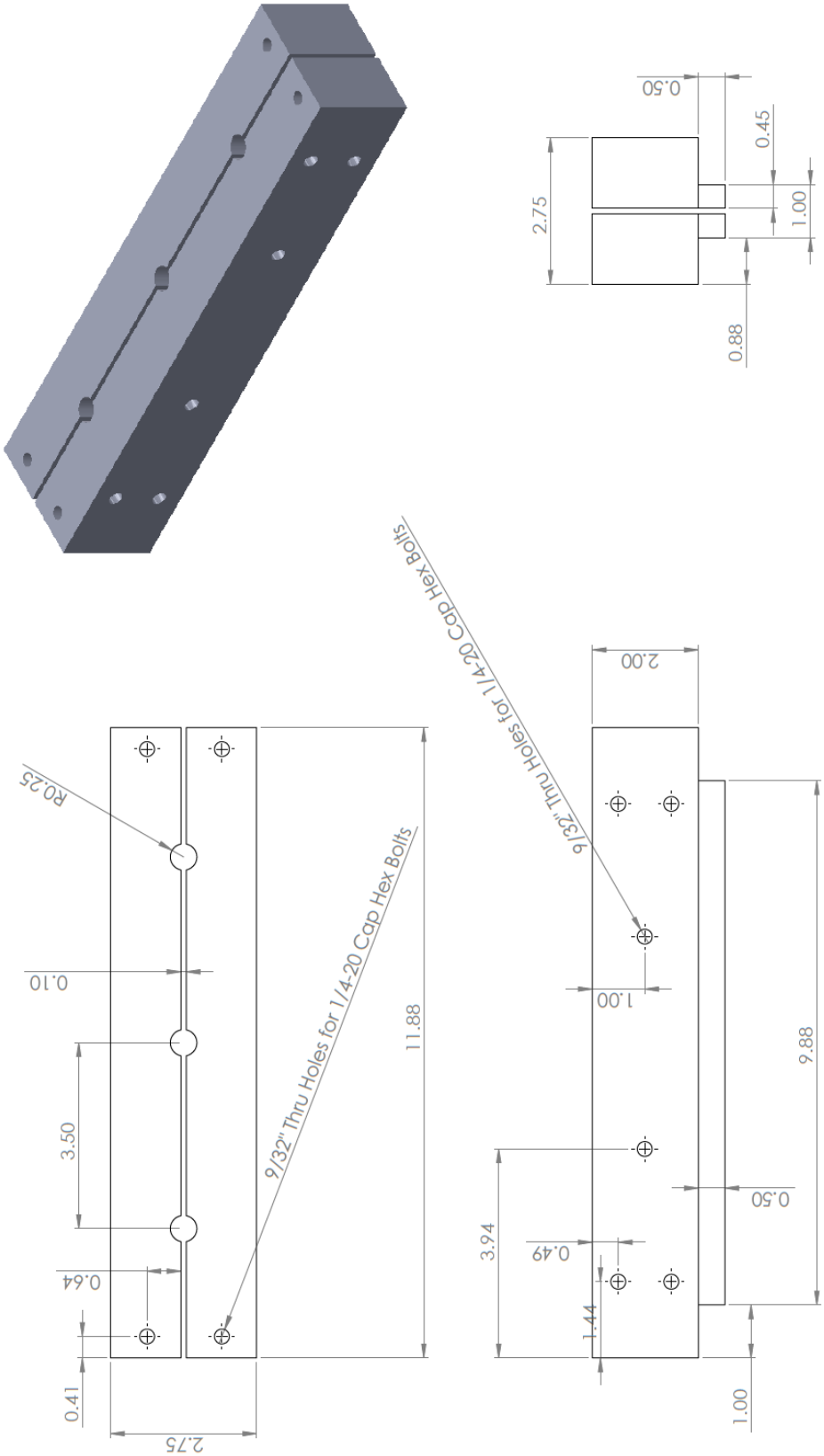

Fig. 135. Electrode holder used in open box experiments. All dimensions shown in inches.

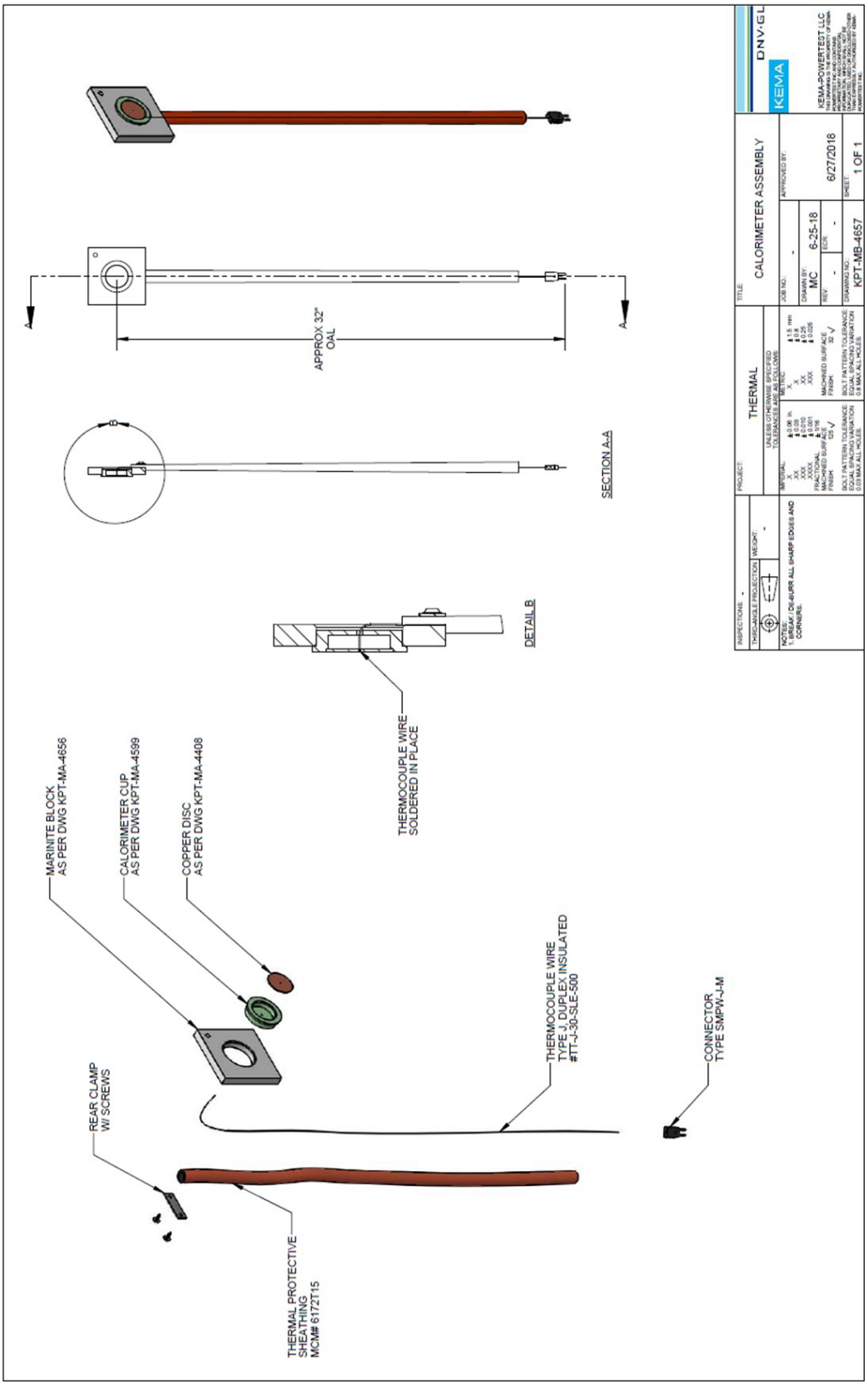

Fig. 136. Drawing KPT-MB-4657, ASTM Calorimeter Assembly

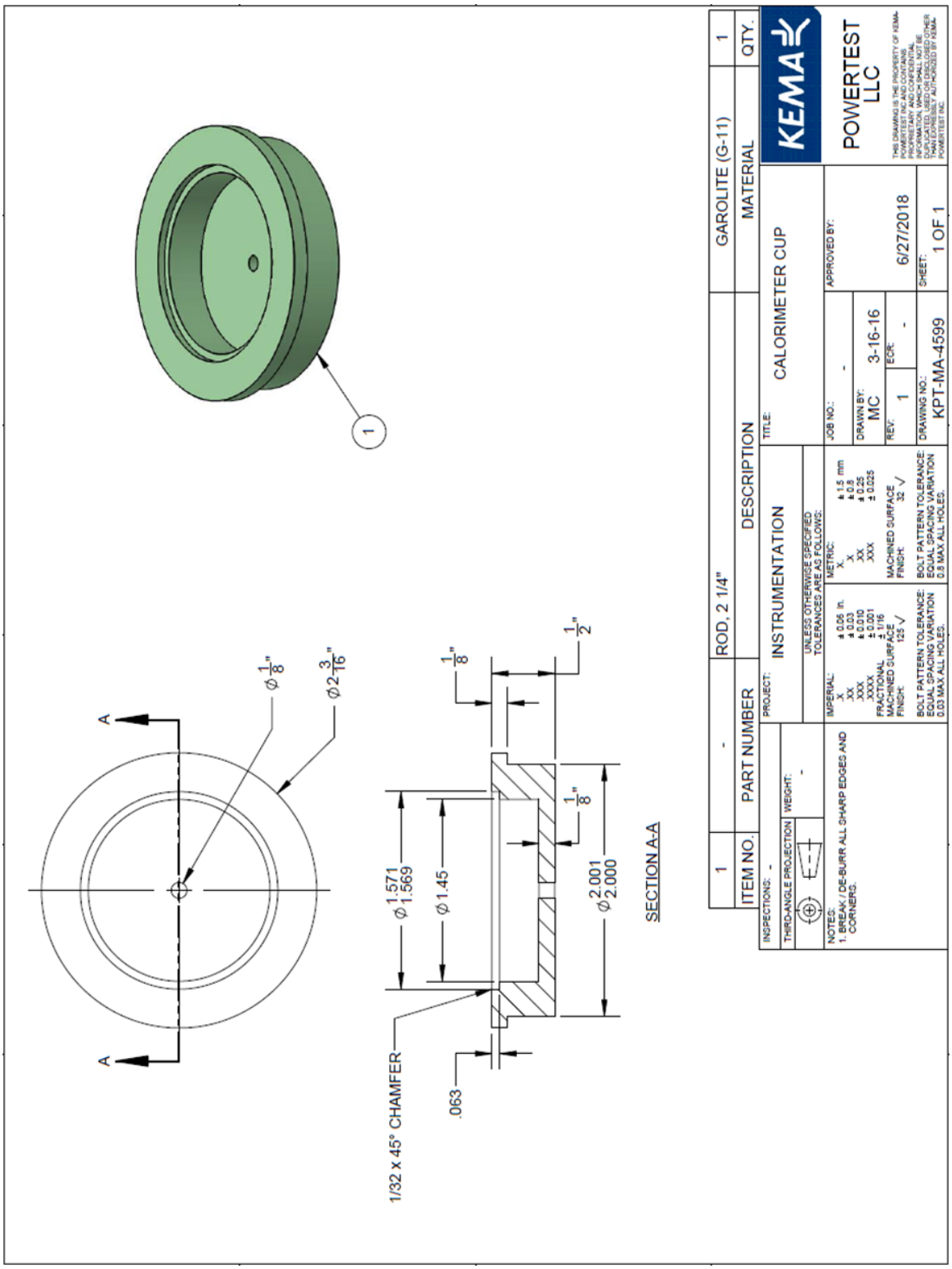

Fig. 137. Drawing KPT-MA-4599, ASTM Calorimeter Cup

Appendix B: KEMA Experiment Report

This appendix provides a copy of KEMA experiment report.